Scaling of Urban Heat Island Simulation:

Validation of the Urban Weather Generator for Varying Boundaries.

Wissenschaftliche Arbeit zur Erlangung des Grades

M.Sc. Bauingenieurwesen

an der TUM School of Engineering and Design der Technischen Universität München.

Betreut von Prof. Dr.-Ing. Werner Lang, M.Eng. Roland Reitberger, M.Sc. Farzan Banihashemi, M.Sc. Nayanesh Pattnaik

Lehrstuhl für energieeffizientes und nachhaltiges Planen und Bauen

Eingereicht von Kristiana Bezha

Eingereicht am Munich, 29.02.2024

Vereinbarung

zwischen

der Technischen Universität München, vertreten durch ihren Präsidenten,
Arcisstraße 21, 80290 München

hier handelnd der Lehrstuhl für Energieeffizientes und Nachhaltiges Planen und Bauen (Univ.-Prof. Dr.-Ing. W. Lang), Arcisstr. 21, 80333 München

– nachfolgend TUM –

und

Frau/Herrn ……

(Anschrift)

– nachfolgend Autorin/Autor –

Die Autorin / der Autor wünscht, dass die von ihr/ihm an der TUM erstellte Masterarbeit mit dem Titel

……

……....

☐ auf mediaTUM und der Webseite des Lehrstuhls für Energieeffizientes und Nachhaltiges Planen und Bauen mit dem Namen der Verfasserin / des Verfassers, dem Titel der Arbeit, den Betreuer:innen und dem Erscheinungsjahr genannt werden darf.

☐ in Bibliotheken der TUM, einschließlich mediaTUM und die Präsenzbibliothek des Lehrstuhls für Energieeffizientes und Nachhaltiges Planen und Bauen, Studierenden und Besucher:innen zugänglich gemacht und veröffentlicht werden darf. Dies schließt auch Inhalte von Abschlusspräsentationen ein.

☐ mit einem Sperrvermerk versehen und nicht an Dritte weitergegeben wird.

(Zutreffendes bitte ankreuzen)

Zu diesem Zweck überträgt die Autorin / der Autor der TUM zeitlich und örtlich unbefristet das nichtausschließliche Nutzungs- und Veröffentlichungsrecht an der Masterarbeit.

Die Autorin / der Autor versichert, dass sie/er alleinige(r) Inhaber(in) aller Rechte an der Masterarbeit ist und der weltweiten Veröffentlichung keine Rechte Dritter entgegenstehen, bspw. an Abbildungen, beschränkende Absprachen mit Verlagen, Arbeitgebern oder Unterstützern der Masterarbeit. Die Autorin / der Autor stellt die TUM und deren Beschäftigte insofern von Ansprüchen und Forderungen Dritter sowie den damit verbundenen Kosten frei.

Eine elektronische Fassung der Masterarbeit als pdf-Datei hat die Autorin / der Autor dieser Vereinbarung beigefügt. Die TUM ist berechtigt, ggf. notwendig werdende Konvertierungen der Datei in andere Formate vorzunehmen.

Vergütungen werden nicht gewährt.
Eine Verpflichtung der TUM zur Veröffentlichung für eine bestimmte Dauer besteht nicht.

Die Autorin / der Autor hat jederzeit das Recht, die mit dieser Vereinbarung eingeräumten Rechte schriftlich zu widerrufen. Die TUM wird die Veröffentlichung nach dem Widerruf in einer angemessenen Frist und auf etwaige Kosten der Autorin / des Autors rückgängig machen, soweit rechtlich und tatsächlich möglich und zumutbar.

Die TUM haftet nur für vorsätzlich oder grob fahrlässig verursachte Schäden. Im Falle grober Fahrlässigkeit ist die Haftung auf den vorhersehbaren Schaden begrenzt; für mittelbare Schäden, Folgeschäden sowie unbefugte nachträgliche Veränderungen der veröffentlichten Masterarbeit ist die Haftung bei grober Fahrlässigkeit ausgeschlossen.

Die vorstehenden Haftungsbeschränkungen gelten nicht für Verletzungen des Lebens, des Körpers oder der Gesundheit.

Meinungsverschiedenheiten im Zusammenhang mit dieser Vereinbarung bemühen sich die TUM und die Autorin / der Autor einvernehmlich zu klären. Auf diese Vereinbarung findet deutsches Recht unter Ausschluss kollisionsrechtlicher Regelungen Anwendung. Ausschließlicher Gerichtsstand ist München.

München, den , den

…… ……

(TUM) (Autor:in)

Erklärung

Ich versichere hiermit, dass ich die von mir eingereichte Abschlussarbeit selbstständig verfasst und keine anderen als die angegebenen Quellen und Hilfsmittel benutzt habe.

_____

Ort, Datum, Unterschrift

Table of contents

Vereinbarung I
Erklärung III
Table of contents 1
Abstract 3
Kurzfassung 4
Acknowledgments 7
List of abbreviations 9
Glossary 11
1. Introduction 13
2. State of research 17
2.1. Urban heat island 17
2.2. Tools for urban climate modeling 18
2.3. Urban Weather Generator 20
2.3.1. UWG case studies 20
2.3.2. UWG parameters 22
2.3.3. Known limitations 24
3. Methodology 25
3.1. Outline of the methodology 25
3.2. Software and tools 27
3.3. Rhino 3D models 28
3.3.1. Model from CADMAPPER 28
3.3.2. Elk plugin and Open Street Map 29
3.3.3. CityGML to Stereolithography 30
3.3.4. CityGML and AntFarm plug in 31
3.3.5. Other methods 31
3.4. Grasshopper model 32
3.4.1. Dragonfly model 32
3.4.2. Urban Weather Generator model 32
3.5. Test with varying parameters 33
3.6. Statistical analyses 34
4. Case study 37
4.1. Location 37
4.2. Area selection 40

4.3. Urban model 41
4.3.1. Buildings' properties 41
4.3.2. Creation of the terrain 48
4.4. Creating the .epw file 53
4.5. Rural model 54
4.6. Running the UWG 55
5. Results and discussion 57
5.1. Graphical results for UHI 58
5.2. Results for the same condition and the same period 61
5.2.1. Urban morphology parameters 61
5.2.2. July simulations 62
5.2.3. December simulations 73
5.2.4. Annual simulations 76
5.3. Results for the same condition but different periods 79
5.3.1. Full sun exposure condition 79
5.3.2. Building shade condition 80
5.4. Results for different conditions but the same period 80
5.4.1. Different conditions comparison, July 81
5.4.2. Different conditions comparison, December 81
5.4.3. Different conditions comparison, annual data 82
5.5. Discussion 83
5.5.1. Radius influence and different conditions 83
5.5.2. UWG behavior and results of intercomparisons 85
6. Conclusion 87
7. List of figures 89
8. List of tables 92
Appendix A 93
Appendix B 97
9. References 123

Abstract

The urban climate change phenomenon is a growing concern severed by the overpopulation of cities, unsustainable consumerism patterns, and inadequate urban planning. One of the main threats in the cities' areas is the urban heat island effect; thus, further attention must be given to climate analysis simulation to develop efficient urban areas or implement new strategies for existing ones. There are already many existing tools, and the main question is the parameters that need to be included in these simulations to truly account for the severity of the urban heat island effect. One main aspect a planner should consider while performing urban climate analysis is the area size. For this reason, in this study, we focused on the influence that the area size has on the climate simulation results, specifically in dry bulb temperature results. To account for the urban heat island effect, we used the Urban Weather Generator, where we varied the boundaries of the urban area starting with a radius of 10 m up to 1500 m. The starting point of our case study was Bordeauxplatz, Munich, Germany. The model was implemented and developed in Rhinoceros 3D and Grasshopper. At the same time, the simulations were run with the help of Dragonfly tools, where the Urban Weather Generator is a plug-in. We considered different parameters of the actual urban area, such as buildings' average height, vegetation covers, sensible anthropogenic heat, etc. For our simulations, we also differentiated the obtained results for different periods, such as July, December, and annual, and between the time spans of a day, as whole day hours, day hours, and night hours. Once we had the results, we compared them with airport data (also used as the engine input) and the measured data, recorded in different conditions such as building shade, full sun exposure, etc. We performed different statistical analyses, where the main focus was the Root Mean Square Error and the Spearman's correlation between the Root Mean Square Error and the variation in radius. We found a maximum urban heat island intensity of nearly 6°C for the case study analyzed. We concluded that the International Munich Airport is an appropriate input for the environmental analysis of Munich. More importantly, there is no specific radius / boundary that displays the lowest error in all cases and conditions; one should consider the period, time span, and condition and look at the radius as a conglomeration of other urban morphology parameters.

Keywords: Dry bulb temperature, Radius, Urban Weather Generator

Kurzfassung

Das urbane Klimawandelphänomen ist ein wachsendes Anliegen, welches durch die Überbevölkerung von Städten, untragbare Konsumgewohnheiten und unzureichende urbane Planung schlimmer wird. In städtischen Gebieten stellt der Wärmeinsel-Effekt eine der Hauptbedrohungen dar. Daher ist es entscheidend, dass der Klimaanalysensimulation weiterhin besondere Aufmerksamkeit geschenkt wird, um effiziente Stadtgebiete zu entwickeln oder neue Strategien für bereits vorhandene umzusetzen. Es existieren bereits zahlreiche Tools, und die wichtige Frage ist, welche Parameter in diesen Simulationen berücksichtigt werden müssen, um die Schwere des urbanen Wärmeinsel-Effekts angemessen zu erfassen. Ein wichtiger Aspekt, den ein Planer bei der Durchführung von Analysen zum urbanen Klima berücksichtigen sollte, ist die Flächengröße. In dieser Studie haben wir uns daher darauf konzentriert, die Auswirkungen der Flächengröße auf die Ergebnisse der Klimasimulation zu untersuchen, insbesondere im Hinblick auf die Ergebnisse der „dry bulb temperature“. Um den Einfluss des städtischen Wärmeinseleffekts zu berücksichtigen, verwendeten wir den Urban Weather Generator und variierten die Grenzen, beginnend mit einem Radius von 10 m bis zu 1500 m des urbanen Gebiets. Unsere Fallstudie begann am Bordeauxplatz in München, Deutschland. Das Modell wurde in Rhinoceros 3D und Grasshopper implementiert und entwickelt. Währenddessen wurden die Simulationen auf Dragonfly-Tools durchgeführt, wobei der Urban Weather Generator als Plug-in integriert wurde. Wir haben verschiedene Aspekte des tatsächlichen urbanen Gebiets in Betracht gezogen, darunter die durchschnittliche Höhe der Gebäude, Vegetationsbedeckung, sensible anthropogene Wärme usw. In unseren Simulationen haben wir auch die Ergebnisse für unterschiedliche Zeiträume betrachtet, darunter Juli, Dezember und das gesamte Jahr, sowie für verschiedene Tagesabschnitte wie Ganztagsstunden, Tagesstunden und Nachtstunden. Nachdem wir die Ergebnisse erhalten hatten, führten wir einen Vergleich mit den Flughafendaten durch, die auch als Eingabe für das Modell verwendet wurden, sowie mit den gemessenen Daten unter verschiedenen Bedingungen, einschließlich Schatten von Gebäuden, voller Sonneneinstrahlung usw. Im Rahmen unserer Untersuchung führten wir diverse statistische Analysen durch, wobei der Hauptfokus auf dem Root Mean Square Error und der Spearman-Korrelation zwischen dem Root Mean Square und der Variation des Radius lag. Wir haben eine maximale urbane Wärmeinsel-Intensität von circa 6°C für die analysierte Fallstudie gefunden. Unsere Analyse ergab, dass der Internationale

Flughafen München eine angemessene Grundlage für die Umweltanalyse von München darstellt. Vor allem zeigt sich, dass es keinen festgelegten Radius oder keine klare Grenze gibt, die unter allen Bedingungen den niedrigsten Fehler hat. Man sollte sowohl den Zeitraum, als auch die Bedingungen berücksichtigen und den Radius als eine Kombination anderer Parameter der urbanen Morphologie sehen.

Acknowledgments

I am grateful to my supervisors, Roland Reitberger, Farzan Banihashemi, Nayanesh Pattnaik, and Prof. Dr.-Ing. Werner Lang, for their unwavering support and valuable recommendations throughout the entire duration of my thesis work. I truly appreciate their prompt responses to all my queries. Additionally, I would like to extend my thanks to Vjosa Dervishi, Priscila Stark da Silva, and Leila Parhizgar for their help in providing some of the necessary data. Much gratitude goes to Nazli Kök for her insightful software advice during the initial stage of my thesis.

Secondly, I would like to thank my friends who have supported me during this challenging period. Thank you for giving me both fun and courage.

Lastly, I would like to express my thanks to my families. To my family in Albania, thank you for supporting me, and encouraging me to pursue my education and take advantage of every opportunity, no matter how far away from you the opportunities were. Mom, dad, and dear sister, I appreciate all the sacrifices you have made for me. To my family in Munich and my soul friend, Emre, with whom I have shared the Master's degree journey from day one, thank you for always being there for me, no matter what. Thank you for making this the most beautiful journey I have taken until now.

List of abbreviations

AV	Average
BS	Building Shade
DBT	Dry bulb temperature
DF	Dragonfly
EPW	EnergyPlus Weather Format
FS	Full Sun
GML	City Geography Markup Language
MAE airport	Mean Absolute Error between simulated and airport data
MAE measured	Mean Absolute Error between simulated and measured data
MBE airport	Mean Bias Error between simulated and airport data
MBE measured	Mean Bias Error between simulated and measured data
R^2	Coefficient of determination, Linear Regression Analysis
R^2 airport	Linear Regression Analysis between simulated and airport data
R^2 measured	Linear Regression Analysis between simulated and measured data
Rhino	Rhinoceros 3D
RMSE airport	Root Mean Square Error between simulated and airport data
RMSE measured	Root Mean Square Error between simulated and measured data
SHGC	Solar Heat Gain Coefficient
TS	Tree Shade
UHI	Urban Heat Island
UWG	Urban Weather Generator
WE	Wind Exposure
WP	Wind Protected

Glossary

Albedo – varies from 0 to 1, showing the part of the solar radiation reflected from a surface / material.

Average building height – refers to the average buildings' height in the urban area.

Dry bulb temperature – also referred to as the air temperature is the temperature measured by a thermometer unaffected by the moisture in the air.

Facade to site ratio – is the ratio of the wall surfaces to the urban area.

SHGC – shows the part of the solar radiation transmitted through the window and its parts after hitting them. It varies from 0 to 1.

Site coverage ratio / Footprint density – the ratio between the building footprint and the site area.

U value – gives the rate of the heat transferred through a structure, material, or different compositions.

1. Introduction

Urbanization is an essential part of global development, but its rapid and uncontrolled expansion poses significant threats to cities and the planet.

Cities are now witnessing increased greenhouse gas (GHG) emissions, a loss of green spaces and biodiversity, escalating pollution, increased resource consumption, etc. [1]. It is important to acknowledge that the deterioration of the environment is caused not only by natural factors but also by human activities such as inefficient urban planning and consumerism. Even though cities only occupy 2% of the Earth's surface, they consume 75% of all material resources. [2] They are responsible for over 70% of global GHG emissions and consume more than two-thirds of the world's energy [3].

Moreover, the global urban population is expected to increase by 2.5 billion between 2018 and 2050 [4]. This indicates that the urban sprawl will expand. Urban sprawl is also linearly related to the built environment activities, which consume 50% of all extracted materials and produce 35% of waste in the EU [5].

Urban sprawl increases the severity of the main threat of the last decades, climate change, whose impact was felt explicitly in Europe in 2022, with several intense heatwaves passing through the continent. Germany broke its record with a temperature of 40.1°C in Hamburg [6]. Moreover, heat waves pose significant threats to human society as one of the most harmful climate extremes; they are expected to be more frequent and severe. On the other hand, the development of urban spaces and infrastructure involves the conversion of agricultural lands and forests, leading to the extensive clearing of vegetation, creating stress on nearby regions and affecting ecosystems [7]. It changes the local climate; the areas of high density and low greenery transform into “islands” with a higher temperature compared to surrounding or rural zones. They are called urban heat islands (UHI), whose effect also exacerbates heat stress for urban residents. [8, p. 2]

To withstand all the threats mentioned before, creating resilient cities through practices of climate change adaptation and mitigation is essential [9, p. 748]. Assessing climate change, especially UHI, is necessary while designing and planning an urban area. The buildings and the surroundings coexist together. The optimization of their performance needs to be done on an urban level in the early stages; this holistic approach blends

simultaneously with SDG 11, developing sustainable cities and communities, and SDG 13, climate adaptation and mitigation [10]. Another crucial approach to urban planning is to involve multiple stakeholders [7]. Part of these stakeholders can be the residents who participate in decision-making processes to ensure that urban areas are planned with a human-centered focus. Additionally, the government can implement policies, as is happening in Europe, where urban policies are shaped by HABITAT III and the 2030 Agenda [11]. A contribution is also needed from academics researching new approaches and urban planners adhering to policies and fulfilling demands.

As discussed previously, among many threats that should be tackled considering their interdependencies, the aggravation, and the effect that the urban UHI has needs a higher focus. For this reason, this thesis will analyze if there are certain boundaries or if a particular area can be analyzed to better assess the UHI and understand the microclimate effect. We will utilize the Urban Weather Generator (UWG) model to accomplish this task. The answer to the question and the results of the thesis will be implemented in the work of the Research Training Group 2679 - Urban Green Infrastructure (RTG-UGI), which aims to improve city life by considering urban transformation, climate resilience, and sustainable stormwater management within a social-ecological-technological framework [12].

The content of this thesis includes the following. A state of research regarding the UHI, the UWG with its case study and parameters, and especially we will look into previous studies regarding the radius as a parameter in the UWG. A general methodology follows, related to the running of the engine and the analysis of the radius effect. We describe the parameters more in detail in our case study chapter. Lastly, we have the results discussed and compared to previous studies, and the conclusion ends the thesis with some key points and suggestions.

Research question and hypothesis:

The research question of this study is:

Is there any optimal radius or boundaries used in an urban model to obtain dry bulb temperature values near the measured ones, in the UWG engine?

To answer our research question, we will look into the case study of Munich and, specifically, the area of Bordeauxplatz, where simulations run for the modeled urban area with different radii will be compared to measured in-place data. The data comes from sensors placed in different conditions, such as building shade, full sun exposure, etc. It was decided to compare the dry bulb temperature (DBT) not because it is one of the results values of the engine but because it is crucial for UHI identification and energy-building analysis [13]. The availability of the data in different conditions gives us the opportunity to analyze not only the radius influence but as well the UWG behavior. To look more into details, the data is differentiated for the 24-hours span (time spans) and seasons.

To the aim of this thesis and what was previously discussed, we considered two central hypotheses:

1. The boundaries do not have a significant statistical influence on the result of DBT for the case study of Munich, Bordeauxplatz.

2. While comparing different conditions, different statistical results are reached for the case study of Munich, Bordeauxplatz.

2. State of research

2.1. Urban heat island

The UHI is a climate-related physical event, showing a difference in temperature between urban and rural areas [14]. The effect is mainly seen at nighttime [15]. The urban heat islands are caused by different factors as the conversion of natural surfaces to sealed surfaces, the type of material used, urban geometry, heat from human activity, etc. [16]. In an urban area, man-made structures imbibe more heat than natural areas, and they do not have the evapotranspiration cooling effect [17]. UHI is present in all urban areas regardless of the city's size or climate [18]. It varies and depends on the city's climatic, meteorological, anthropogenic, and morphological conditions, creating artificial microclimates. The phenomenon is also local and can change from one neighborhood to another. [15] The variation concept also lines up with the example in the USA where researchers show that usually, cities compared to their surroundings have a temperature difference of nearly 0.5°– 4.0°C during the daytime while at night it can be as severe as 1.0°– 2.5°C. It has been stated that the difference is higher in denser cities and cities with humid climate [19]. Moreover, a study done for 70 European cities for UHI and heat waves, has shown that the cold climate cities are more vulnerable to UHI and heat waves [20].

To evaluate the UHI, there are two methods: the UHI intensity, as used in the USA example, which compares mean and maximum air temperature between urban and rural areas [14], and the energy balance concept. It considers the various heat fluxes emitted in the studied zone and accounts for their influence on the UHI. [21] The energy balance method is widely used in climate analysis software.

The UHI can be classified according to its vertical occurring positions as the Surface UHI, the Urban Canopy UHI, and the Urban Boundary Layer UHI [15]. The comfort indicators at the neighborhood level rely on the Surface UHI (temperature difference of surfaces a few centimeters above the ground) and the Urban Canopy UHI (air temperature difference inside the city) [22]. On the other hand, evaluations of simulated data with measured data have shown that to correctly assess the UHI effect, the analyzing tools must consider both the canopy and the urban boundary layer [23].

Since UHI is a representative phenomenon of urban climate change with indicators as the temperature increases [24], and its severity is increasing with the situation of global and urban climate change, when we assess the UHI, we are also assessing mainly the urban climate change. Moreover, UHI not only changes many ecological and meteorological patterns as precipitation, air motion, etc., but also has a negative impact on human health, such as heat stress, stroke, exhaustion, or even suicidal tendencies [25]. Considering all the effects and variations that the UHI has, a specific case-dependent study must be performed while designing or planning an urban area. By performing simulations, urban planners will know how and where to implement solutions to reduce the UHI effect, such as careful planning, the right choice of building materials, the creation of unsealed surfaces, the implementation of green infrastructure, etc. [26].

2.2. Tools for urban climate modeling

Even though accounting for the effect on microclimate is necessary, many construction projects do not perform it. This issue occurs due to companies' lack of knowledge [26] or insufficient interdisciplinary cooperation. It cannot be attributed to the lack of methodologies or tools, as many have existed for decades.

There are two main approaches to urban climate modeling: observational approaches and simulation approaches [27, p. 2192]. Observational approaches are expanded more into urban microclimate analysis, related to measurements in the studied area or remote sensing [28, p. 1615]. An example of remote sensing is the Land Surface Temperature (LST) method, using satellite data [15]. On the other hand, the numerical simulation approaches, where more important are the Computational Fluid Dynamics (CFD) and the Energy Balance Models (EBM), allow to look into different scenarios compared to the observation methodology [28, p. 1615]. Moreover, there are different scales in climate modeling, as seen in Figure 1.

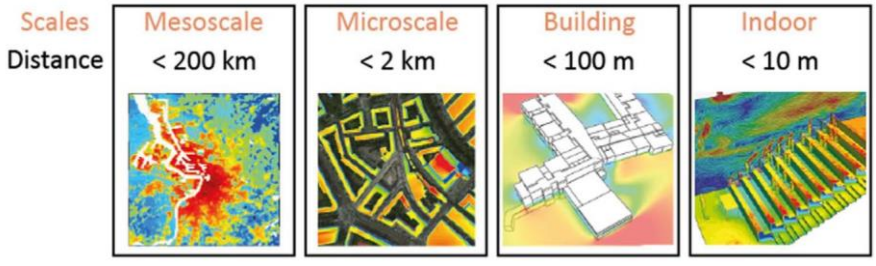

Figure 1 Representation of spatial scales in climate modeling [28, p. 1615]

Various tools can be used depending on the tool's scale and ability. Some worth mentioning microscale numerical models are ENVI-met, Ladybug tools, ANSYS (ENVIMET decoding urban nature), GREENPASS (also based on Envi-met), uhiSolver, Urban Weather Generator (UWG) etc. [26].

Some studies compare different tools to select the most appropriate one for their needs. An example from Abu Dhabi states that ENVI-met can simulate urban temperature, humidity, wind speed, and various heat maps but needs improvement in calculating anthropogenic heat and mean radiant temperature. Meanwhile, UWG results in a detailed energy model on a mesoscale model, also considering the seasonal effect [13]. The UWG was also compared with the Crawley temperature alteration algorithm [29] by Street. After validating the Energy Usage Intensity (EUI) data, Street recommends using UWG for urban design feedback with available urban morphology data and Crawley for magnitude results without urban site data. [30]

As can be seen from the previous information and the examples in comparison, urban planners and environmental specialists have several tools to choose from for climate analysis. They can use the numerical simulation models for climate-efficient urban development, predictions, and adaptation measures for existing urban areas [28, p. 1613]. The tool selection depends on various factors, such as the scale of analysis, level of detail, data availability, and tool accessibility. Hence, comparing different methods before proceeding with the analysis is recommended.

For our case, we decided to use the UWG for two main reasons: it gives dry bulb temperature value, and we can access it in our designing platform. This tool has been getting more attention lately due to its accuracy and straightforward user interface [23]. Moreover, UWG has a stand-alone version, and it is now also a tool of the Dragonfly (DF) plugin in Grasshopper [31, 32]. The translation from the original Matlab into a Python code made many benefits to be integrated into DF, more variety of parameters at the urban and building level, improvement of results, etc. [33]. This version enables architects, urban planners, and engineers to use UWG directly in their designing platform. Additionally, the Python file is open-source, meaning anyone can generate results quickly by knowing specific parameters and having an EnergyPlus weather (.epw) file [34].

2.3. Urban Weather Generator

UWG, created by Bueno [23], is an urban design tool with UHI considerations into thermal comfort and energy [35]. The UWG requires two main inputs: the .epw file and an Extensible Markup Language (.xml) file containing the urban and rural properties. [35]. The outputs of the UWG are hourly urban air temperature and humidity values (part of the urban EnergyPlus weather file) morphed from the reference weather data measured outside the city. When coupled to energy simulation tools better results can be obtained compared to conventional methods. The tool uses a building energy model (BEM) that relies on the Town Energy Balance (TEB) scheme [36, p. 433] and EBM which controls volumes between urban canopy and boundary layers. The volume control and information exchange happen between the four UWG composing modules. The Rural Station Model (RSM) calculates heat fluxes at the weather station, the Vertical Diffusion model (VDM) controls air temperature profiles, the Urban Boundary Layer (UBL) manages temperatures above the urban canopy, and the Urban Canopy and Building Energy Model UC-BEM analyzes heat fluxes and provides air temperature and humidity values for the urban canopy. [23] How the information is exchanged can be seen in Figure 2.

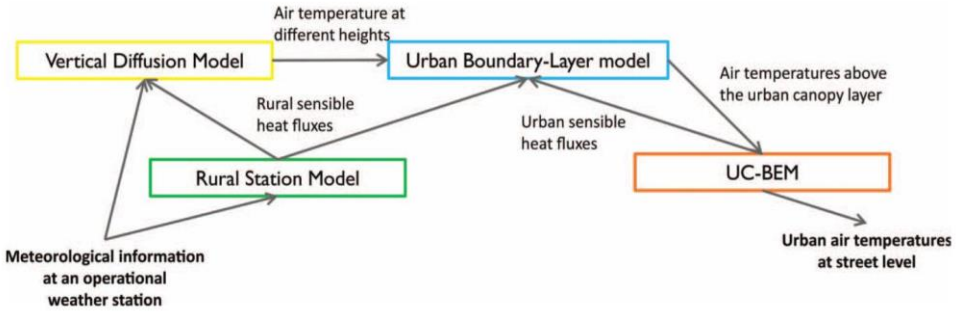

Figure 2 Information exchanged between the four modules of the UWG [23]

2.3.1. UWG case studies

The Urban Weather Generator (UWG) has been utilized in various cities across the globe, each with its unique climate. The engine capability has been assessed in nine cities: Toulouse (France) and Basel (Switzerland), Singapore, Boston (USA), Rome (Italy) and Barcelona (Spain), Mendoza (Argentina), Campinas (Brazil), and Abu Dhabi (United Arab Emirates) [37]. Moreover, the engine is also evaluated for a fictional urban area [32].

The two European cities, Toulouse, France (city diameter 7500 m) and Basel, Switzerland (city diameter 5000 m), were the first to be used as case studies for the UWG evaluation. The simulated urban air temperatures have been compared to previous studies as BUBBLE in Basel [38] for the summer period (10 June - 10 July) and CAPITOUL in Toulouse [39] for July, October, and January. For Basel, the Root Mean Square Error (RMSE) resulted in 0.9°C, while for Toulouse, it was 0.7°C - 1.1°C. For these two cities, key parameters were the morphological characteristics such as building footprint and the façade to site ratio; for Basel, vegetation is also an essential factor. As it concerns the engine performance, from the first study, it was stated to work better for homogenous cities with scarce vegetation, and the rural site should be far from the urban mountains, and large water bodies' influence. [23]

The case study of Singapore has evaluated a new version of UWG, examining various land uses, building types, and morphology parameters for multiple neighborhoods in a new tropical climate. The data was compared to eight HOBO sensor air temperature measuring devices data placed in different urban configurations for February and July, also by differentiating between day and nighttime. It has shown that the UWG can be used in different climates and urban configurations, and the choice of the rural site does not have a great impact, except for the temperature difference. [40, p. 51]

Salvati et al. analyzed two Mediterranean cities, Barcelona (Raval) and Rome (Boncompagni and Arenula). The simulated values were compared with measured in place and airport data. Their average RMSE comparing simulated and measured data was between 0.5°C and 1.5°C and complied with previous studies. They stated that the UWG's behavior also depends on the urban site's location and characteristics. [41]

The fictional urban area (250 m x 250 m) case study examined the impact of the city's morphology on UHI. They used Local Climate Zone, specifically LCZ1 protocol to divide the blocks (high density of buildings, high-rise structures, and increased human activity). The model was created using parametric modeling and optimization techniques in Rhino and performing simulation in Grasshopper without vegetation. They concluded that increasing the building height minimizes the UHI. [32]

Carmes case study 2024, a high building density area, showed a RMSE value of 1.73°C. In contrast to previous studies, this study stated that selecting an appropriate rural site is important for error results. [37]

2.3.2. UWG parameters

To create and run the UWG model, urban planners, architects, and others need to input 50 parameters, which may not always be available. [42]. These parameters are organized in the .xml file in different scale categories:

1. Reference site: describing the case study's position and radius.
2. Urban Area: urban morphology parameters, vegetation ratio, sensible anthropogenic heat, etc.
3. Buildings: building usage, the average floor height, façade parameters, glazing ratio, etc.
4. Elements: albedo values, thickness regarding (road, roof, wall) urban and for rural station. [41]

It was challenging to use the engine widely due to its 50 parameters. For this reason, Nakano, in her master's thesis, performed a sensitivity analysis to reduce the number of parameters and simplify the user interface. The sensitivity analysis aimed to test the significance of important parameters for urban planners and ensure that hard-to-find parameters did not influence the results. The metrics were thermal and energy, where each parameter is changed at a time and compared to a base situation. The parameters in Nakano's work are grouped as shown in Figure 3. [42]

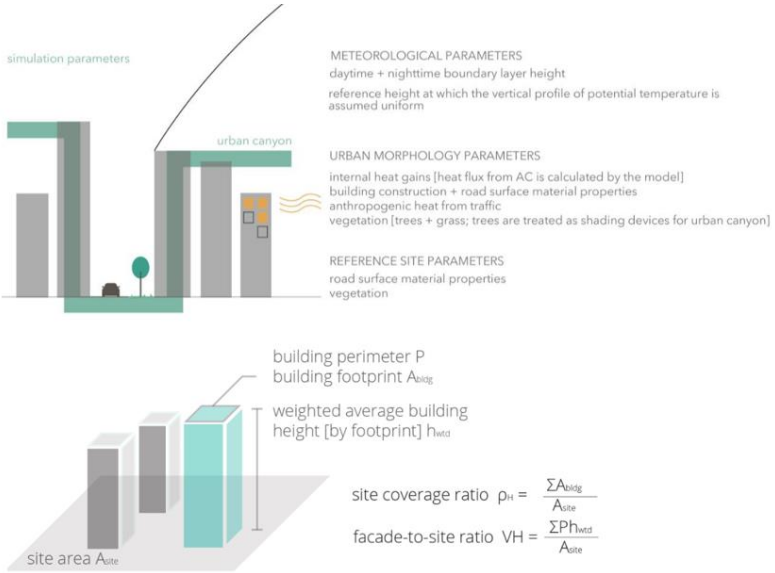

Figure 3 UWG inputs from the urban and reference site environments [42]

Nakano analyzed the Boston Financial District, MA, and Punggol, Singapore; she also compared her findings with previous case studies in Toulouse and Basel [23] to see if the parameters are important in all climates. As a result, the three main key parameters were site coverage ratio (footprint density), façade-to-site ratio, and sensible anthropogenic heat. There are also other parameters, such as albedo roof material or vegetation, which are essential for some cities. The input parameters were reduced by 46 %, and the rest were placed as default values. [42]

Hamdi et al. did a Morris sensitivity analysis distinguishing the parameters of having a negligible, linear/additive, or nonlinear effect on the output. The albedo, grass cover, and daytime boundary did not affect the output, while tree cover, footprint density, average building height, and façade site ratio have a linear influence. [37] Moreover, Salvati et al. reported that morphology parameters are relevant for energy calculation [41].

The user interface of Grasshopper also gives a report with the mentioned parameters. We will discuss them and many other inputs in the case study chapter.

The radius as a parameter

Many studies do not explain or give importance to the area that needs to be analyzed to observe the effect of UHI and obtain better results by using the UWG. Moreover, the radius/area studied also influences the calculation for all the other parameters [30]. Nakano states that the city size is not a key input in Boston and Punggol [42]. On the other hand, Street, throughout his thesis, case study Cambridge, MA, uses a radius of 500 m, suggesting that it generally gives correct values. He elaborates more on the effect of radius variation by using the UWG and considering the EUI. Street suggests altering the area depending on the site's morphology and the surroundings' influence. [30] Salvati et al. analyzed a portion of a circle area with a radius value of 500 m for Barcelona (Raval) and Rome (Boncompagni), while for Arenula, a whole circle area with a 500 m radius. Raval and Arenula's results were appropriate, but not for Boncompagni, since a nearby park that, in reality, affects the local climate was outside the 500 m radius. They suggested that the site’s selection should consider the dominant winds. [41] Bueno et al., in the Singapore case study, considered different boundaries of the neighborhoods without specifying any reason [40]. Due to varying boundaries in different studies and the reasons outlined in the introduction, we will focus on the radius parameter.

2.3.3. Known limitations

Previous studies have shown not only the capabilities of the UWG but also its well-known limitations. One of the main limitations is related to the fact that it only modifies DBT and relative humidity; on the other hand, all the simplifications do not allow it to analyze very site-specific microclimates, especially in heterogeneous urban areas [35]. Moreover, the engine performs better in areas of low winds [41] and does not compute local winds [42]. Another limitation regarding vegetation, particularly the trees, is due to the shade-convention approach that neglects the impact the trees have on longwave radiation [23].

3. Methodology

This chapter presents the methodology used to create the model and obtain results. We will highlight the software used and provide authoritative websites that we referred to.

3.1. Outline of the methodology

An outline of the whole methodology is illustrated in Figure 4. The explanation of each step follows:

To run the engine, the two main inputs, the .xml file, and the .epw file were needed. The .xml file consisted of the model created in Rhino and modified in Grasshopper. A certain radius corresponds to specific values of average building height, footprint density, and other parameters. On the other hand, the .epw file was related to the Munich Airport's location, and additional climate data to enhance the .epw file were retrieved from the Deutscher Wetterdiesnt [43].

After running the engine with our two main inputs, we were interested in retrieving the hourly simulated data for DBT. These take into account the UHI effect.

Our objective was to analyze the engine performance at various radii. To achieve this, we compared the measured data obtained from air temperature measuring devices (refer to Figure 4). Moreover, a comparison was made with the airport DBT to examine the engine's behavior and the data's transformation. Various statistical analyses were performed to do the comparison.

The methodology involved performing the same procedure multiple times using varying radii, starting from the smallest one, 10 m, and progressing up to 1500 m. For each radius, we obtained the result of a linear regression analysis (R^2), Mean Absolute Error (MAE), Mean Bias Error (MBE), and RMSE, followed by the Spearman’s correlation analysis. The errors were related to the measured in-place data and the airport ones. After conducting the statistical analysis, we compared the errors corresponding to different radii to identify any maximum or minimum errors or patterns resulting from changes in radius.

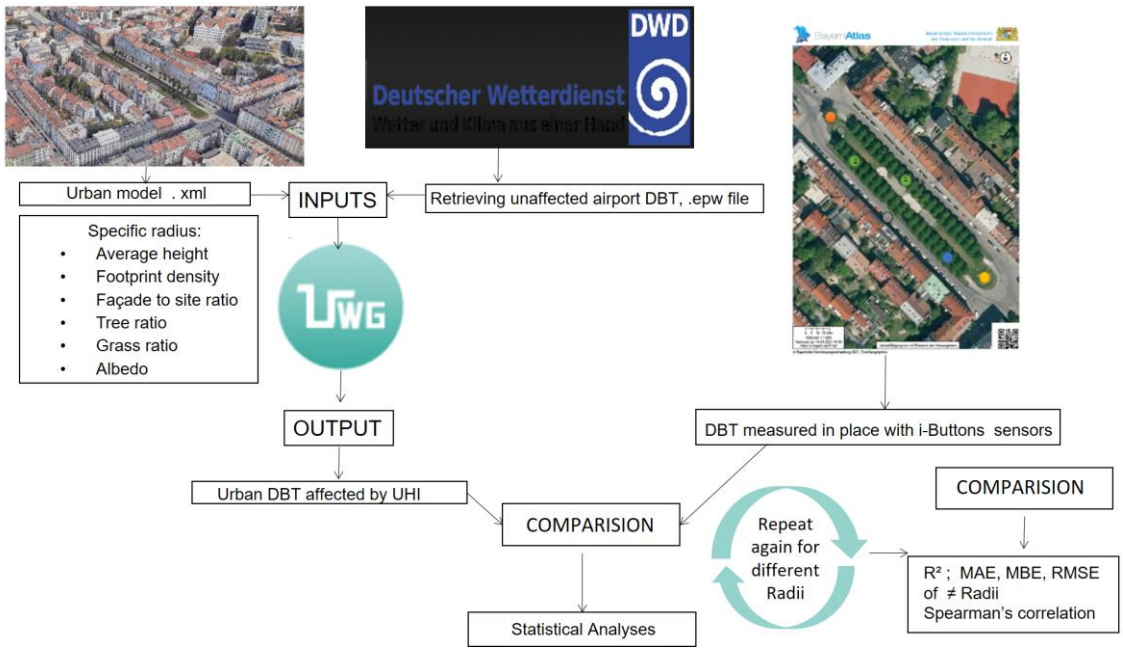

Figure 4 Methodology scheme

Our research methodology involved a detailed analysis of different period spans. Specifically, we performed annual simulations with 8760 DBT values. These datasets enabled us to see how the engine behaves considering all year. Additionally, we ran the engine for December and July, representing winter and summer. Each of these sets consisted of an output of 744 simulated values. This way, we could observe if the engine behaves differently for different seasons. The study by Salvati et al. also distinguished the period of analysis [41]. It must be mentioned that they use monthly averages of diurnal cycles, while we looked at the whole data sets of hourly simulations for each period. Another aspect is that in the methodology of this thesis, we differentiated between the time spans of a day, considering whole day hours, day hours from 10 AM to 3 PM, and night hours from 11 PM to 4 PM. This particular consideration is made because there are variations of the effect of the UHI, which is observed to be more intense during nighttime in various cases [44].

In addition, the temperature measuring devices, whose data we used to compare with our simulated data, were situated in various locations, such as under building shades, in full sun exposure, under tree shade, and so on. For this reason, we also have run the simulation considering their locations. More information will follow in the “Case Study” chapter.

Figure 5 illustrates the division of the period and time span and presents the different conditions.

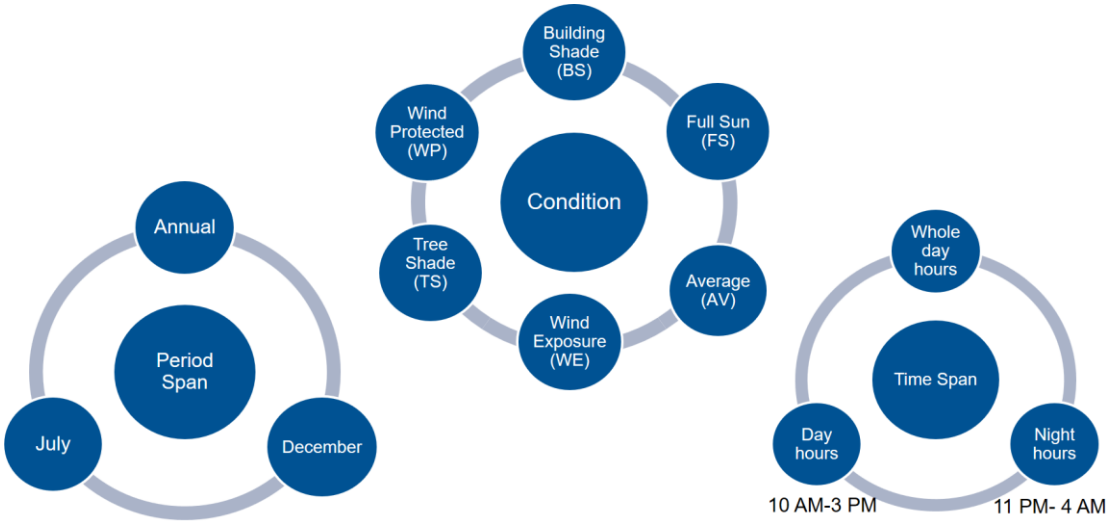

Figure 5 Period spans, time spans and different conditions used in the study

3.2. Software and tools

We used different software, tools, and websites to follow the methodology explained in the previous section, as shown in Figure 6.

To begin with, we needed to create an urban model. After considering many approaches we will cover in the following sections, the most feasible one was using Citygml (.gml) files. These files were provided from Bayern Atlas, open-source data, where 3D building models of Level of Detail 2 (LoD2) are available between many files and formats for the state of Bavaria [45]. The model was imported in Rhinoceros 3D software version 7, where modifications (such as closing poly surfaces and creating Non-Uniform Rational B-Splines (NURBS)) needed to be made to link the model with the Grasshopper and for the engine to run. The UWG is now also a tool inside the DF plug-in of Grasshopper. For this reason, we created the DF model, inserted the needed properties of the urban model, and ran the UWG engine, as shown in Figure 6. From our Grasshopper model script, we made it possible to obtain the data, specifically DBT data, in an Excel file. After, the data was compared with the measured and the airport values with a Python script. Moreover, specifically for the RMSE values and radius, we performed the Spearman's correlation by using R studio.

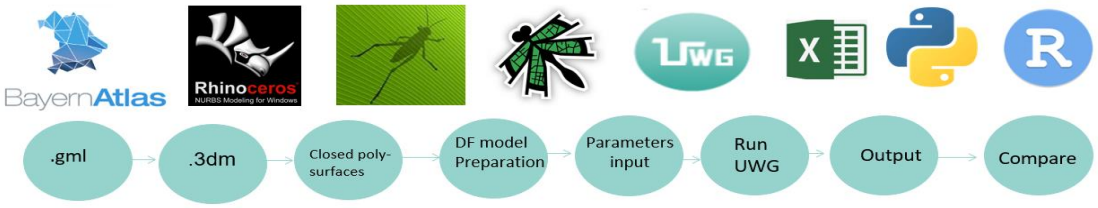

Figure 6 Software and tools used in the study

3.3. Rhino 3D models

In this chapter, we will look at the approaches we studied to create and have our case study's model (buildings and terrain) in the Rhino software. To create the model in Rhino, we explored various methods, including OpenStreetMap (OSM), CADDMAPPER, shape files, and .gml files.

To import a model into Rhino, one can use plugins or perform a file conversion from one format to a supported format. During the process of converting and utilizing various software programs, data can be lost. The loss of information during data exchange is an underlying subject in the architecture, engineering, and construction industry, and we experienced it in our steps, too. Moreover, Chelyshkov et al. state that the increasing use of information modeling technologies throughout building lifecycles and structures highlights the need for efficient digital data exchange tools in information systems, notably to support urban planning activities [46, p. 1]. Adding to the previous argument, the planning and construction of the built environment involve many stakeholders and tools, passing models from one professional to another. This process needs to look into interoperability, which refers to transferring information between software products developed by different companies without any loss or corruption. [47] Considering the great interest in this topic, we present the approaches we followed to create our model below. We will go through the advantages and disadvantages of each of them.

3.3.1. Model from CADMAPPER

The fastest and easiest way to import urban models in Rhino is by using CADMAPPER's website. It offers maps for all locations worldwide, including buildings, surrounding information, and topography. CADMAPPER's website offers free maps up to 1 km^2, as shown in Figure 7. The maps of this website can be used in many software, such as AutoCAD, ArchiCAD, and, most importantly, Rhino. [48]

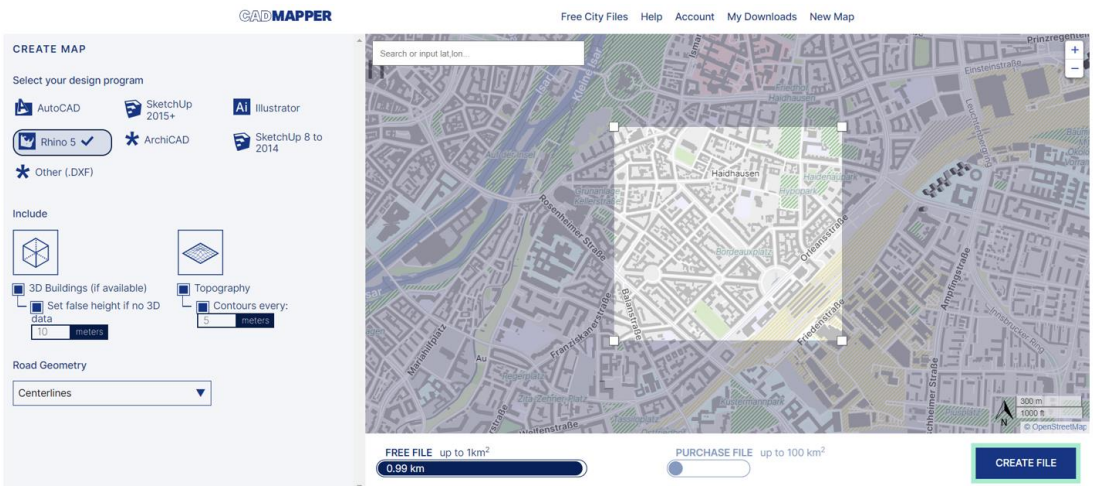

Figure 7 CADMAPPER website [48]

The model in Rhino had many urban features as buildings in closed extrusion format and the terrain as curves, shown in Figure 8. However, most buildings lacked a 3D version in the map (height is assumed while creating the model from CADMAPPER to a .3dm supported in Rhino). This approach is unsuitable for our case; we suggest using it only when 3D versions of buildings exist for the location of interest.

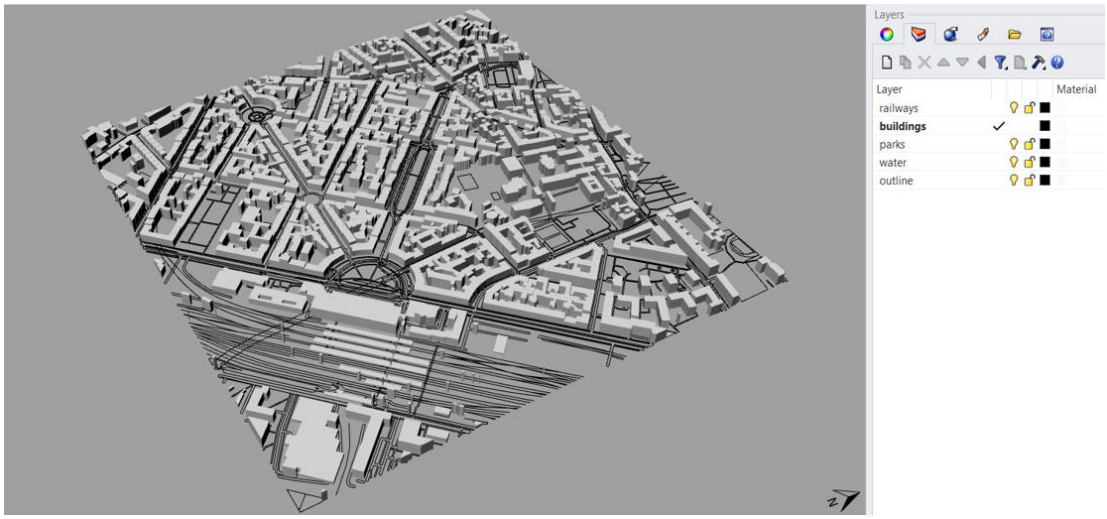

Figure 8 3D view of the model created with CADMAPPER

3.3.2. Elk plugin and Open Street Map

Elk is a set of tools inserted as a plugin in Rhino to create maps and topographical surfaces using USGS and OpenStreetMap.org [49]. The obtained result from this method can be seen in Figure 9; no 3D element was created since OSM has no data points related to the height for our location.

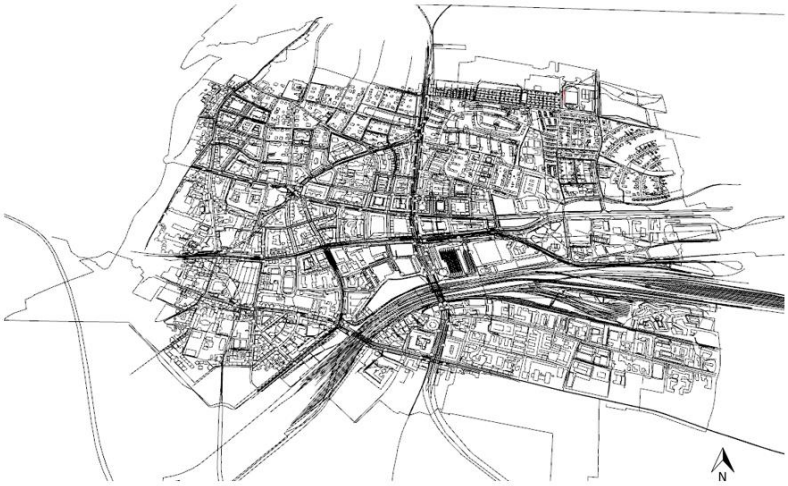

Figure 9 Model created with Elk and OSM

3.3.3. CityGML to Stereolithography

Rhino cannot directly support a .gml file. For this reason, we converted the file into a format that can be opened in Rhino. Rhino 7 can open file formats such as Rhino 3D model .3dm, AutoCad drawings (.dwg), OBJ Wavefront (.obj), Stereolithography (.stl), and many more [50]. The key is to find the most accessible tool to convert in the correct format. We used the FZK Viewer tool [51] to convert the .gml file to a .stl file. The .stl export resulted in an unusable model for the DF and UWG engine, as many buildings became open and unrepairable meshes. Figure 10 shows the model.

Figure 10 3D view of the model from the .stl file

3.3.4. CityGML and AntFarm plug in

Using the AntFarm plugin in Rhino 3D was the most beneficial approach for our case. AntFarm is a plugin for Rhino 3D that allows users to pair Rhino objects with data types using a user-friendly interface and command line operations with available tutorials [52]. This plugin can support .shp, .gml, .tif (geoTIFF), and .osm [52]. We combined four 2 km x 2 km .gml files using AntFarm. These files contained LoD2 data, including building geometry, height, function, and other properties [53]. These characteristics are needed to create the DF model. Figure 11 shows the buildings' functions, available with codes and different colors. We used an external code list related to the .gml files to translate the code into a function. For example, 31001_1100 stands for mixed-use residential buildings, but some buildings have undefined functions [54]. To identify all the buildings' functions, we did a site analysis and used Google Earth Pro.

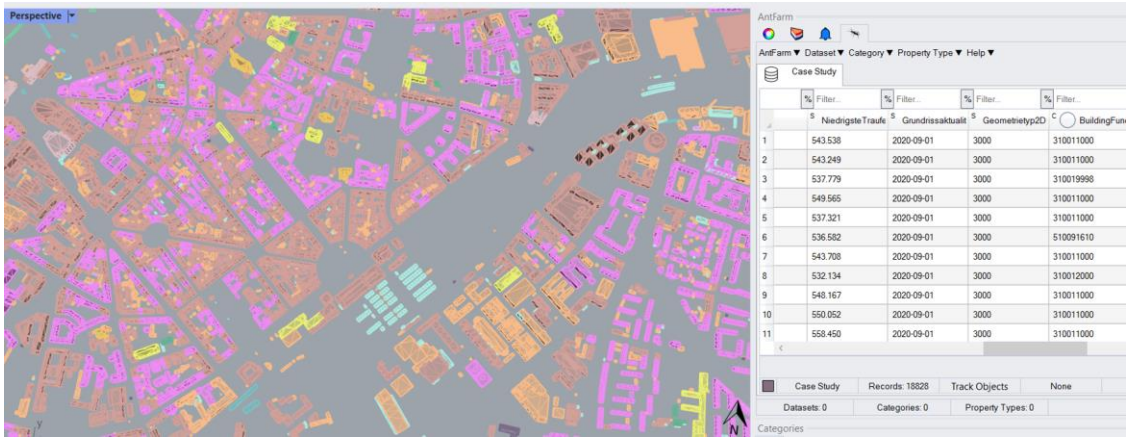

Figure 11 3D view of the model after using AntFarm

When using the AntFarm, the buildings will come as open meshes. To make them closed poly surfaces, we exploded the blocks, joined them, unified the normal, and turned them from meshes to closed surfaces, but some meshes were non-manifold, so they could not be modified. [55] We used Grasshopper functions to extrude and recreate these buildings and proceeded with the project's next steps using this model.

3.3.5. Other methods

There are also other approaches for data exchange and reaching interoperability. Using Urbano and OSM files (if all the information is available for the case study) with Urbano, 3D site models that include terrain, buildings, and streets can be generated [56]. Another

method includes Python scripts used for data conversion from .gml files to .obj files created at the Technical University of Munich (TUM) [57] based on the previous work of the Technical University of Delft (TU Delft) [58].

3.4. Grasshopper model

To use the UWG, we need to prepare the model with Grasshopper's DF tools. In this section, we will present some main tools with a simplified scheme for creating the Grasshopper Model.

3.4.1. Dragonfly model

DF makes it possible to create models of buildings and areas up to urban districts. Except for analyzing UHI with the UWG, it also analyzes the district thermal systems, optimizes photovoltaics usage, etc. The plugin is a conglomeration of many other tools categorized into create, visualize, serialize, energy, and alternative weather. [59]

To create the DF model, we connected Rhino's buildings to Grasshopper using Boundary Representation (Brep) components, where one Brep component groups buildings of the same function. Each Brep was connected to a separate "DF Building from Solid," where we assigned different parameters for all the buildings [60]. In the urban model, we also have other elements, such as canopies, generators, etc., which are considered as context shade. We used the "DF Context Shade" tool, which not only considers geometry as objects, but once the "uwg_is_veg_" parameter is set as true, it will also represent the tree canopy in the UWG simulations [61]. We now have buildings with assigned properties and other objects as context shades, so we can create our DF model using the "DF model" tool [62].

3.4.2. Urban Weather Generator model

To run the UWG engine, we need to create the UWG model with tools that are part of the "Alternative Weather" of DF. The "Assign Model UWG Properties" tool uses the DF model we created as a base. Moreover, we assigned the information for the terrain, sensible anthropogenic heat, and the vegetation cover. [63] Another essential component is the "UWG Simulation Parameter," which connects to the run period and accounts for the rural/airport station properties related to the input .epw file [64]. Both components behave as a base for the "Run Urban Weather Generator," which morphs the rural epw

considering all the urban information inserted and gives an urban .epw file, JavaScript Object Notation (.json), and a report as output. [65].

Figure 12 shows a simplified scheme of the main tools regarding the DF model and UWG model. It is worth mentioning that we have utilized several other tools and steps to develop the model and execute the engine. However, we will delve deeper into these methods in the "Case study" chapter, where we will introduce and integrate the unique features of our location into these tools.

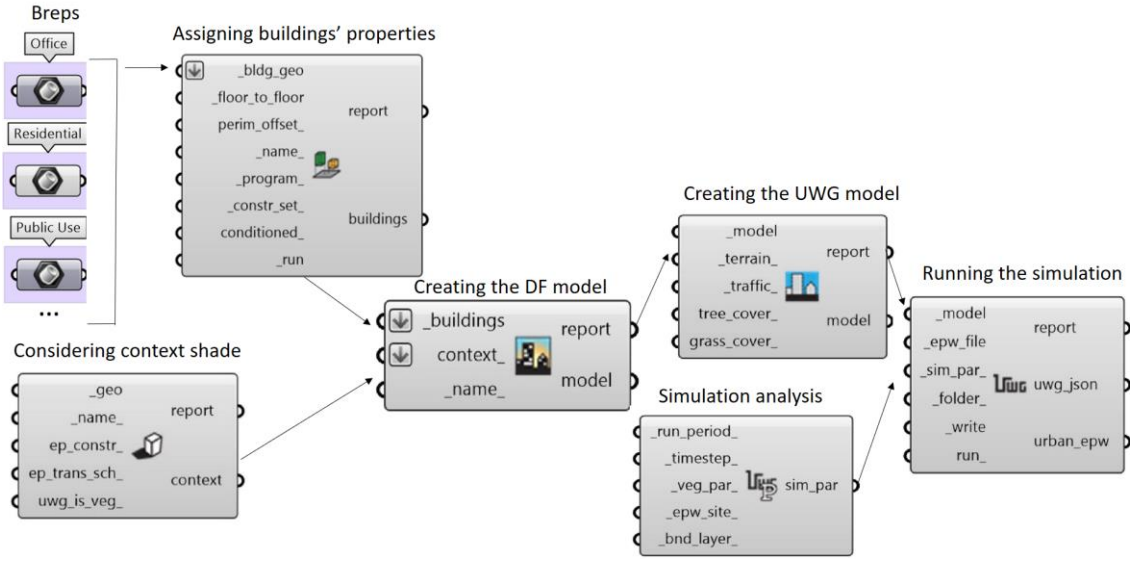

Figure 12 Simplified scheme with DF and UWG tools based on [59]

3.5. Test with varying parameters

When Grasshopper script was prepared, we ran some tests with a small model. We first had some initial conditions; afterward, all the other variations were compared to the initial one. The variations were created by changing one parameter while keeping the other parameters constant. The period of the simulation was the month of July. The parameters that we considered and varied were the average buildings' height (h), footprint density (d), tree cover ratio (t), grass cover ratio (g), and albedo of the terrain (a), as can be seen in Table 1.

Table 1 Variations of each parameter for the test

Initial Condition	h = 20 m; d=0.27; t=0; g=0.02
Variation in average buildings‘ height	h = 5 m; h=10m; h = 30 m
Variation in footprint density	d = 0.02; d = 0.46; d = 0.65
Variation in tree cover	t = 0.3; t = 0.5; t =0.9
Variation in grass cover	g = 0.3; g = 0.5; g = 0.9
Variation in albedo of the terrain	a = 0.1; a =0.3

We conducted 14 test simulations and looked into all the hours of the month to see if there was a change or a pattern in it. What was concluded for them were two main points discussed in previous sections.

- There was no pattern, while tree or grass cover was at a maximum or minimum ratio, likely due to the mentioned limitation of the vegetation.
- At 0.65 footprint density, an average hourly temperature increase of 0.2 ºC was observed, showing the strong influence of the parameter, as in previous studies.

Since the test model was small, we manually calculated grass and tree cover ratios. We compared them to the automatic ones to see if the way we had chosen to create and interpret them was correct. It proved to be correct.

3.6. Statistical analyses

This section focuses on the statistical analysis many studies have followed to compare weather or more specific temperature data.

A method used to compare weather data sets is the Finkelstein-Schafer statistic (FS statistic) [66]. It assesses the likeness between two distributions where a high value implies dissimilarity. Equation (1) is composed of the cumulative distribution function

(CDF) of a particular weather parameter (x) and n total number of values (data points) in a CDF. The FS statistic resulted useful for comparing weather data sets in Cyprus. [67, p. 289] Another version of the equation is used to generate epw files, as was done for the meteorological year in different climates of Turkey [68, p. 144] and Hong Kong, considering hourly data of 25 years [69, p. 87].

$$FS_x = \frac{\sum |CDF_{x,data\ set\ 1} - CDF_{x,data\ set\ 2}|}{n} \quad (1)\ [66]$$

A study focused on comparing air temperature measured in a vineyard canopy and at a standard weather station in France used linear regression analysis to compare the daily maximum and minimum temperatures with result the R-squared (the coefficient of determination) [70]. Le Bras and Masson found the coefficient of determination as well. They compared temperature data occurring at 3 AM for a year (distinguished seasonally) between the results of the Spatial UWG simulations for Paris and an existing atmospheric model. They used two other statistical methods, the RMSE and MBE. [71]

Simple linear regression predicts values $\hat{y}_i$ based on known values y_i and relationships [72]. While having both data sets, such as our case we can use linear regression, R^2 value to analyze how comparable the data are and their fitting.

RMSE is a method that removes the sign and gives the average value of the error. [41] It accounts for variability and biased error. The equation follows, where ŷi and yi are the simulated and the actual value for the i-th observation while n is the sample quantity.

$$RMSE = \sqrt{\frac{\sum_{i=1}^{n} (\hat{y}_i - y_i)^2}{n}} \quad (2)\ [73]$$

MBE is a method where the error sign is not erased to show if the data are under or overestimated compared to the actual values [41]**.**

$$MBE = \frac{\sum_{i=1}^{n} (\hat{y}_i - y_i)}{n} \quad (3)\ [74]$$

The RMSE and MBE methods were used in Basel and Toulouse, where a season differentiation was also done [23]. Salvati et al. did the same by comparing the monthly average diurnal cycle of simulated urban air temperature (for summer and winter months) with two stations, one of which was an airport [41]. Street assessed his outcomes using (RMSE and MBE), focusing on different periods [30].

In our work based on the previous studies, we will consider these main statistical methods as mentioned in previous chapters: R^2, RMSE, MBE, and as well to support them,

MAE, which is the mean of absolute differences. Moreover, we also wanted to analyze the correlation between the RMSE and radius, so we looked into Pearson's correlation (linear relationships) [75] but after observing the behavior of our data and having a short consultation with the statistical consulting TUM|Stat [76], it was decided to proceed with Spearman's correlation (non-linear relationships) [75].

4. Case study

In this chapter, we will analyze the case study's details, its location, and all the parameters and characteristics that define it. We will be examining these aspects closely and translating them into inputs for running the engine. By understanding the nuances of the case study, we can create a more accurate and reliable simulation that reflects real-world conditions.

4.1. Location

The center of our case study is Bordeauxplatz in Munich. Figure 13 illustrates the location with an example area with a certain radius. As mentioned earlier, we will be increasing the radius and expanding beyond the boundaries of Bordeauxplatz. Munich (area 310.7 km^2), home to more than 1.5 million inhabitants [77], is the capital of Bavaria, located in the southeast of Germany and is in proximity to the Alps. The city has a humid continental climate with warm summers and no dry season. Before, the temperature range for the year was from -4°C to +24°C, according to the German weather services [78, pp. 4692-4693]. The average temperature for the period between 1991 and 2020 was recorded to be 10.1°C [79], while in 2022 was 11.3 ºC with 20 hot days (maximum 30°C or higher) and the sub-zero days were 7. The precipitation of 2022 was 598 mm. [77]. It is expected that the average temperature and precipitation will increase, bringing also flooding and very hot summers [80].

Bordeauxplatz is part of Haidhausen, a central district, located in the eastern boundaries of the Isar River [81]. Bordeauplatz is named after the French city of Bordeaux. The square has a large park placed in its center with an area of nearly 5700 m^2, [82] the green infrastructure is made out of trees, shrubs, and lawn/grass and together with the surrounding roads and side walks has an area of 14000 m^2 [83]. Bordeauxplatz was chosen as the starting point of our study for the following reasons:

- Central part of the city
- Near Ostbahnof (Munich East Station)
- High vegetation ratio

- Near water bodies
- Various land use
- Recreational area and various businesses

Figure 13 Location of the case study, Bordeauxplatz, Munich [84]

Figure 14 Various land use

Figure 15 Recreational area

Figure 16 Various businesses

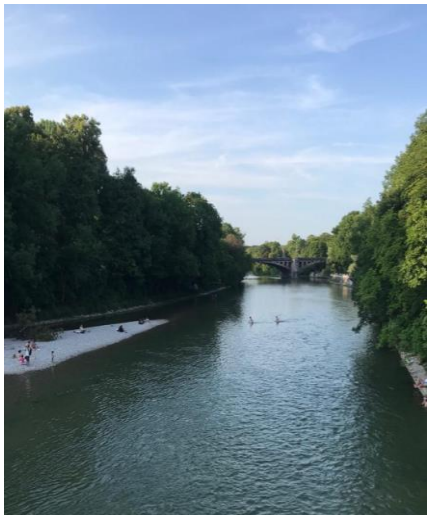

Figure 17 Isar River

The main reason was the availability of the measured DBT. In the area, we had five measuring i-Buttons devices, placed in different conditions as shown in Figure 18. These devices collected DBT and relative humidity values every 10 minutes [85]. Solar shields were used to protect the devices from wind, rain, and sun exposure [83]. i-Button devices were installed for the "Ecosystem Services of Urban Green at Public Squares in Munich" project funded by the Bavarian State Ministry of the Environment and Consumer Protection [86].

Figure 18 Top-View Bordeauxplatz, location of i-Buttons devices, P.Stark [87]

4.2. Area selection

Since we analyzed various radii, we needed the automation of the process to select a certain area. Once we changed the radius, we had to select and perform the analysis only for the buildings and elements that fell under the area depicted by the radius. For this reason, we developed the part of the script as seen in Figure 19, where the centers depend on conditions (of i-Buttons) such as tree shade, building shade, etc., and the radius selection was made by a numerical slider. This created the boundaries and the circled area (with different radii in each case) that later was used to select only buildings and elements inside the area. Moreover, the created area was used as the terrain, and connected to DF model tool.

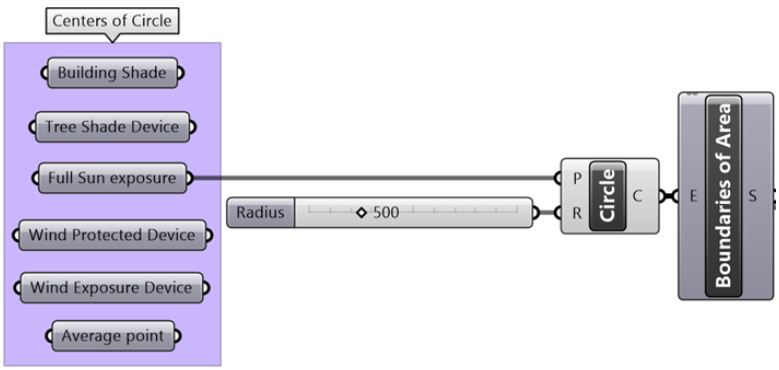

Figure 19 GH Script for area selection

Figure 20 shows a blue-colored representation of the model's part within a radius of 500 m with FS center (as an example of one of the simulations).

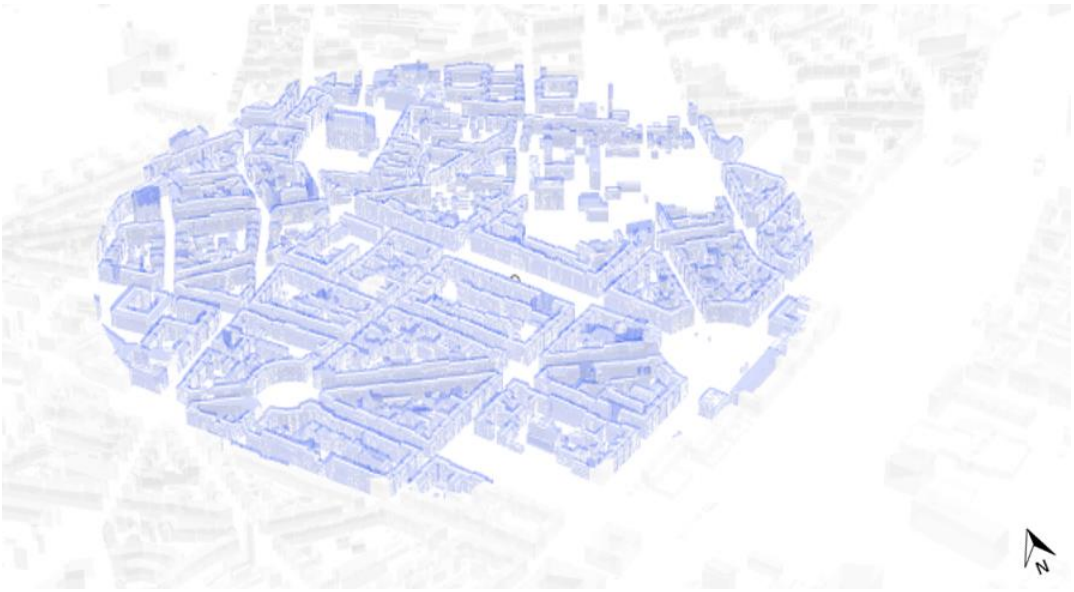

Figure 20 Area and elements selected automatically, example radius 500 m, FS

4.3. Urban model

In this step, everything is related to our case study to mirror the exact characteristics of real life in the urban model, specifically in DF and UWG tools. We would be looking into the characteristics of the buildings and terrain.

4.3.1. Buildings' properties

There are many properties that had to be assigned to the buildings for the engine to run, such as programs, floor to floor heights, construction sets, facade parameters, UWG parameters for buildings, and so on.

Buildings' programs

As we discussed before, we identified many buildings with different functions; after we grouped them in same Breps (buildings of same functions) and we assigned the available programs of the DF tools. Table 2 summarizes the assigned program for each group.

Table 2 Buildings' function and assigned available programs

Buildings' function in Rhino 3D model	Assigned programs DF model
Residential	Midrise apartment
Big hotels	Large Hotels
Church	Warehouse
District Government	Large Office
Education Research	Secondary school
Hospital	Hospital
Kinder Garden	Primary School
Police Station	Medium Office
Factory	Warehouse
Fire Department	Medium Office
Show Rooms	Retail
Public Use	Strip Mall
Office	Large Office
Garage/Warehouse	Warehouse
Canopy	Context shade
Weir	Context shade
Generator	Context shade

Buildings' floor to floor height

The .gml files we used to create our model had no information regarding floor to floor heights. To find this height for the residential buildings, we considered various reasons.

First, a previous study done in Kempten considers that the minimum clear height of the floors in Bavaria is 2.4 m, and in DIN EN 1520 concrete ceiling being 50 cm, the floor-to-floor height was inputted as 3 m [88]. During the site analysis, it was observed that the first floor-to-floor height of the residential buildings were higher compared to the upper floors. For these reasons, we have considered the first floor as having a 3.5 m floor-to-floor height and the other floors as 3 m. For offices, it was chosen higher than the residential buildings as 3.5 m. For the buildings that function as showrooms, factories, churches etc., we measured their full building height in Rhino and used it as floor to floor height as done previously for a church [88].

Table 3 Buildings' functions and their floor to floor heights

Buildings' function	**Floor to floor height**
Residential	1st floor 3.5 m; upper floors 3 m
Big hotels	1st floor 3.5 m; upper floors 3 m
Church	13 m
District Government	4 m
Education Research	4 m
Hospital	3.5 m
Kinder Garden	3 m
Police Station	4 m
Factory	10.4 m
Fire Department	4 m
Showrooms	13.6 m
Public Use	4 m
Office	3.5 m
Garage/Warehouse	3 m

Construction set

To ensure a detailed design, we specified the required information in the construction set. The construction set is essential to create an energy model [60]. The component "HB Construct Set by Climate" needs the following information as the Climate Zone; Vintage (construction year); and the construction type [89]. For Munich's climate zone we chose the cool climate zone, among eight other options. For the age of the buildings, we followed two paths. First by considering the map from the Geoportal Munich [90] shown in Figure 21, where we see that the buildings (of all types) mainly were built before 1980, especially for the area of Bordeauxplatz. Secondly, a representative of the Statistics Office of Munich [91] provided us with 2 data sets regarding the number of buildings build in certain periods, one for a small area around Bordeauxplatz and the other for a greater area. It was seen that the share of buildings built before 1980 was 79 % and 81% for small and big area respectively. A map and more details regarding it can be found in Appendix A, section A.1. We chose the construction year as pre-1980, considering the information from Figure 21 and the fact that even in our Rhino model, 84 % of the buildings are residential (without considering garages) making valuable the second resource from the Statistics Munich office.

Figure 21 Map of Buildings' age [90]

Regarding the construction type, between steel-framed, wood-framed, mass, and metal frame, the most appropriate type of construction to be assigned was mass-type.

Facade‘s parameter

An important parameter related to the facade is the window to wall ratio (WWR), or short window parameter. To decide about it we considered the buildings’ functions.

Referring to the residential buildings, the majority of them were multi-family houses (MFH), this was seen during the site analysis and compared to the buildings’ type in Typology Approach for Building Stock Energy Assessment (TABULA) web tool [92]. Furthermore, based on data derived from a report focused on Germany and based on TABULA [93], the average window ratio for the residential buildings MFH type was calculated as 0.24. More information on how the value was derived can be found in the Appendix A section A.1

For Germany's administrative public buildings and offices, a maximum WWR of 0.3 is suggested [94]. The suggestion was followed also in the Kempten case study [88]. We decided for public use, government buildings, fire departments and police stations to assume a window ratio of 0.25.

Special attention was given to the offices, where in site analysis, we noticed a higher WWR. Based on a previous study that found that the optimal ratio for office buildings is between 0.3 and 0.45 [95] and considering the suggestion for Germany, for office buildings it was decided to continue with the ratio of 0.3. The same ratio was assumed for the university, large hotels and other business commercial buildings.

For the kindergartens, the only information that could be found on guidance on how to build a safe environment for the children was a suggestion of having a window area of approx. 1/10 of the room floor [96, p. 42]. We selected a ratio of 0.2.

For the WWR of the hospitals, we inputted a 0.25 ratio, lining up to a previous study on hospital performance in Italy [97, p. 1152] and also with the Germany suggestion.

For the churches, in a previous study considering energy analysis in Sweden a ratio of 0.08 was chosen [98] in our case we inputted a ratio of 0.1. The ratio of 0.1 was chosen even for factories and garages since they usually have small glass areas.

The buildings for which we decided to have a WWR 0.4 were the showrooms that needs to have a visibility for their displayed items.

UWG buildings' parameters

To conduct the simulation, we were required to add other parameters falling in the category of UWG buildings' parameters.

For the SHGC of the windows, we used again the data of the greater area which were provided by the Statistics Office of Munich [91]. Having the buildings periods we matched them with the MHF types of TABULA [92] to find the corresponding U values. We considered an energy performance level 2 meaning a standard refurbishment, based on the requirements of EnEV 2009/2014/2016. Table 4 shows the number of buildings constructed in certain periods and the corresponding U values. Combining this information, we performed a weighted average for the U value, which resulted to 1.34. A double glazing, argon filled, low-E, type of glass with a U value of 1.3 W/(m^2K) was assumed, matching the SHGC value of 0.6 [99]. We applied the same assumption to buildings with other functions.

Table 4 Buildings' construction year and their U values of the glass

Construction Year	Number of residential buildings	U values (W/(m^2K))
before 1919	29469	1.6
1919 - 1949	17136	1.3
1950 - 1950	29583	1.3
1960 - 1969	23859	1.3
1070 - 1979	12736	1.3
1980 - 1989	11837	1.3
1980 - 1989	7135	1.3
2000 - 2005	3500	1.3
2006 and later	3394	0.7

Other important parameters are the albedo values of the wall and the roof. We did not have the information regarding buildings' façade material construction, but from the site

analysis, we observed facades of white, peach and creamy colors, as Figure 22 shows. As it concerns the roofs we considered a Google Earth image, Figure 23 [84], where it was observed that the main colors were orange and grey.

Figure 22 Buildings' facades

Figure 23 Buildings' roof, Bordeauxplatz [84]

To decide about the specific values for the albedos, we referred to a previous study that considered the colors of the facades and roofs. As can be seen from Figure 24, we took an average value of 0.35 for the wall albedo and 0.33 for the roof albedo.

Wall colour	Wall albedo	Roof colour	Roof albedo
white	0.30	brown	0.12
peach	0.42	Orange	0.33
creme	0.33	Grey	0.30

Figure 24 Albedo values for wall and roof [100, p. 33]

Figure 25 shows how all the buildings' properties for which we discussed above, are inserted and connected in the GH script. The example is for the residential buildings only, but we have performed the same steps and created the same script for each of the building group of different functions. Each of the group was connected to the DF tool to create the DF model as discussed before.

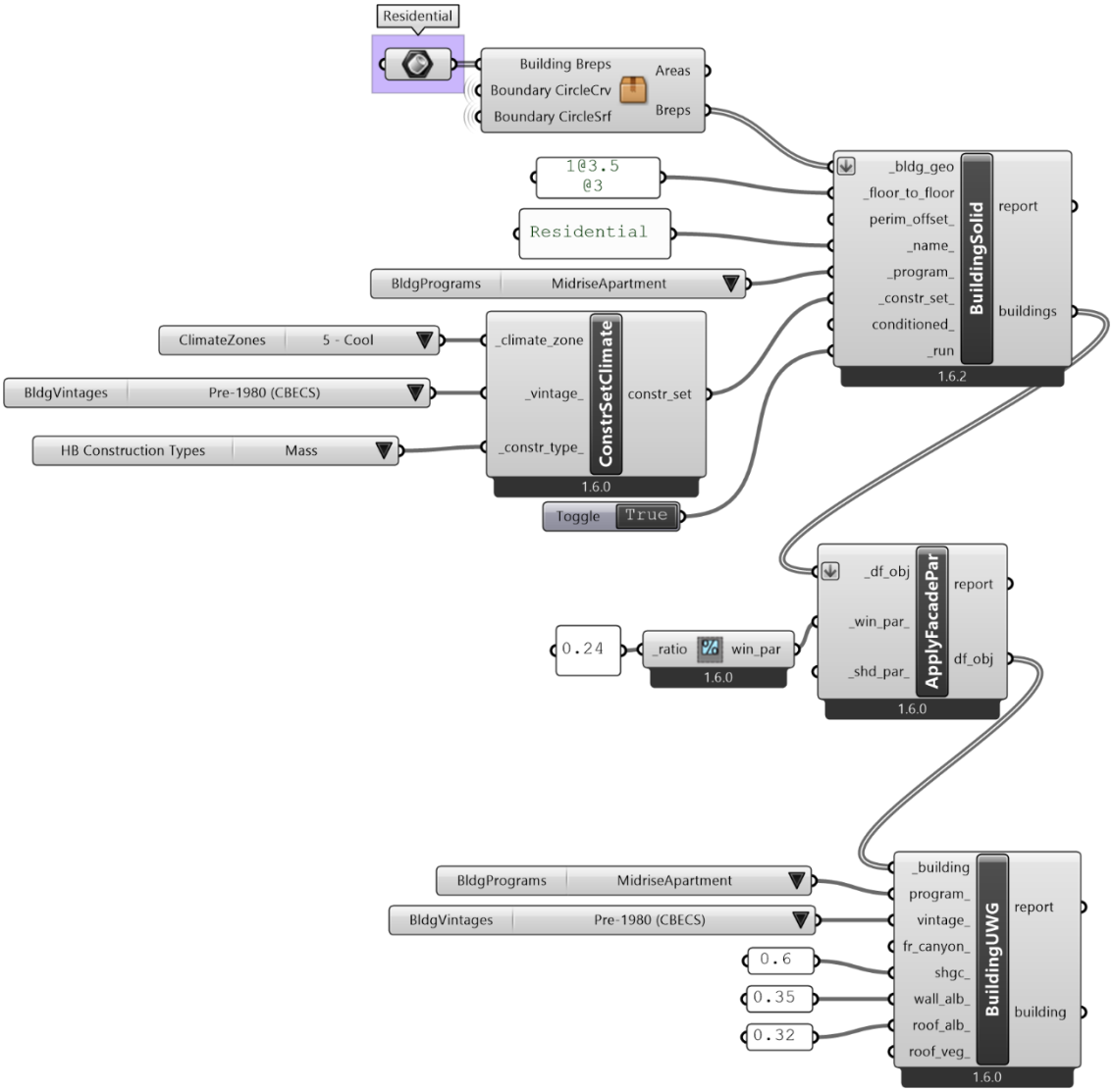

Figure 25 GH script for assigning buildings' properties, residential example

4.3.2. Creation of the terrain

Terrain is an important element during the creation of the DF model. In order to analyze it, we went on a site inspection in Bordeauxplatz. The terrain was composed of different elements such as soil, grass areas, concrete pavement, water bodies, permeable and

impermeable sampietrini, and mostly asphalt. The DF tool concerning terrain creation considers only a single type of surface [101]. Also, water bodies cannot be modeled in the DF tool [102]. After researching to confirm these characteristics, we conducted a discussion in the forum where professionals confirmed that the UWG engine does not account for water bodies or multiple street canyons [103]. To overcome this situation and adapt our model as much as possible to the real-life neighborhood, we decided to create a terrain model in Rhino composed of the elements we mentioned before. Since no data regarding the terrain was available, a Google Earth image was embedded in the model, as can be seen in Figure 26, and all the terrain elements were manually drawn in Rhino 3D as curves distinguished by different layers and different colors. The drawing was made for all centers (different conditions) up to a radius of 1500 m, as can be seen in Figure 27.

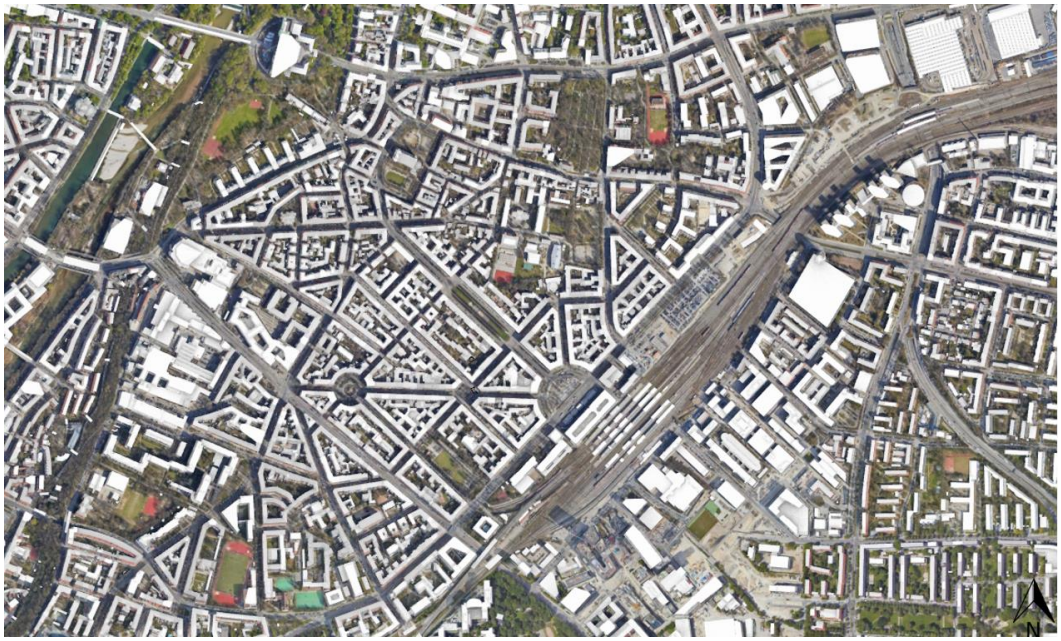

Figure 26 Part of the model and the embedded map

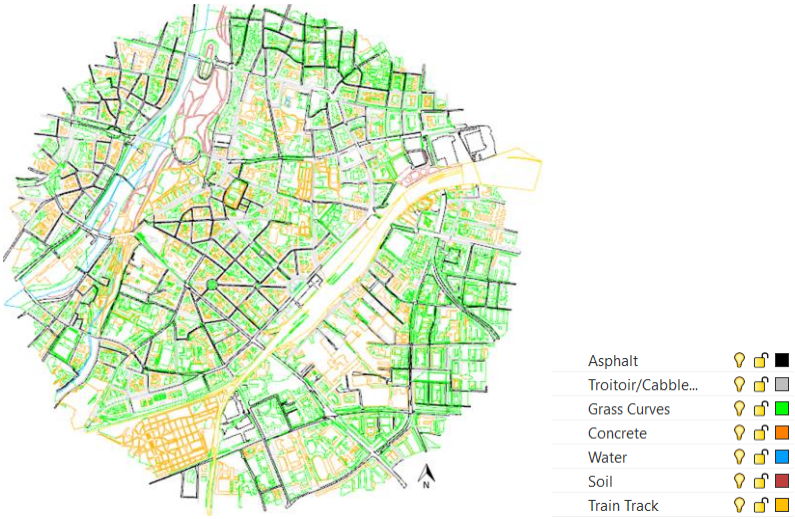

Figure 27 Terrain division

Albedo values

Importance was given primarily to the terrain's albedo value. As mentioned before, having many types of surfaces also means different values of albedos. In order to consider each surface's influence and since for different radii, the area of each surface type changes, we chose to use the weighted average. The weighted average is calculated as shown in Equation 4.

$$albedo_{average} = \frac{Area_{grass} \times albedo_{grass} + Area_{asphalt} \times alebdo_{asphalt} + Area_{concrete} \times albedo_{concrete} + \cdots}{Area_{total}}$$

(4)

Deciding on the albedo values of the different surfaces was a process that included going through many studies for each type of surface. Table 5 gives a summary of the albedo variation for each type, and the chosen values for our case study. More information can be found in the Appendix A section A.2

Table 5 Albedo values variation for different surface types

Surface type	Albedo variation	Albedo chosen	Studies
Asphalt	0.05 - 0.227	0.2	[104], [105], [106], [88], [107, p. 173]
Concrete	0.2 - 0.4	0.3	[108], [109]
Grass	0.16 - 0.27	0.2	[109], [110]

Soil	0.05 - 0.5	0.4	[111]
Sidewalks (sanpietrini + concrete)	0.4 - sanpietrini 0.3 - concrete	0.35	[106]
Water	0.03 - 0.1	0.065	[112], [113]

The weighted average value of albedo will change with the radius, the variation is small and the values are comparable to total albedos of urban areas generally varying from 0.12-0.24 [109].

Terrain thickness

Another essential parameter for the terrain is its thickness. Since we did not have information on all the terrain's components' thicknesses, we decided to go with the default value of the DF terrain tool, which was 0.5 m.

Anthropogenic heat

Anthropogenic heat refers to the heat generated by human activities within urban areas [114]. What affects the most UHI is the sensible heat [42]. The sensible anthropogenic heat refers mainly to the vehicular contribution of anthropogenic heat. Its value varies among countries and within city areas [115]. An example of its calculation comes from Poland, specifically the city of Lodz where the values varied from 12 W/m^2 in summer to 54 W/m^2 in winter [116]. There was no data available for Munich and especially our study area, we decided to consider the values suggested from the traffic component in DF, which derive from previous studies. Maximum sensible anthropogenic heat was 20 W/m2 for a downtown area, 10 W/m2 for the commercial area in Singapore, and 8 W/m^2 for mixed use in Toulouse. [117] We know that the city of Munich has a higher population density compared to Toulouse, and since increasing our radius, we also considered downtown areas; we decided to use an anthropogenic heat value of 15 W/m^2. We kept this value constant in all radii to avoid another variation. For anthropogenic heat seasonal change, we used the default program of DF.

Grass cover

Grass curves were available from terrain creation, and we converted them to surfaces when inside the radius we were simulating. The grass ratio, is related to the fraction of

grass areas to the unbuilt terrain [62], for this reason, from the whole terrain, which is the circle area with a certain radius, we deducted the footprint of the buildings to find the appropriate grass ratio. This process was automatically performed for every radius and condition we considered. Furthermore, our design was made for the summer period, when the grass areas are larger and the trees are full of leaves, but it was confirmed by the experts that the engine takes into consideration the seasonal change of the vegetation [118].

Trees implementation

In regard to trees implementation, we solely took into account their crowns, as it is the primary factor responsible for blocking the sun [119]. We first secured a model in shape file format, based on LiDAR point clouds to 3D tree models [120]. In the file, trees were represented by curves containing the crown and the trunk covering the entire city of Munich. We used the Urbano plug-in [56] to insert the curves for our whole area (considering all centers/conditions up to 1500 m radius), and to distinguish between crown and trunk. Curves where transformed into surfaces and joined in Rhino. Their union does not allow to double count the shade created by two crowns side by side [121]. We inserted them in the Grasshopper model as surfaces, and we performed an intersection to take into account only the trees inside the radius we were considering. They are inserted into the “Context Shade” component and “uwg_is_veg_” is assigned as true and this offers an automatic calculation of tree ratio, for each radii.

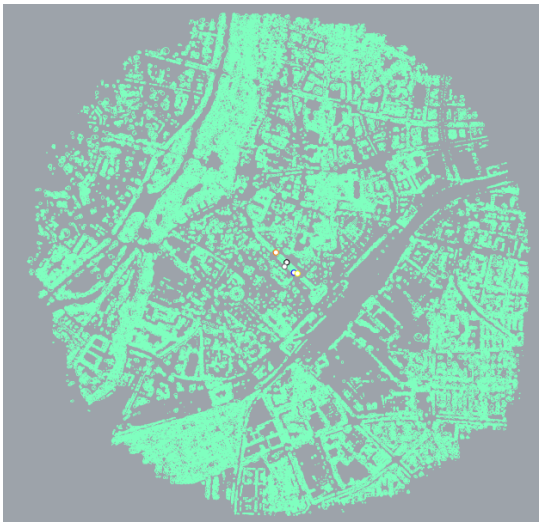

Figure 28 Tree crown curves, from shape file

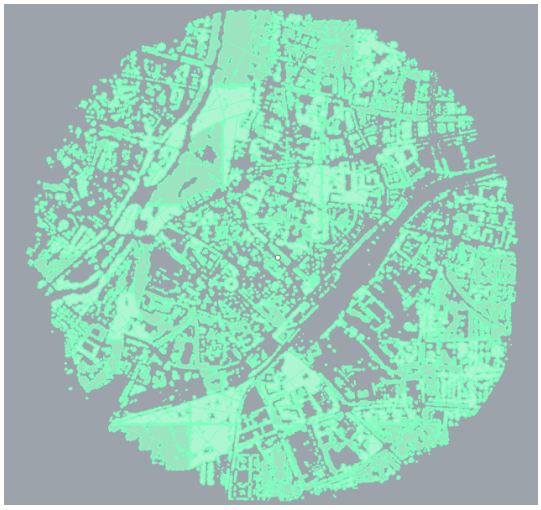

Figure 29 Union of tree crowns as surfaces

4.4. Creating the .epw file

The DF component suggests a website where .epw files for many stations can be found [122]. Upon conducting research on the suggested website, there were no available files compatible with the coordinates of Munich International Airport but only for the city itself. We were able to find .epw files related to the airport data in an open data source website Climate.OneBuilding.Org. The website offered three different compilations of .epw covering the periods 1930-2021, 2004-2008, and 2007-2021[123]. Considering that in the last decades the climate has changed severely, we decided to choose the .epw covering the period 2007-2021. An .epw file contains average data of multiple years, but we were specifically interested in the year 2022. To surpass this issue, we used the component "Create EPW" of the DF [124], as can be seen in Figure 30. Between many inputs, we insert hourly data for the whole year of 2022, for DBT, dew point temperature, wind velocity, and wind direction. We retrieved these data in excel formats from the Deutscher Wetterdienst, for Munich International Airport station under the ID: 1262 [43]. The other remaining inputs were inserted by using the base .epw which in our case is the .epw of the period 2007-2021. The base .epw provides information regarding location, radiations, sky cover, atmospheric pressure etc. Figure 30 displays all the steps for the creation of the .epw file. The created .epw file was connected to the running component of the UWG.

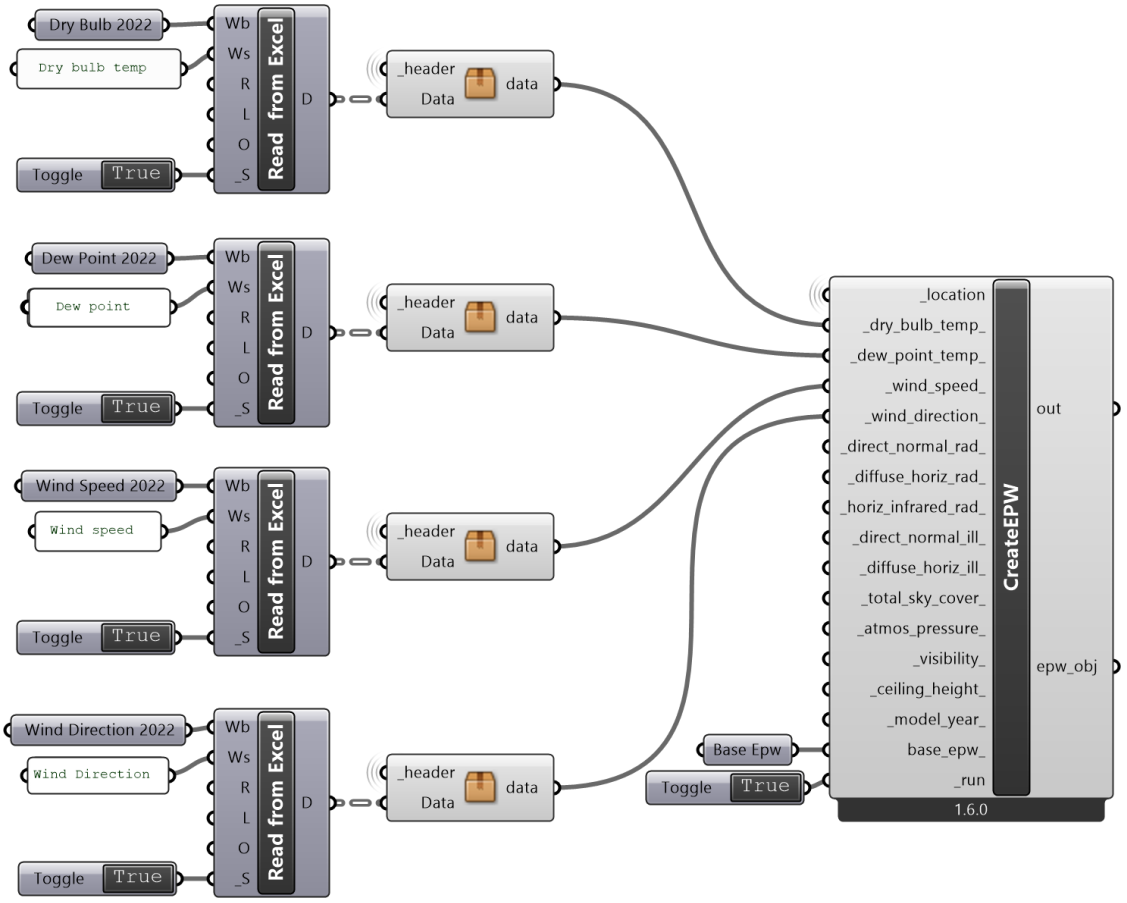

Figure 30 GH script for creating the epw file

4.5. Rural model

The .epw input belongs to a station located in a rural area or an airport. For our case study, Munich International Airport was chosen. Important for the engine to run are also the characteristics of the rural/airport station, as can be seen in the Figure 31. The information regarding the height where the temperature and wind is measured was attached to the Excel files retrieved from the Deutscher Wetterdienst [79]. The values were 2 m and 10 m respectively. To insert the other remaining features, we created the airport model in the same way the urban model was created. Referring to Figure 32, we embedded the map of the area into the model, and to find the vegetation cover, we used a circle with a 500 m radius centered at the measuring station, as previously done and suggested [41], [125]. We drew curves, and transformed them into surfaces, and found the vegetation cover to be 0.79. Furthermore, there were no buildings present within a 500 m radius to act as obstacles. Thus, we used the default value of 0.1.

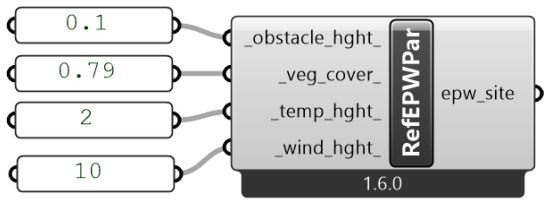

Figure 31 Properties of reference rural/airport site

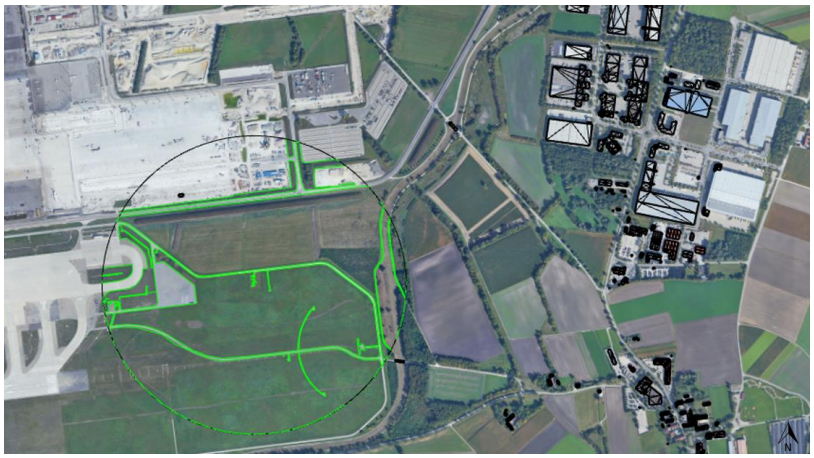

Figure 32 Airport site, model created with the vegetation curves

4.6. Running the UWG

Until this point, we have created all the components necessary to run the engine. The UWG model connects directly to the “UWG Run” component. Meanwhile, we have the .epw file and simulation parameters which includes the airport model (RefEPWparameter) and the analysis period. The analysis period was adjusted to align with annual, July, and December simulation. A detailed scheme of all the connections and values of our urban model can be seen in Figure 33.

The simulations were performed for areas with different centers, matching with the conditions where the i-Button devices were placed.

After running the engine, two primary outputs are generated: the uwg_json and urban_epw files. The simulatable .json file follows the UWG schema and has all the properties of the designed model. While the urban morphed .epw file contains the UHI effect in the urban areas. [65] The .json file can be opened and interpreted easily in other programs as well. As it concerns the urban .epw file we were interested at the DBT values, for this reason we retrieved the data by the help of “Write to Excel” component

of the TTTtoolbox, plug-in [126]. Having the data in Excel eased the process of comparison between simulated DBT values with the measured and airport data, which also were in Excel files. We performed the comparison with a Python Script, which made a differentiation between night and day values as well, and accounts for all the statistical analysis we mentioned before. The results of these comparisons can be found on the next chapter.

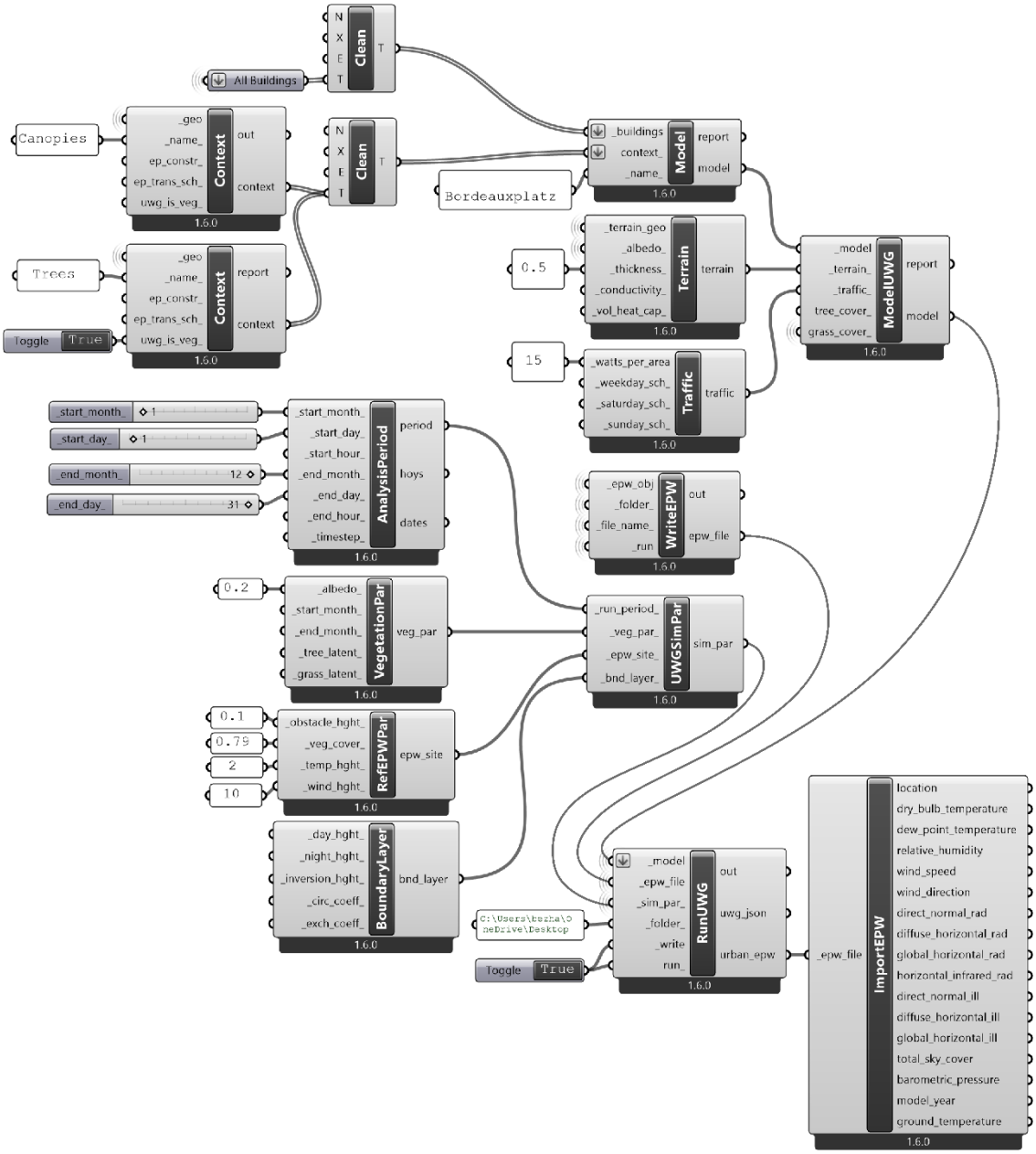

Figure 33 GH script to run the UWG

5. Results and discussion

In the upcoming chapter, we will be sharing the outcomes of the simulations carried out in different conditions, periods, and time spans. We will display the comparisons between the simulated DBT and the actual measurements, along with the airport values. These comparisons will help us identify any patterns and examine the impact of decreasing or increasing the radius.

Additionally, we will be examining different conditions as FS, BS, AV, WE, WP, and TS, allowing us to compare different cases. Thus, we will not only be analyzing the influence of the radius but also conduct intercomparisons. These intercomparisons are distinguished as follows:

1. Same condition and same period span
    - Radius influence – How does the radius influence the statistical results?
    - Time spans – Is there any time span for which the values are better estimated?
2. Same condition but different period spans
    - Annual FS vs December FS vs July FS – Under the FS condition which period span is better estimated?
    - Annual BS vs December BS vs July BS – Under the BS conditions which period span is better estimated?
3. Different conditions but same period span
    - July BS vs July FS vs July AV – Which condition shows better estimation when considering data from the month of July?
    - December BS vs December FS – Which condition shows better estimation when considering data from the month of December?
    - Annual BS vs Annual FS – Which condition shows better estimation when considering annual data?

5.1. Graphical results for UHI

It is worth noting that the UWG does not produce temperature maps that can help us identify the extent and severity of the UHI effect in different areas. Instead, it gives hourly values of an averaged area temperature. By having these values, we can create graphs and charts together with the airport data to show the time and period where the UHI presents itself the most. We used the LB tools specifically “Monthly Chart” which gives monthly averages diurnal cycles for a whole year [127] and “Hourly Chart“ illustrating hourly representations [128]. By using these graphs, we even compared the results of different radii, but there was no clear evidence of having a change since the data in the graphs are averaged. In this section, we are presenting the annual results of 500 m radius for the FS condition. As illustrated in Figure 34, the UHI effect is present throughout the year, where at night hours and late afternoons 6 PM to 6 AM, we have a visible DBT difference between the urban simulated data and the airport data.

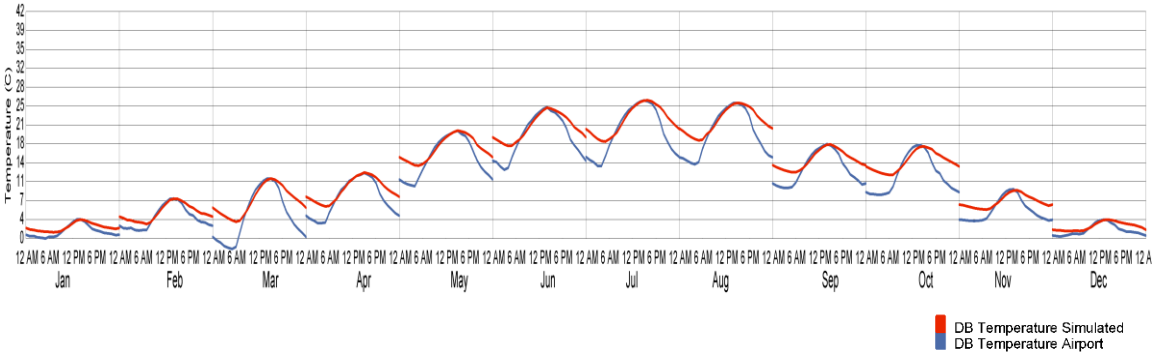

Figure 34 Monthly averages diurnal cycles 2022, Munich

We would like to focus on the month of July and January to compare the behavior to previous studies. According to the Figures 35, 36, and 37, regarding the month of July, we see that the simulated urban DBT pattern from the UWG and the airport data pattern are comparable with previous case studies, such as those conducted in Barcelona and Singapore (some shift in hours is present). On the other hand, the UHI effect is visible in all the Figures. We do expect a different UHI intensity in different case studies as the climate and urban planning change; in our case, we reached values of 5 ºC - 6 ºC during the time span of 12 AM to 4 AM, as can be seen in Figure 35.

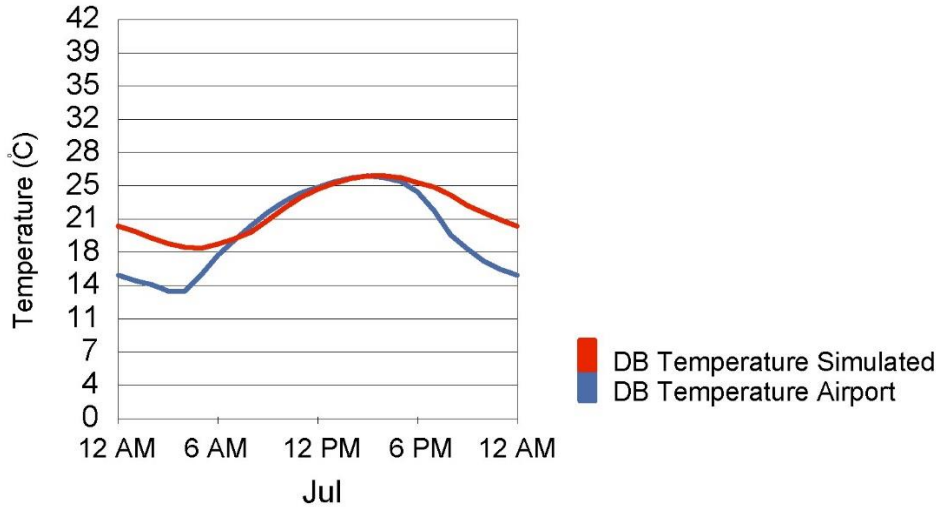

Figure 35 July monthly-average diurnal cycle, DBT, Munich

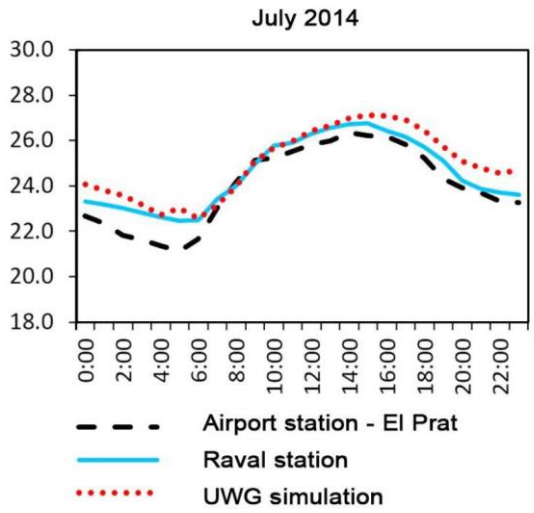

Figure 36 Barcelona Case Study Results (July monthly-average diurnal cycle) [41]

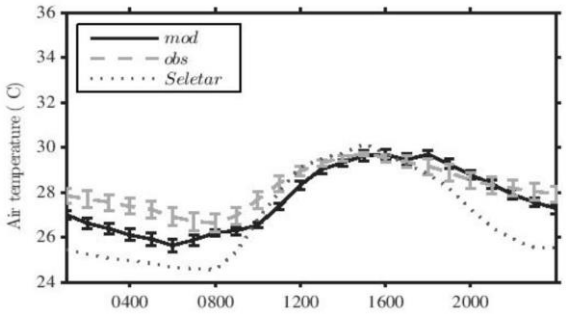

Figure 37 Singapore Case Study July 2010, Seletar (rural station) [129]

Figure 38 and Figure 39 referring to the month of January present the comparable pattern of the simulated urban data and the rural/ airport station values between Munich

and Barcelona (some shift in hours is present). For our case, Figure 38, the simulated urban data are nearly equal to the airport values in the time span from 8 AM to 2 PM with the airport data, while for the other time spans, the simulated are higher by 1 ºC - 2 ºC.

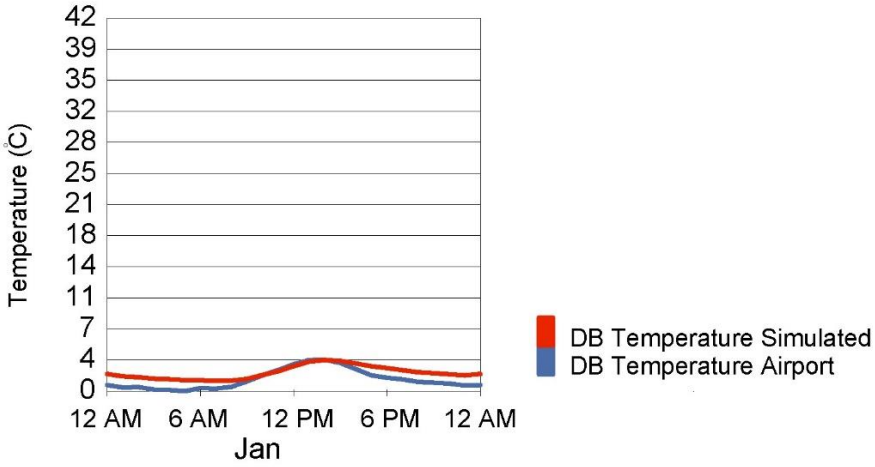

Figure 38 January monthly-average diurnal cycle, DBT, Munich

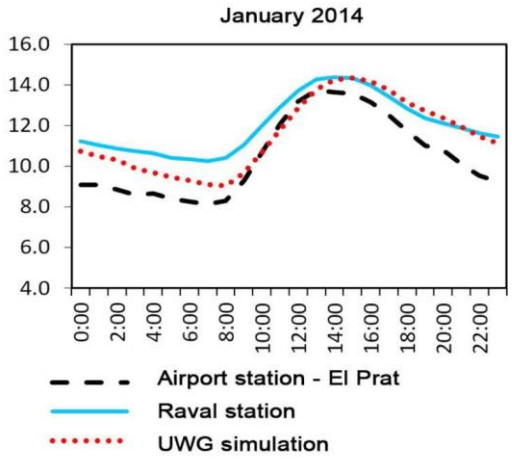

Figure 39 Barcelona Case Study Results (monthly-average diurnal cycle) [41]

Figure 40 and Figure 41 illustrate the hourly values of the simulated DBT and the airport station DBT respectively. Focusing on the summer months, we see that in the simulated values, we have high-temperature values throughout the whole day, day and night included, while for the airport station, we see that between 6 AM - 6 PM, there is a drop in temperature.

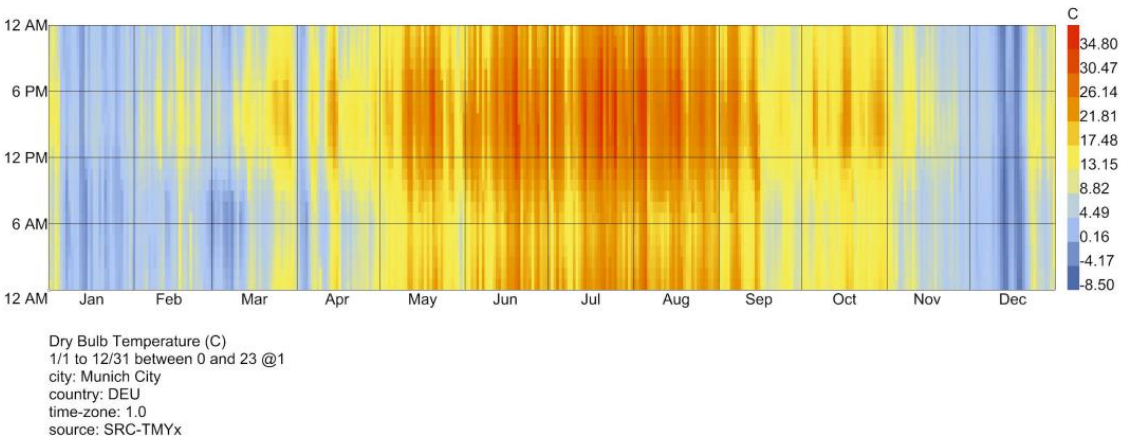

Figure 40 Hourly values of DBT for the whole year 2022, simulated

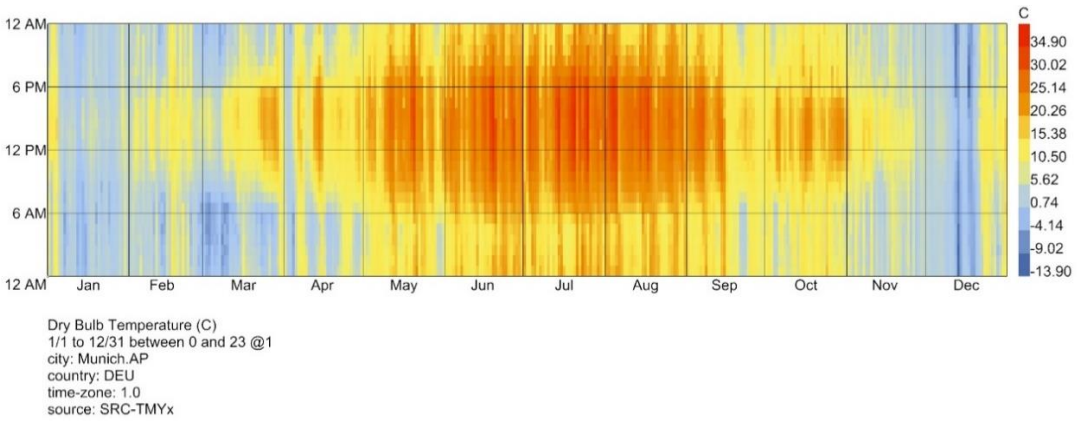

Figure 41 Hourly DBT values for the whole year 2022, Munich Airport

5.2. Results for the same condition and the same period

In this section, we will be looking into the comparison results of FS for July, December, and annual periods; for each of them, there is also a distinguishment between whole day hours, day hours, and night hours. Simulation results regarding other conditions can be found in Appendix B. From now on, the statistical analysis and results comparing simulated DBT and measured values will be referred to as “measured,” while the ones regarding simulated and airport values will be referred to as “airport.”

5.2.1. Urban morphology parameters

After having created the model with the buildings and the terrains characteristics, the UWG model component gives automatically a report. The report includes properties as the average buildings’ height, footprint density, façade to site ratio, tree cover and grass

cover. Another parameter, which we added to make a differentiation based on the terrain usage, is the terrain's albedo value. Each radius has its own combination of the mentioned parameters; as also stated by Street in its work, they vary based on the radius considered to define the urban site [30]. In our case, we performed the simulations for radii of value 10 m, 20 m, 30 m, 50 m, 100 m, and from 100 to 1500, the simulation is performed for every 100 m. We had the same number of parameters' combinations as the number of radii we analyzed and the different conditions. Table 6 shows the variation of these parameters for some of the radii. The change of grass cover and tree cover during season change is also taken into account, except those two parameters, the others stay the same even for annual simulation and for December. The combination of the parameters for each radii for FS can be found in the Appendix B, section B.1.

Table 6 Urban morphology parameters combinations for different radii

Parameter	30 m	100 m	500 m	1000 m	1500 m
Average height	22.4 m	15.8 m	14.3 m	15.3 m	15.3 m
Footprint densiy	0.02	0.39	0.32	0.3	0.27
Facade to site	0.47	2.14	1.55	1.25	1.1
Tree cover	0.18	0.49	0.46	0.52	0.59
Grass cover	0.34	0.32	0.28	0.34	0.38
Terrain's albedo	0.211	0.234	0.263	0.259	0.248

5.2.2. July simulations

For the month of July, we had 744 simulated DBT values. As discussed, we also analyzed different time spans as whole day hours, day hours, and night hours. We will present all the statistical analyses. We must note that the same approaches and statistical analyses that are performed for this period and condition are performed for all other periods and conditions. More can be found in Appendix B, section B.2, where in some of them, we stop at the most important analyses as RMSE values and Spearman's correlation.

Whole day hours

The results of the MAE analysis in Figure 42, show that the error for the measured is lower than the error coming from the airport comparison. Moreover, the error is higher

at small radius but the highest difference of MAEs measured is seen to be 0.05 ºC (1.04 ºC – 0.99 ºC), which is negligible for our engine since the UWG gives numbers with one digit of precision after the decimal point.

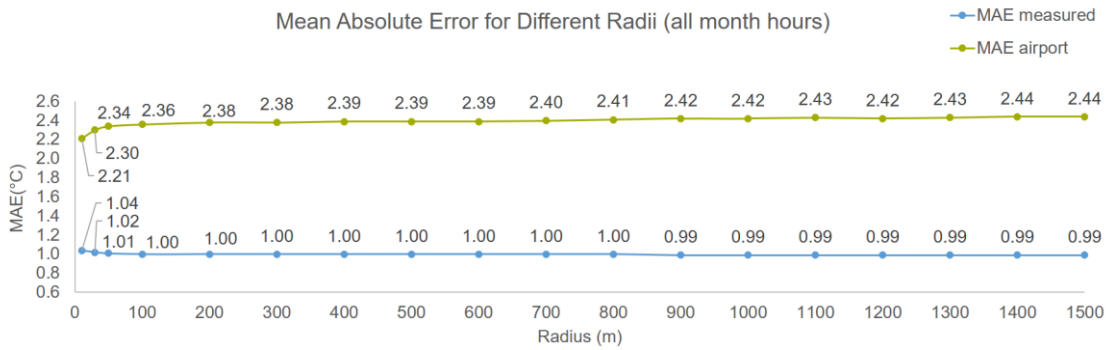

Figure 42 MAE analysis results for July FS, all month hours

The regression analysis between the simulated and the measured values, Figure 43, displays a constant high value of R^2= 0.94 throughout the radius change. On the other hand, we do have a variation in the R^2 airport values.

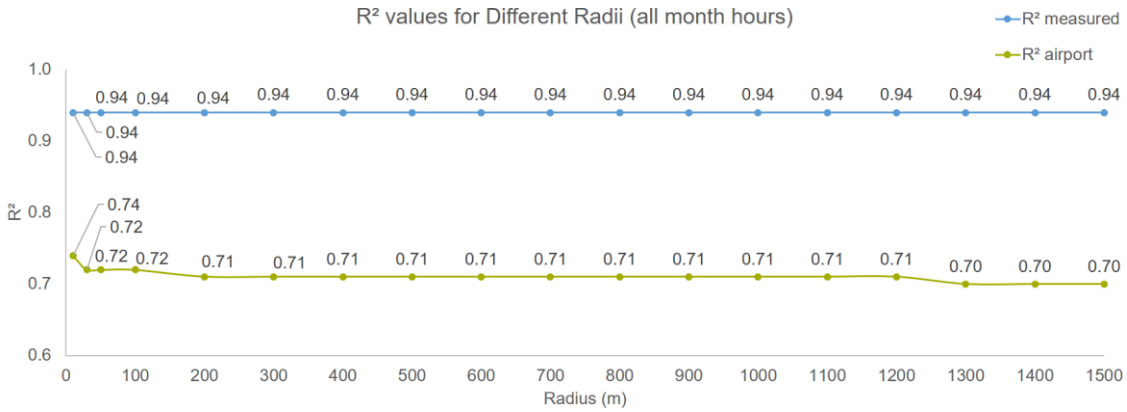

Figure 43 Linear Regression Analysis results for July FS, all month hours

In Figure 44, MBE shows an overestimation of the simulated data compared to the measured data, while the MBE related to the airport shows an underestimation.

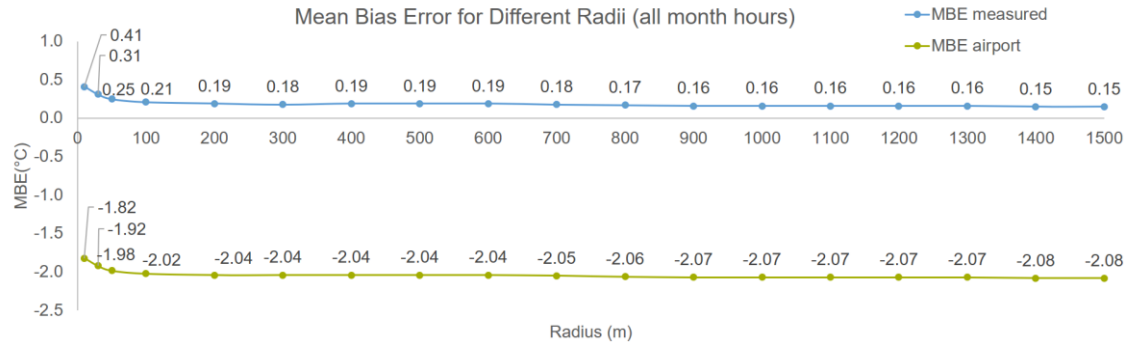

Figure 44 MBE analysis results for July FS, all month hours

Referring to Figure 45, for RMSE measured we see higher error in the 10 m and 30 m radius. After this value, we have a constant error. The highest difference between the RMSEs measured is 0.02 ºC (1.30 ºC – 1.28 ºC) insignificant for the engine. The RMSE measured is lower compared to the RMSE airport for all radii.

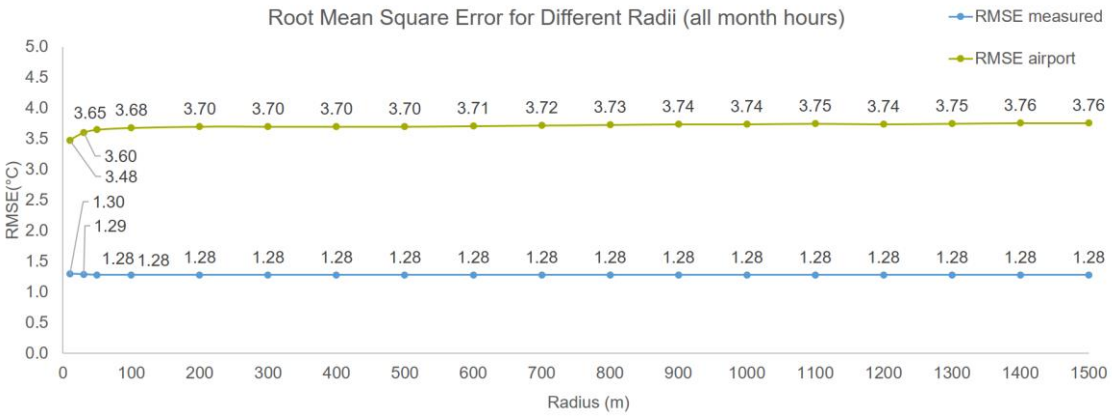

Figure 45 RMSE analysis results for July FS, all month hours

Day hours

Figure 46 presents the MAE analysis. MAE measured does not show any increasing or decreasing pattern. In the small radii values, we have higher errors, and a maximum difference of 0.03 ºC (0.91 ºC - 0.88 ºC), which is again negligible. In the case of the day, we observed that the simulated-airport errors are lower than the simulated-measured errors.

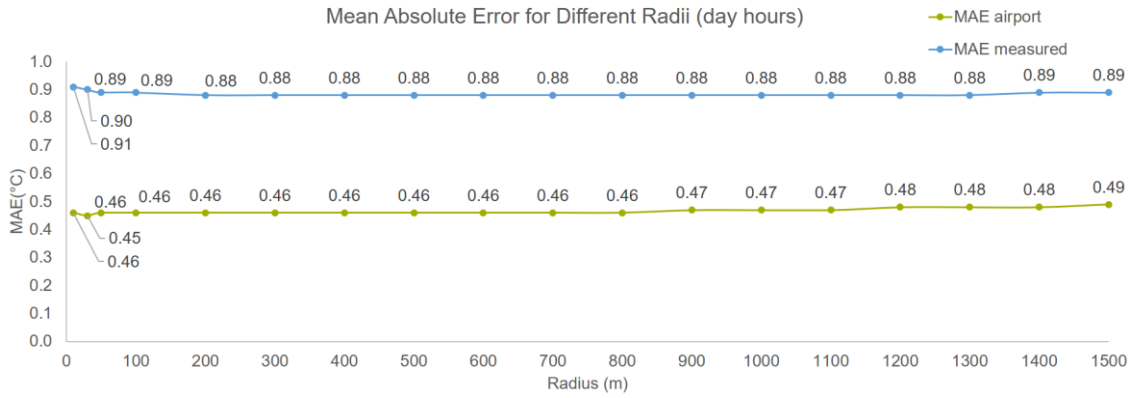

Figure 46 MAE analysis results for July FS, day hours

The regression analysis, Figure 47, shows a constant value of 0.96 for the R^2 measured throughout the change of radius. The R^2 airport stays constant as well. It is noticed that we have again a better fitting of the simulated data to airport values than to the measured data.

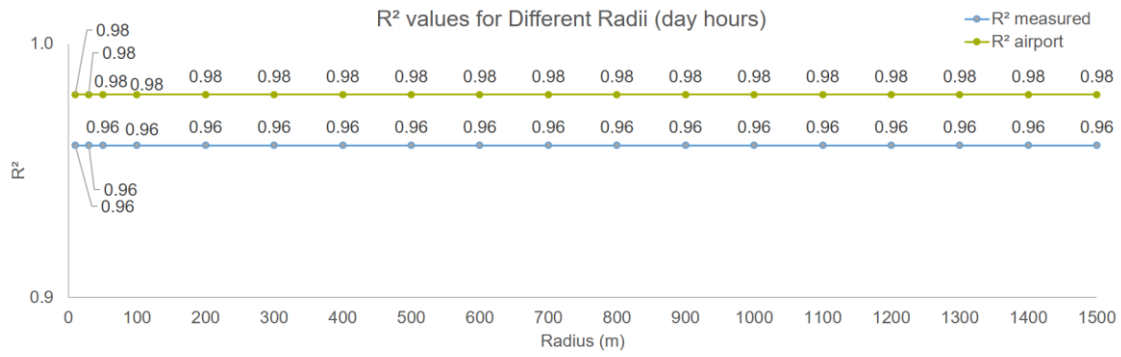

Figure 47 Linear Regression Analysis results for July FS, day hours

The MBE measured and the MBE airport show an overestimation of the values as observed in Figure 48.

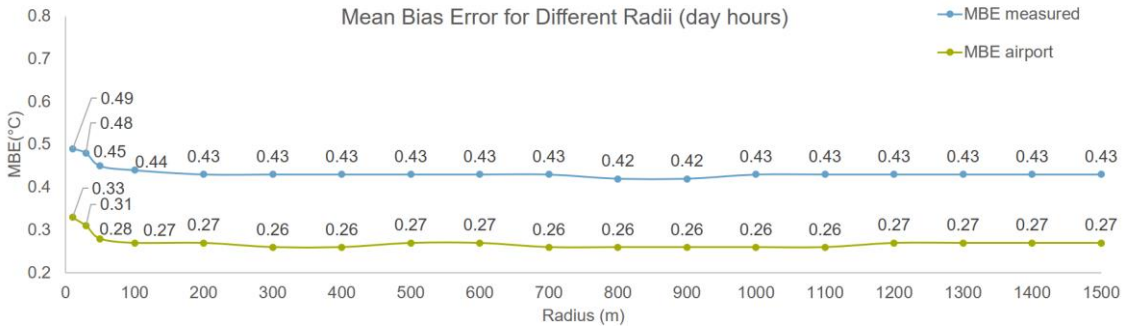

Figure 48 MBE analysis results for July FS, day hours

For the RMSE measured, there is no pattern with regard to the varying radius (Figure 49). We see a slightly higher error when the radius is 10 m. The highest difference between RMSEs measured values is 0.04 ºC (1.13 ºC – 1.09 ºC) thus, not significant for our engine. Again, for day hours we observe that the error related to airport is lower than the one related to measured data.

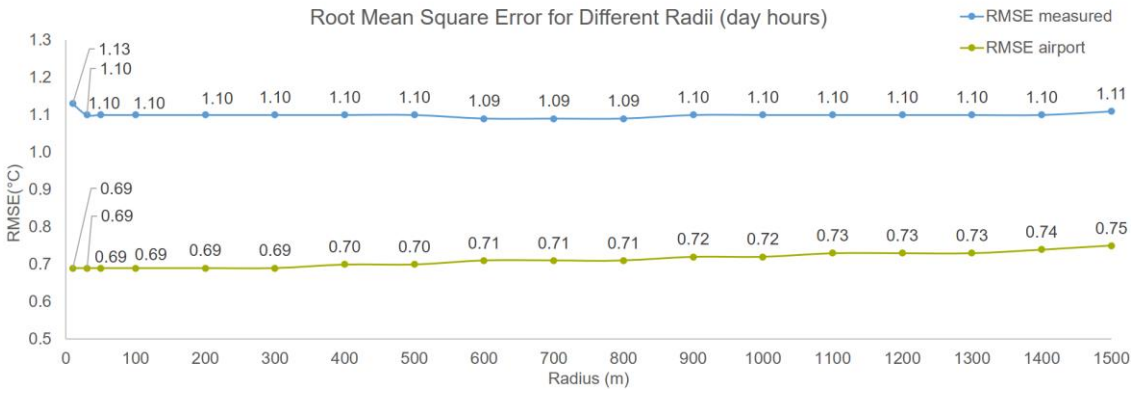

Figure 49 RMSE analysis results for July FS, day hours

Night hours

In Figure 50, the MAE measured has no patterns with varying boundaries. The maximum difference in errors observed is 0.03 ºC (0.89 ºC – 0.86 ºC). However, the simulated-airport errors are noticed to have high values.

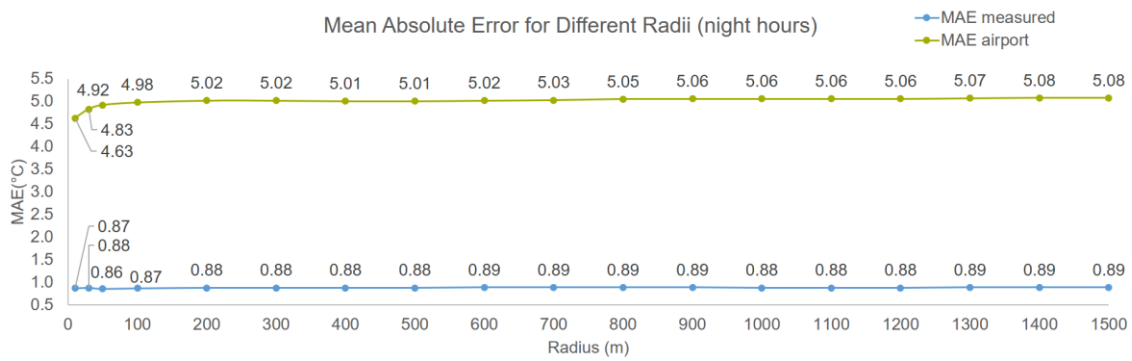

Figure 50 MAE analysis results for July FS, night hours

The regression analysis that can be seen in Figure 51 indicates a better fit for small radii values, but only with a 0.01 difference. As expected, the R^2 airport is lower compared to the R^2 measured.

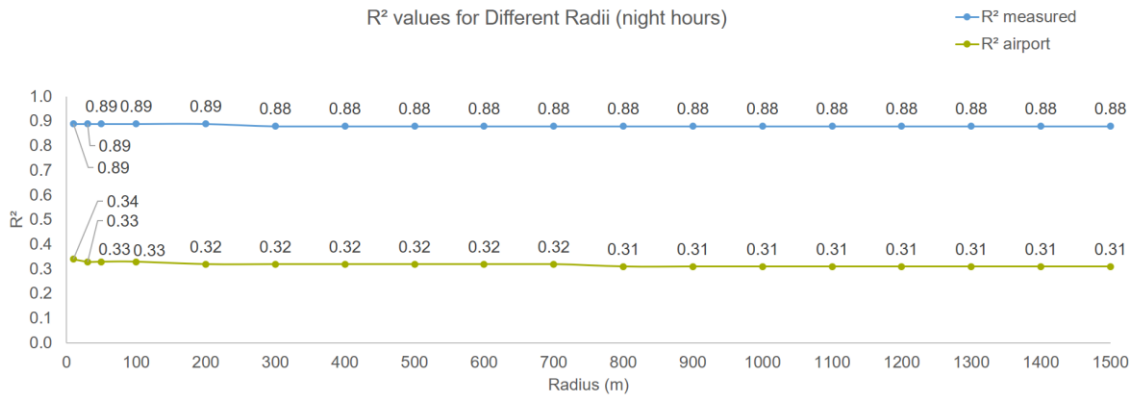

Figure 51 Linear Regression Analysis results for July FS, night hours

Referring to Figure 52, MBE analysis we see mostly an underestimation of the simulated values compared to the measured ones, the same applies from MBE airport.

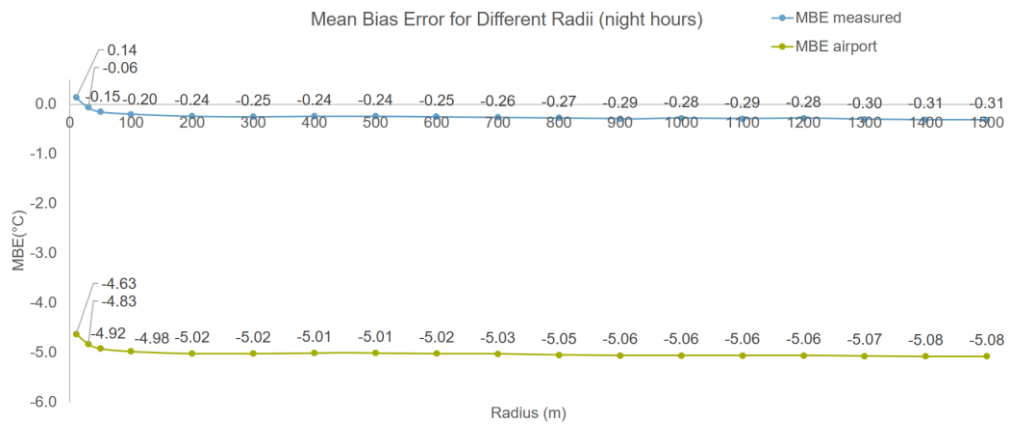

Figure 52 MBE analysis results for July FS, night hours

RMSE related to the measured values shows small errors for small radii, the highest difference for RMSEs measured is 0.09 ºC (1.15 ºC – 1.06 ºC). Again for July we have high errors when comparing simulated values to airport data, as Figure 53 presents. These high errors are refering also to the UHI intensity, meaning the difference in DBTs when comparing urban and airport data.

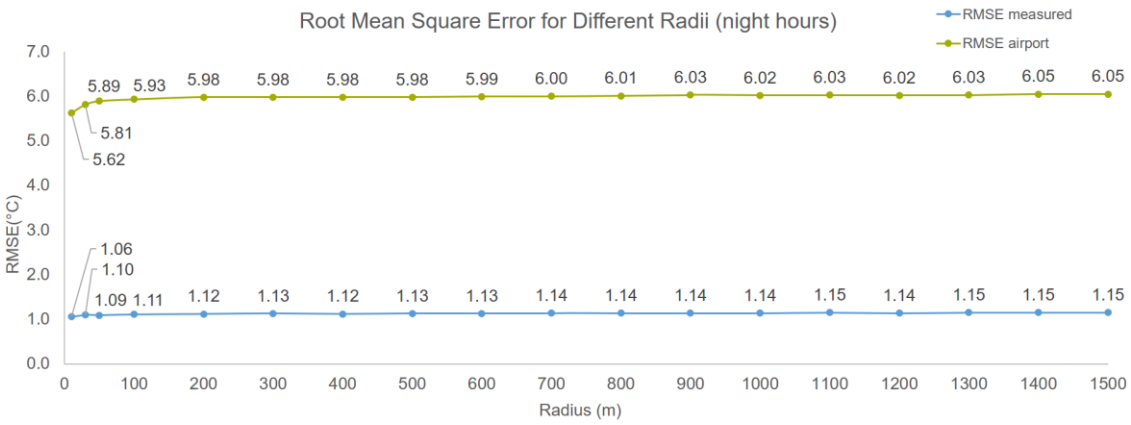

Figure 53 RMSE analysis results for July FS, night hours

Spearman’s correlation between RMSE and radius for whole day, day, and night

We performed Spearman’s correlation, using R studio, between radii values and the RMSEs measured values for each time span, focusing on having or not a correlation, Spearman's rank correlation coefficient (ρ), and the significance value of the correlation (p) (0.05). Table 7 presents a summary of Spearman’s correlation and the highest difference observed between RMSEs measured values (Δ_{RMSE}). Figures that were obtained from R studio follow.

Table 7 Summary of Spearman's correlation and Δ_{RMSE} for July FS

	Spearman's correlation	ρ	Significance p	Δ_{RMSE}
Whole day hours	Not applicable	-	-	0.02 ºC
Day hours	Not applicable	-	-	0.04 ºC
Night hours	Applicable	+0.96	1.025×10^{-10}	0.09 ºC

During the analysis of the whole day hour's case using Spearman's correlation (Figure 54), no correlation was observed. Additionally, as mentioned previously, the highest difference between the RMSEs measured was 0.02 ºC, which we consider negligible for our engine. Therefore, selecting a specific radius in this scenario will not make any significant difference in terms of error.

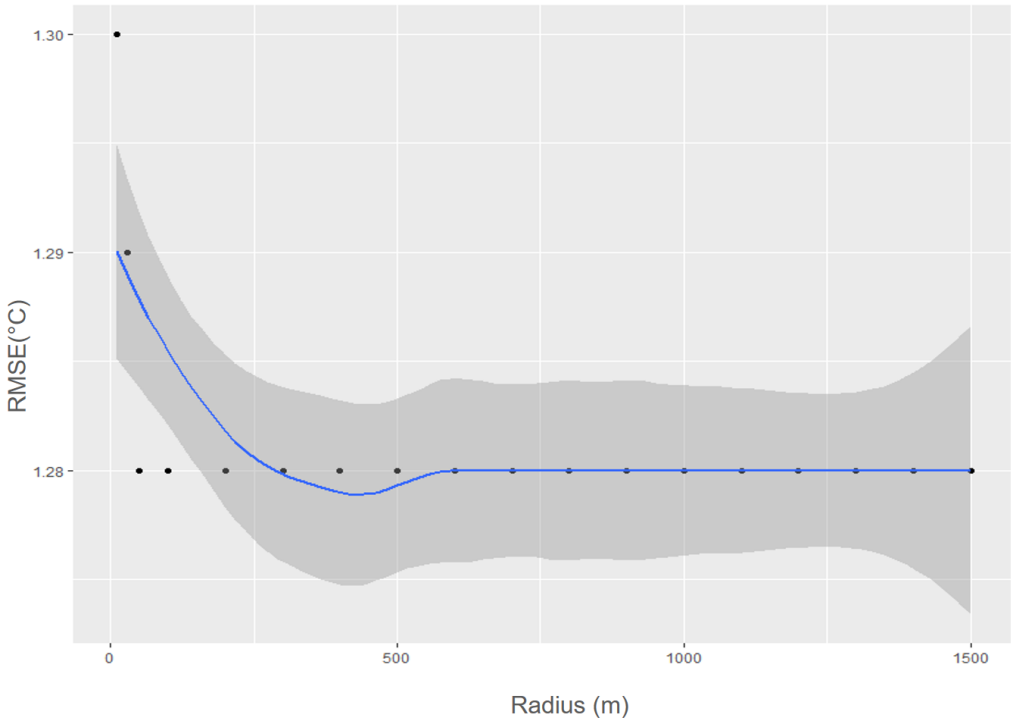

Figure 54 RMSE vs Radius in R studio for July FS, all month hours

There was also no correlation between RMSEs measured and radii values for day hours. Additionally, the highest difference of RMSEs measured is 0.04 ºC, which is negligible. Figure 55 presents the graph from R studio.

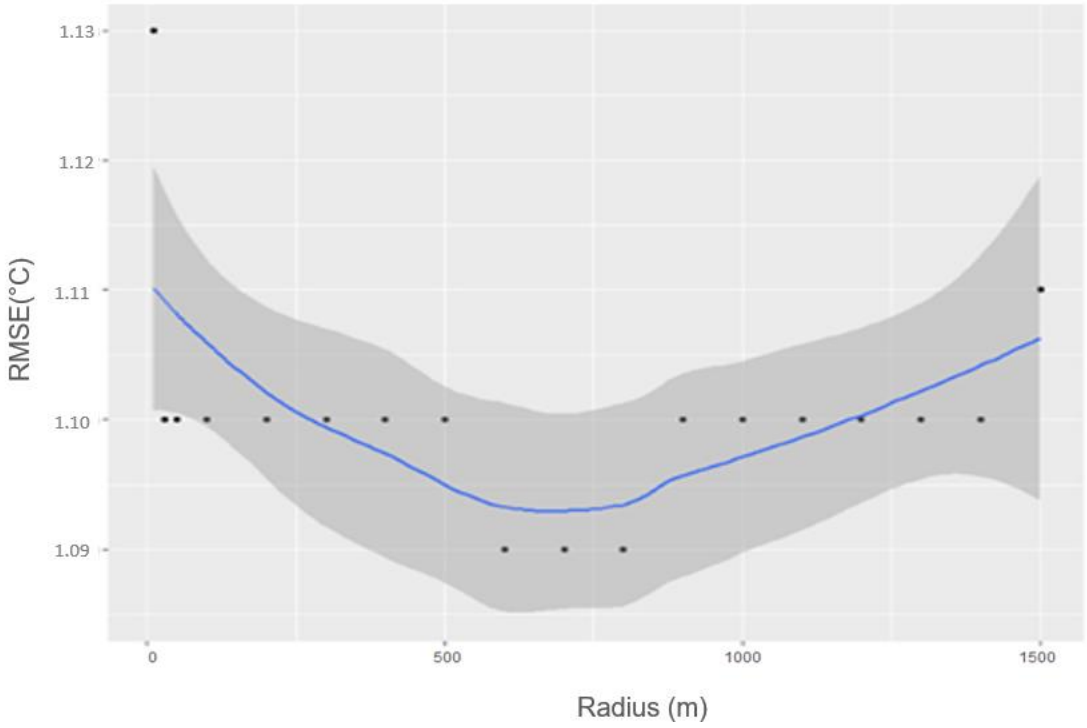

Figure 55 RMSE vs Radius in R studio for July FS, day hours

As it concerns the night hours, we obtained a high value of the Spearman correlation coefficient as ρ=0.96, showing a strong correlation. With significance level p-value= 1.025×10^{-10}. From Figure 56, we can even see some deviations; some of them are noted with red; thus, when deciding to suggest a radius, we also take into account the highest difference between the RMSEs measured values. In this case, it is 0.09 ºC (1.15 ºC - 1.06 ºC). Thus, if the urban planners consider a change of 0.09 ºC in error as significant, then we would suggest using a radius of 100 m or lower to perform the simulations.

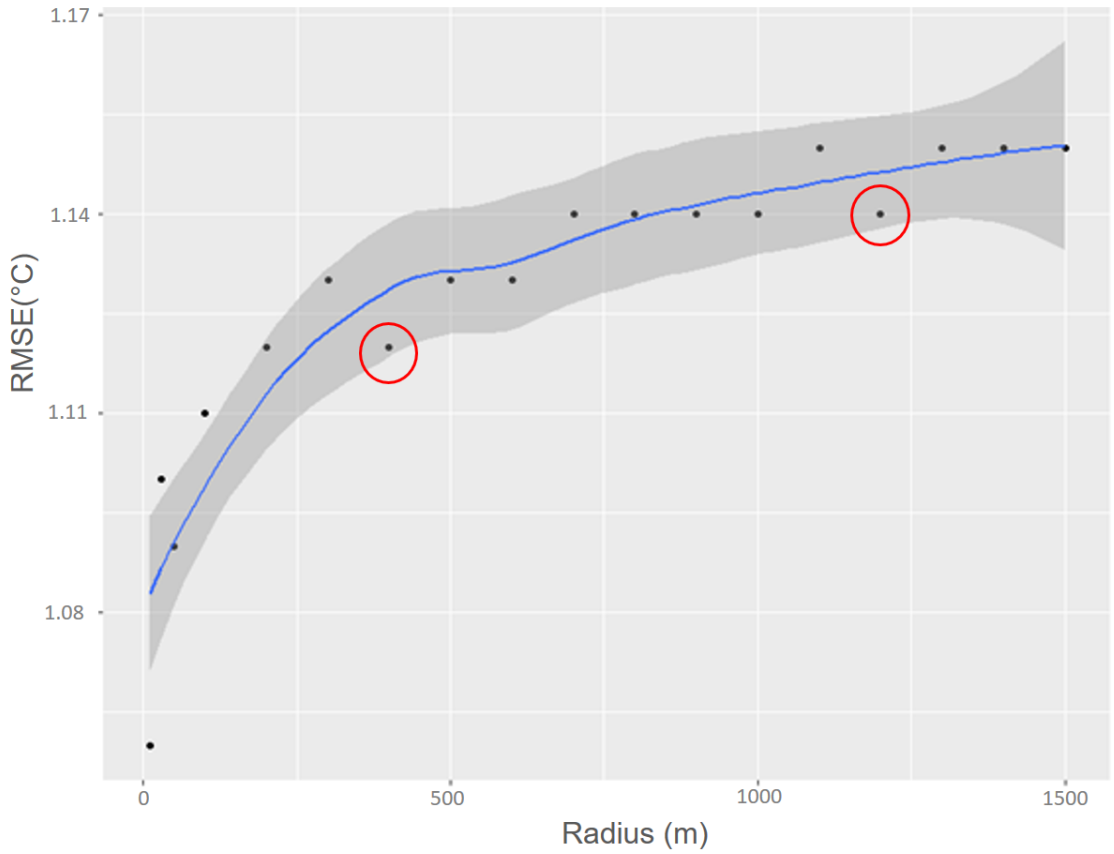

Figure 56 RMSE vs Radius in R studio for July FS, night hours

Time span comparison

To make the comparison between different time spans we used the RMSEs measured values. We took an average to consider all radii values and, as error bars in the graphs, we used the max and min RMSE values. It can be concluded that the engine, in this case, displaying values of 1.28 ºC, 1.10 ºC, and 1.13 ºC for whole day hours, day hours, and night hours, respectively, as shown in Figure 57, gives a better estimation for the day hours and displays a higher error when considering the whole hours in a day.

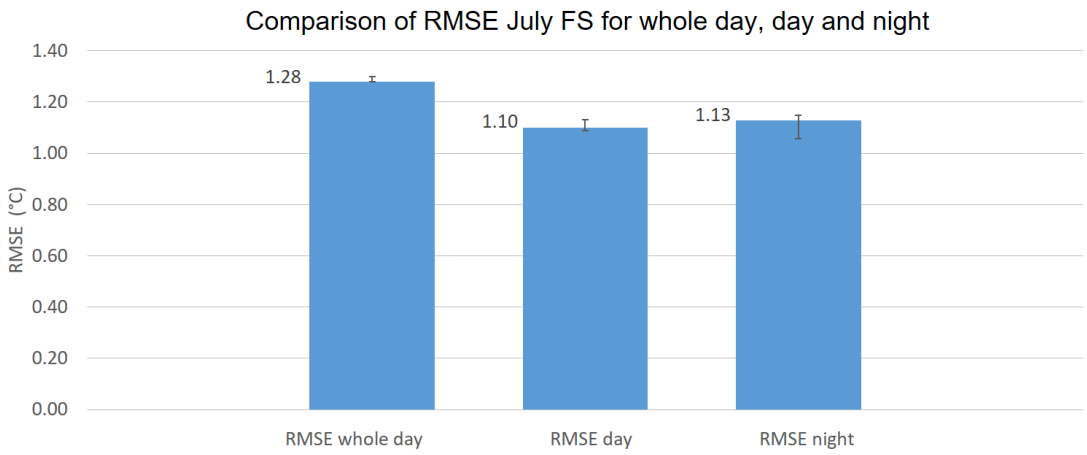

Figure 57 RMSEs measured comparison for different time spans, July FS

Overheating hours and tropical nights

Other methods that we delved into to see the behavior of the engine and if the radius had an influence was analyzing the overheating hours and the tropical nights. The overheating hours are hours where the air temperature > 30 ºC, [130, p. 42] for our case we considered air temperature ≥ 30 ºC. A tropical night refer to a night in which the minimum air temperature is ≥ 20 ºC for the time span of 6 PM to 6 AM [131]. We divided the simulated values into two time spans: 12 PM to 4 PM and 6 PM to 6 AM. This helped us to analyze the overheating hours and tropical nights (we considered hourly values, not minimum air temperatures but all DBTs data from 6 PM to 6 AM) for each radius separately. We followed the same approach for the measured data and the airport DBT. The results are as shown in Table 8. It can be seen that the overheating hours in this case are underestimated, for all radii values, it can be argued that this may happen since the measuring device is placed in FS. As it concerns the tropical nights, except for the 10 m value of the radii, there is an overestimation of the hours from the engine compared to the measured data. It should be noted that the engine overestimated the occurrence of tropical nights in all conditions of July as well as for the annual data.

Table 8 Overheating hours and tropical nights (in terms of hours) July FS

Radius	Overheating hours, DBT ≥ 30°C	Tropical nights, DBT ≥ 20°C
10	21	207
30	22	213
50	22	216
100	21	218
200	21	218
300	21	220
400	22	218
500	22	217
600	22	218
700	22	218
800	22	218
900	22	218
1000	22	218
1100	21	219
1200	22	218
1300	22	218
1400	21	218
1500	21	218
Measured in Full Sun	32	207
Airport values	23	95

5.2.3. December simulations

December period has 744 simulated DBTs values. We will present below the RMSE statistical analysis since it accounts for both bias and variation in error and Spearman's correlation for each time span. The other statistical analyses can be found in Appendix B, section B.2.

Whole day hours

As in Figure 58, RMSE for the measured values throughout the whole day shows a significant change of error, with the highest difference of 0.23 ºC (1.74 ºC - 1.51 ºC). The greatest fluctuation occurs between 10 m and 200 m radius, with a difference of 0.21 ºC, while between 200 m and 1500 m radius, the difference is 0.03 ºC, which is negligible. Therefore, we suggest modeling and simulating an area with a radius of at least 200 m, for this case. Even the airport values show a high range of change. Small radii values give lower errors, which is contrary to the RMSEs measured data.

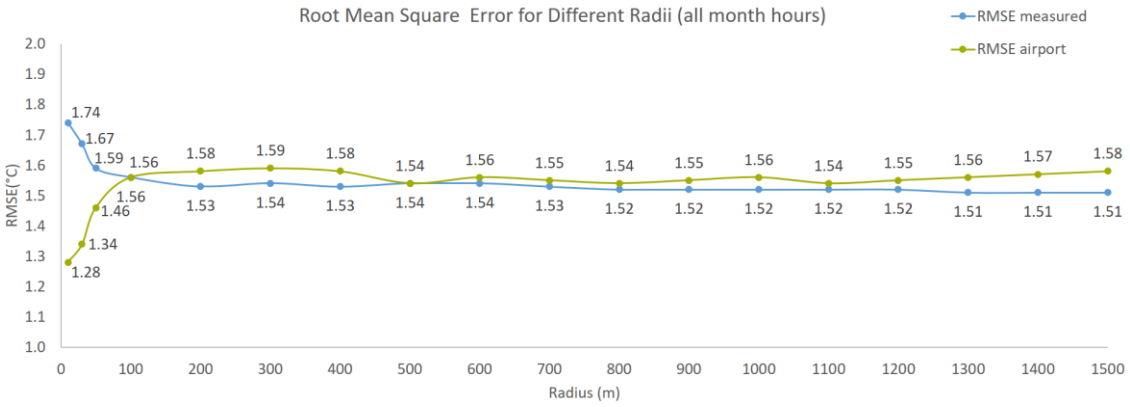

Figure 58 RMSE analysis results for December FS, all month hours

Day hours

Referring to Figure 59, the RMSE measured for day hours, we see that there are higher errors for the small radii. The highest difference between RMSEs measured is 0.15 ºC (2.08 ºC -1.93 ºC) happening between 10 m and 200 m radius and we have a maximum difference of 0.02 ºC (100 m to 1500 m), which is negligible. For this case we suggest a radius of at least 100 m. The RMSE airport for the day hours is lower compared to the RMSE measured.

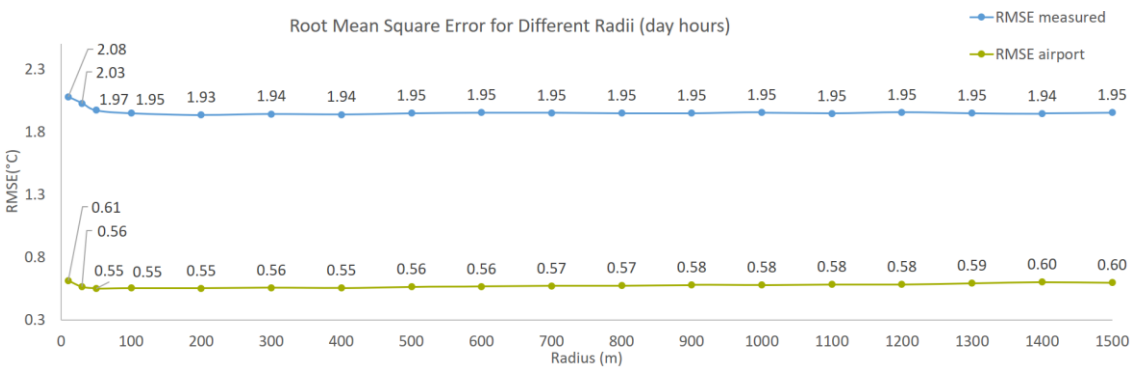

Figure 59 RMSE analysis results for December FS, day hours

Night hours

In this case, compared to all other periods, time spans, and conditions, we saw the highest difference between the RMSEs measured values, Figure 60. The difference is of 0.29 ºC (1.71 ºC -1.42 ºC). We must mention that the highest drop happens between 10 m and 600 m in this case with a difference of 0.24 ºC, and after these radii, the difference between RMSEs measured is a negligible value of 0.03 ºC (from 700 m to 1500 m). For this case, we suggest a simulation with a radius of at least 700 m.

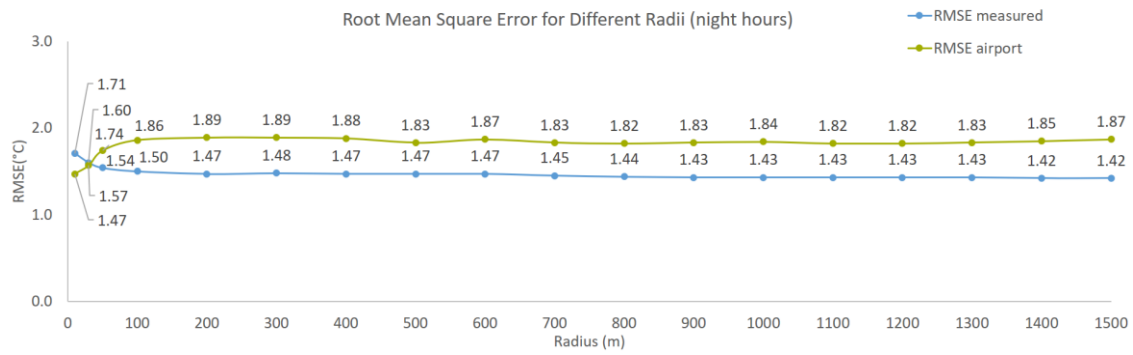

Figure 60 RMSE analysis results for December FS, night hours

Spearman's correlation between RMSE and radius for whole day, day, and night

Table 9 presents the summary of Spearman's correlation, where we see a negative correlation for RMSE measured and radius. More details can be found in Appendix B, section B.2.

Table 9 Summary of Spearman's correlation and Δ_{RMSE} December FS

	Spearman's correlation	ρ	Significance p	Δ_{RMSE}
Whole day hours	Applicable	-0.95	1.25×10^{-9}	0.23 ºC
Day hours	Not applicable	-	-	0.15 ºC
Night hours	Applicable	-0.98	2.05×10^{-12}	0.29 ºC

Time span comparison

We also compared the RMSEs measured values for different time spans for December. As presented in Figure 61, the highest error is observed during daytime, while we have a better estimation of the DBTs values for the nighttime.

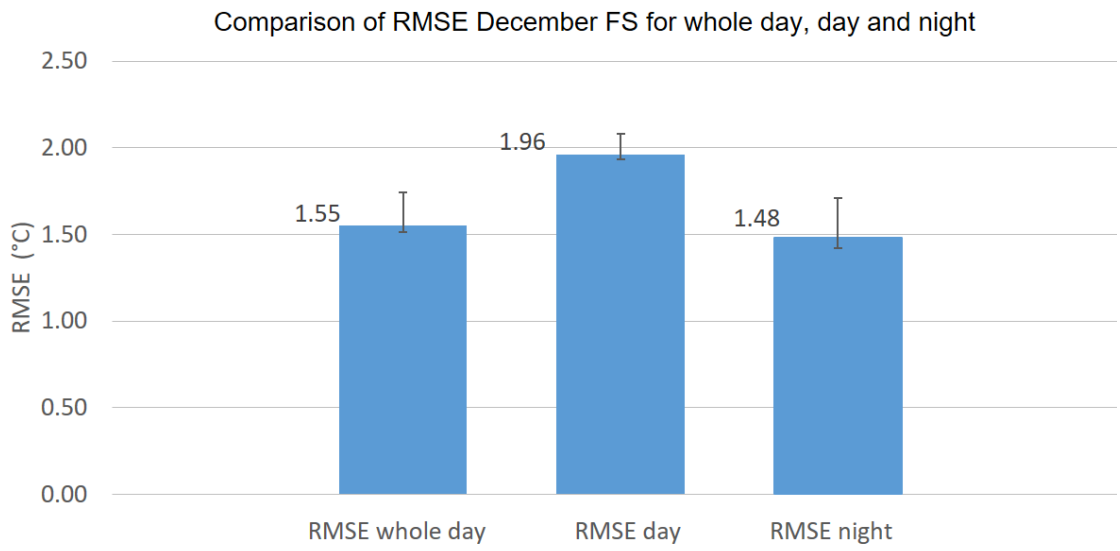

Figure 61 RMSEs measured comparison for different time spans, December FS

5.2.4. Annual simulations

The current section of the subchapter shows the results related to the annual simulation. For the annual period, we will present the RMSE analysis and the results of the Spearman's correlation. Other statistical analyses for this period and condition are available in Appendix B, section B.2.

Whole day hours

We considered all the hours of the annual simulation, 8760 hours. Figure 62 shows the RMSE for the all year hours for different radii. We see that the RMSE airport is higher compared to RMSE measured for all radii values. The highest difference between RMSEs measured values is 0.03 ºC (1.49 ºC - 1.46 ºC), which is negligible, also there is no pattern observed.

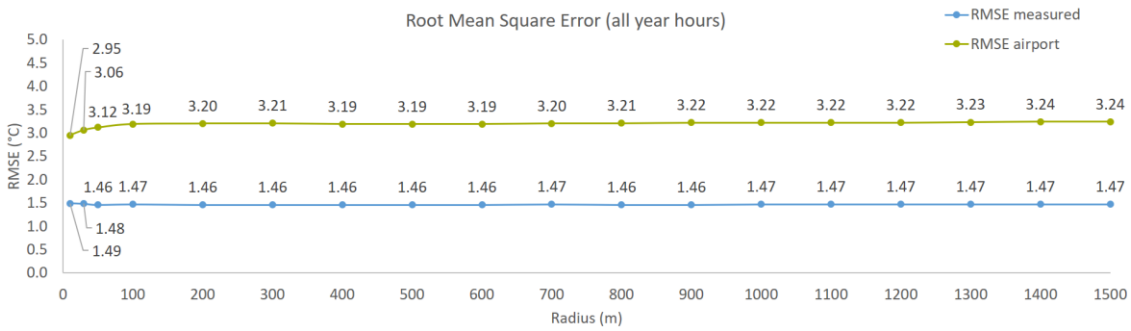

Figure 62 RMSE analysis results for annual FS, all year hours

Day hours

For the day hours comparison, as seen in Figure 63, we observe the highest errors are related to small radii; the highest difference between RMSEs measured is 0.08 ºC (1.71 ºC -1.63 ºC). Furthermore, the RMSE airport is lower compared to the RMSE measured.

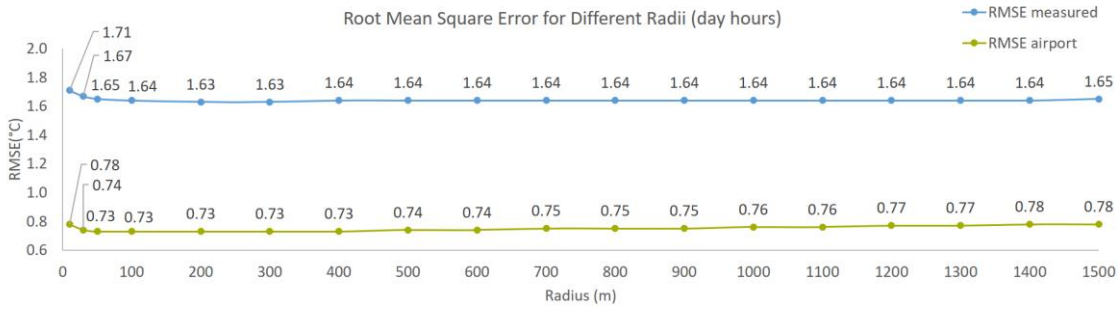

Figure 63 RMSE analysis results for annual FS, day hours

Night hours

The RMSEs measured data shows smaller values at the small radii, the highest difference is again observed to be 0.08 ºC (1.40 ºC -1.32 ºC). The RMSE related to the airport

is higher than the one related to the measured data for all radii values. As can be seen in Figure 64.

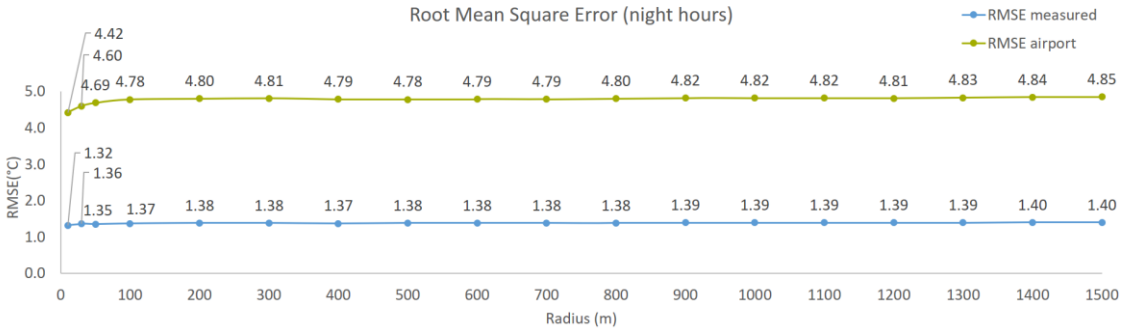

Figure 64 RMSE analysis results for annual FS, night hours

Spearman's correlation between RMSE and radius for whole day, day and night

Table 10, presents a summary of the correlation and the highest RMSEs difference Δ_{RMSE}. More information regarding the correlation and the analysis with graphs from R studio can be found in Appendix B, section B.2

Table 10 Summary of Spearman's correlation and Δ_{RMSE} annual FS

	Spearman's correlation	ρ	Significance p	Δ_{RMSE}
Whole day hours	Not applicable	-	-	0.03 ºC
Day hours	Not applicable	-	-	0.08 ºC
Night hours	Applicable	+0.95	1.43×10^{-9}	0.08 ºC

Time span comparison

Figure 65 shows the comparison of different time spans for annual errors. The engine showed a better estimation for the nighttime period (1.38 ºC) while the error was higher for daytime (1.65 ºC). Therefore, for the annual period FS condition, we can conclude that the best estimation accuracy of DBTs values is for the nighttime as was observed in December.

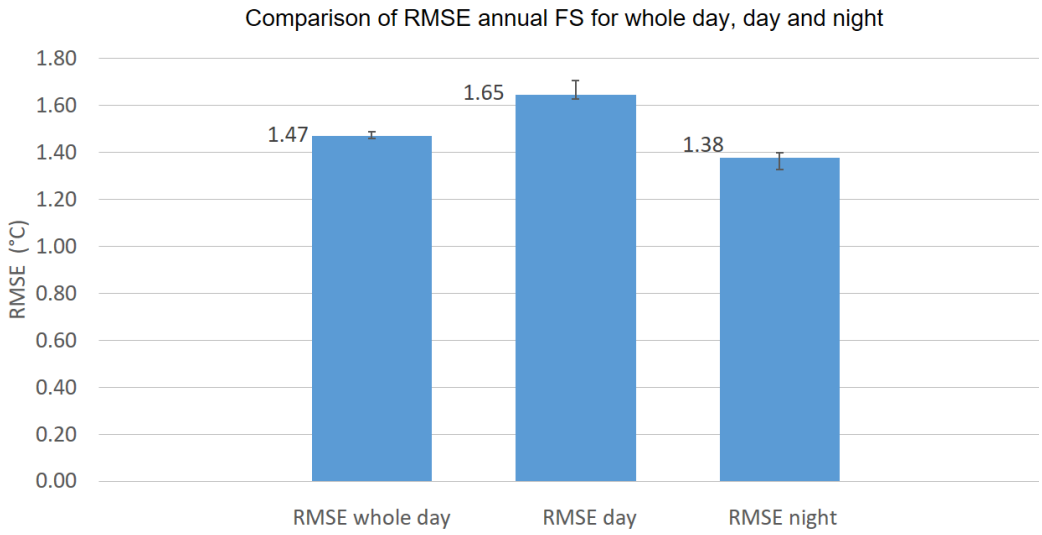

Figure 65 RMSEs measured comparison for different time spans, annual FS

5.3. Results for the same condition but different periods

In this section, we will explore how the RMSE between simulated and measured data changes across various periods: annually, in December, and in July. Firstly, we will look into the full sun exposure condition and then into the building shade condition. In these comparisons, we included the different time spans as well.

5.3.1. Full sun exposure condition

When considering the FS condition Figure 66, we can see that the month of July is better estimated compared to the annual and December estimation, across all the time spans (1.28 ºC, 1.10 ºC, 1.13 ºC). On the other hand, the month of December displays higher errors, exceeding the annual errors. Furthermore, December also has a higher variation in terms of error, inside a time span.

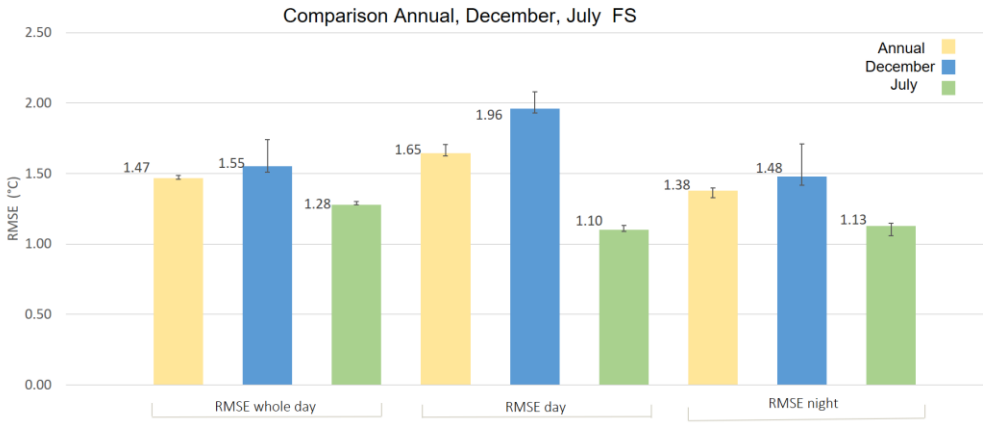

Figure 66 RMSEs measured comparisons different periods and time spans, FS

5.3.2. Building shade condition

Referring to Figure 67, for BS condition it appears that July is more accurately estimated compared to December and the annual values. This holds true for all time spans, including the whole day, day, and night (1.21 ºC, 1.09 ºC, 1.18 ºC). In regards to the annual data compared to the December values, we noticed that the annual data has a higher error rate, except during the day hours where December's error surpasses the annual one, 1.51 ºC and 1.32 ºC respectively.

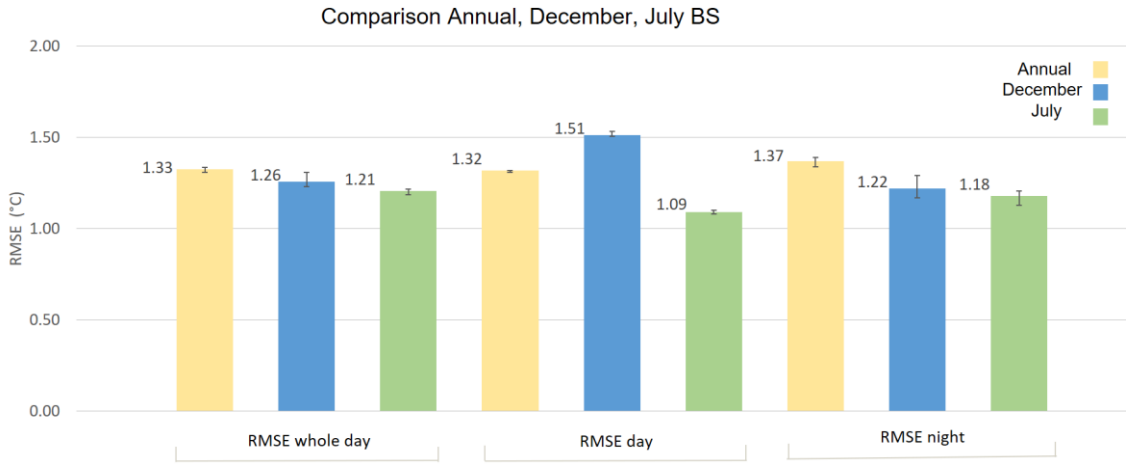

Figure 67 RMSEs measured comparisons different periods and time spans, BS

Based on our intercomparisons, we concluded that the engine provides more accurate estimations for the month of July in all conditions, corresponding to the summer period.

5.4. Results for different conditions but the same period

In this subchapter, we will compare different conditions for the same period. We analyzed July data considering FS, BS condition and the AV condition. This condition was simulated by taking the center of the circled area (with varying radius) between the centers of other conditions and comparing it with the averaged values of the measured data of all the other conditions (FS, BS, TS, WP, WE). For December and annual data we will look into the comparison of FS and BS. We also differentiated among the three different time spans.

5.4.1. Different conditions comparison, July

When comparing the FS and BS, we observed higher error for the FS during the whole day, and day time span while not the same behavior was observed at night. When comparing the three conditions, the average condition provided the most reliable temperature estimation for all time spans, with lower RMSEs values of 1.17 ºC, 0.89 ºC, and 1.13 ºC for whole day, day, and nighttime, respectively. Figure 68 shows the comparison among the three conditions for July.

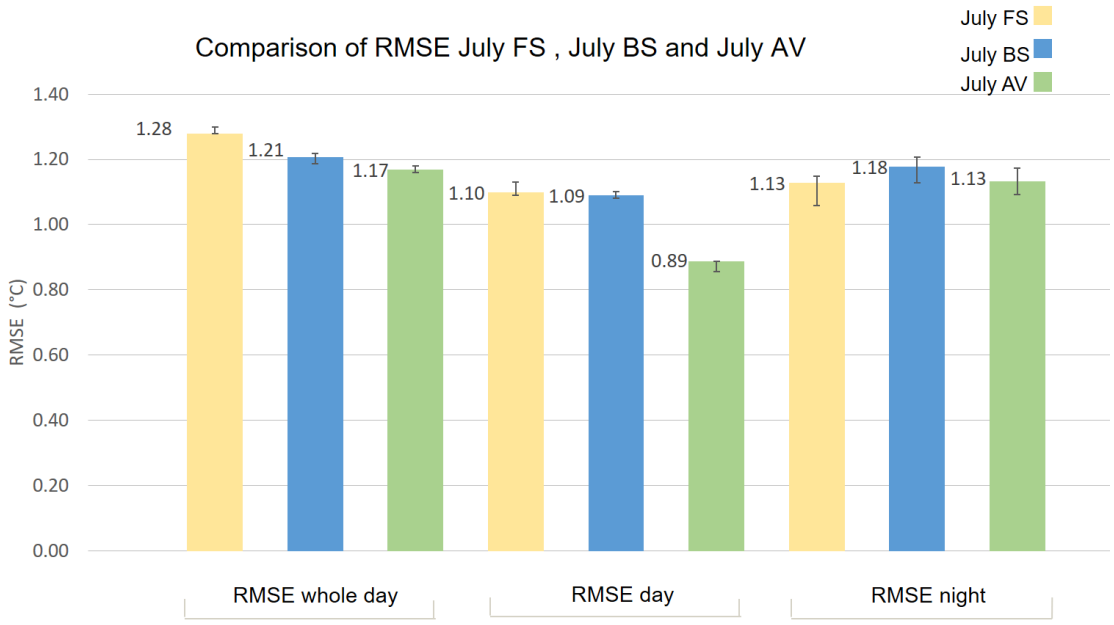

Figure 68 RMSEs measured comparisons FS, BS, and AV for July

5.4.2. Different conditions comparison, December

When analyzing December RMSEs for the two conditions, Figure 69, we observe that a more accurate estimation is obtained for the BS condition, across all time spans. Furthermore there is a higher variation in the error for the FS conditions during the whole day, day, and night.

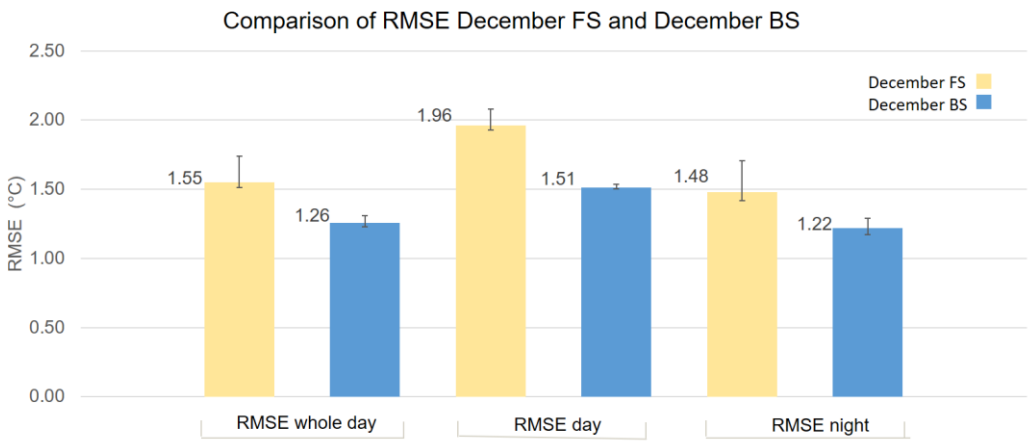

Figure 69 RMSEs measured comparisons FS, BS for December

5.4.3. Different conditions comparison, annual data

When comparing the annual FS and BS conditions, it becomes clear that the BS condition shows better estimation and lower errors for all time spans as can be seen in Figure 70. Furthermore, if we compare the errors during the whole day and during the day in different conditions, we can observe a significant difference in error, especially during the day span where we see 1.65 ºC and 1.32 ºC respectively. However, during nighttime, the errors are comparable. We also see more variation of the error for the FS condition than for the BS for all time spans.

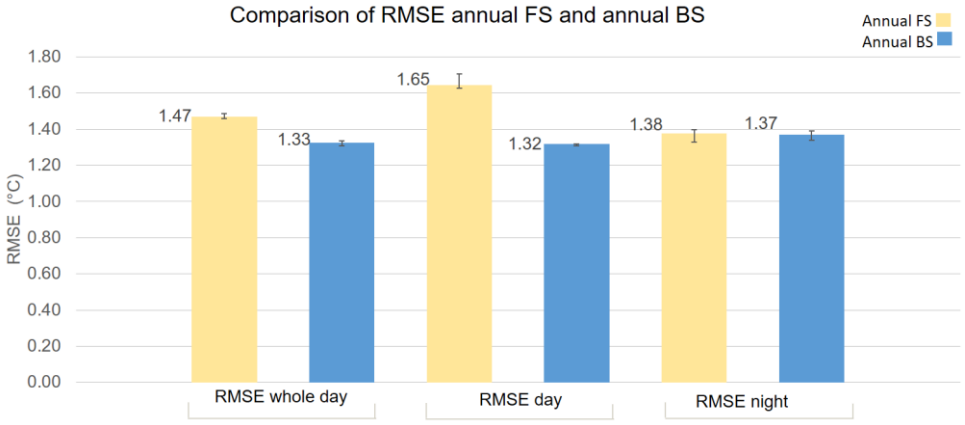

Figure 70 RMSEs measured comparisons FS, BS for annual data

From the intercomparisons, same period, and different conditions, we concluded the following: We have a better estimation for the BS condition than the FS condition for the annual, December, and July periods, mainly for all time spans. On the other hand, when considering the AV condition, we observed even a better estimation for the month of July.

5.5. Discussion

The upcoming subchapter summarizes the main findings and compare some of them to similar studies. The first section relates to our two main hypothesis: the influence of the radius on the results and the various considered conditions. Furthermore, we also provide a summary of our findings regarding UWG behavior.

5.5.1. Radius influence and different conditions

We have previously presented the results related to the radius influence for three different periods, considering three time spans and one condition, specifically FS, where we looked mainly into RMSE analysis and Spearman's correlation.

In order to test our hypothesis, we conducted several statistical analyses (as presented in the July FS). After careful consideration, we focused on the RMSE measured results, which take into account both bias errors and error variation. Additionally, we examined the Spearman's correlation between the RMSEs values and the radii values to reinforce our findings.

As part of our research, we performed a thorough analysis of the obtained results considering all cases, which enabled us to create a guideline table, displayed in Figure 71. It suggests an appropriate radius (Rs) for UWG based on our study of Bordeauxplatz in Munich. The LCZ map [132] classifies the majority of the areas in Munich as LCZ2 (compact midrise), including Bordeauxplatz [133]. The table may be a helpful guide for urban planners and future researchers, considering other areas classified as LCZ2. It is important to note that we did not compare other LCZ2 cities (can be explored in future research), and we used the LCZ as a scaling concept for our results.

In the table, we considered two main criteria to suggest a radius that gives the lowest error for the analyzed condition:

- The highest difference between RMSEs measured
- The Spearman's correlation

In relation to the greatest observed difference between RMSEs measured values, a conservative range was selected with consideration given to the fact that the engine supplies values with only one digit after the decimal point. Our analysis regards any

difference in errors that is equal to or less than 0.05°C as insignificant, while differences exceeding 0.05°C as significant. Moreover, we also have the correlation which can be positive or negative. These 2 criteria create 4 different combinations, as seen in the legend of the table. We suggest a Rs in two of these combinations:

- There is a correlation and the $\Delta_{RMSE} >$ 0.05 °C
- There is no correlation and the $\Delta_{RMSE} >$ 0.05 °C

Regarding the other combinations, we did not recommend any specific radius as the difference for our engine is considered insignificant. Furthermore, the range of Δ_{RMSE} can be chosen subjectively by each urban planner. In this particular case, we have taken a more conservative approach. For a more in depth results of these differences and the correlations, refer to Appendix B, section B.3.

	Annual		December		July					
	BS	FS	BS	FS	BS	FS	TS	WP	WE	AV
Whole Day			Rs ≥ 200m	Rs ≥ 200 m					Rs ≤ 50 m	
Day		Rs ≥ 50 m		Rs ≥100 m					Rs ≤ 50 m	
Night		Rs ≤ 100 m	Rs ≥ 900 m	Rs ≥ 700 m	Rs ≤ 200 m	Rs ≤ 100 m	Rs= 50 m; 200 m	Rs ≤ 30 m	Rs < 30 m	Rs ≤ 200 m

Legend

- Correlation and $\Delta_{RMSE} \leq 0.05$
- No Correlation and $\Delta_{RMSE} \leq 0.05$
- No correlation and $\Delta_{RMSE} > 0.05$
- Correlation and $\Delta_{RMSE} > 0.05$

Figure 71 Summary of the results, case study Bordeauxplatz Munich, guideline

To explain this guideline, we look into the AV condition of the July period. For the whole day and day time span, there is a correlation, but the $\Delta_{RMSE} < 0.05$ °C; for these cases, we see that there is no significance to suggest any value of radius. On the other hand, as it concerns the night span, we have a correlation and, at the same time, $\Delta_{RMSE} > 0.05$ °C. In this case we recommend, when running the analysis to consider an area with a radius ≤ 200 m, the range of radius from 10 m to 200 m where we have the smallest RMSEs values and the $\Delta_{RMSE} < 0.05$ °C.

Regarding our main hypothesis, influence of the radius, we should first note that correlation does not mean causation. We saw that the radius (varying from 10 m to 1500 m) did not have the same behavior in all cases as increasing or decreasing the error. We

observed negative correlation for December and positive for July and annual data. Furthermore, we had always a correlation in the night span except July TS. Upon thorough consideration of our case study, we have concluded that the selection of a suitable radius should be based on various factors as season, time span and to be careful with the conditions of the measured data. It is important to note that different radii are recommended for different cases such as winter versus summer or day versus night. Additionally, it is crucial to take into account the urban morphology parameters, and the radius should be viewed as a combination of these parameters. Street has also suggested the same in his work [30]. It is worth noting that there is no specific boundary or radius that will result in the lowest error in every case or condition.

5.5.2. UWG behavior and results of intercomparisons

When comparing the predictions of the engine for different periods, but same conditions Figure 66, Figure 67 we observed that the errors vary across the different seasons. The engine results are better estimated for the summer period, in our case the month of July. The finding lines up with the previous case study as Barcelona, Figure 72, where the RMSEs values are 1.42 °C for December and 0.56 °C for July [41]. A comparable conclusion can be seen even in the results of the CAPITOUL case [23], presented in Figure 73.

	MBE	RMSE
December	-1.3	1.42
January	-0.5	0.77
February	0.7	0.86
June	0.1	0.41
July	0.4	0.56
August	0.7	0.79

Figure 72 Statistical results, Raval station, Barcelona [41]

Month	RMSE (K)	MBE (K)
BUBBLE		
Summer	0.9	−0.6
CAPITOUL		
Summer	0.7	0.2
Fall	0.8	−0.1
Winter	1.1	−0.2

Figure 73 Statistical results, BUBBLE and CAPITOUL case study [23]

We identified that there is a variation in errors even when we compared different time spans within the same period and same condition. This variation is evident in Figures 57, 61, and 65. Our analysis revealed that the values of December are overestimated across all time spans, while in July, we have underestimated values during nighttime. These findings are consistent with Hamdi et al.'s study, which reported that in previous

case studies the engine overestimated urban air temperatures during winter's daytime and underestimated the summer's nighttime values [37].

Furthermore, during the daytime, we saw lower RMSEs airport values compared to RMSEs measured, in contrast with the nighttime values. We concluded that the nighttime data goes into more adjustments from the engine to account for the UHI effect, which presents itself more during nighttime.

The estimations also varied depending on the data conditions we compared the simulated values with, which verifies our hypothesis regarding the difference between different conditions. The conditions also depend on the availability of the measured data. When having data measured in building shade they give better results than the one of full sun exposure while comparing. Thus, if there is a possibility or availability to choose between them we would suggest a shading condition. On the other hand, if values that consider different conditions can be found, average values can be derived and compared to the simulated values; this will show a better estimation, as was observed in the July comparison, Figure 68. Nakano also confirms that the UWG gives an average temperature value for an urban area [42].

It is important to note that the rural station, which in our case is the Munich International Airport, is a suitable input station for performing climate analysis for the city of Munich. This is due to its location far from any major geographical features, urban areas, and obstacles. Additionally, we have obtained low RMSEs measured values, particularly during the summer period, where we never exceeded an RMSE value of 1.3 °C. This aligns with the findings of Hamdi et al., who reported that UWG performance error is around 1°C. Moreover, in the same case study they emphasize the importance of the rural station choice. They compared the simulated data and the urban data, considering different rural stations, Figure 74, where we see a high variation with the smallest RMSE being 1.73 °C for the rural station Centre equestre. [37]

Rural Station	RMSE °C	MBE °C
Mondouzil	3.48	−2.24
Meteopole	3.39	−2.22
Centre équestre	1.73	0.02

Figure 74 Statistical results based on 3 rural stations, Carmes [37]

6. Conclusion

This study focused on the radius influence during climate simulations of urban areas. For this purpose, a validation of the Urban Weather Generator model for varying boundaries was performed, by using the dry bulb temperature data. The range of radius considered starts from 10 m to 1500 m.

Bordeauxplatz, Munich, Germany, classified as Local Climate Zone 2 (compact midrise buildings area) was used as the case study. We used Rhino 3D and Grasshopper to model the urban area. In order to mirror the same conditions of the real-life area in our model, we did a site inspection, used available data regarding our case study, and made assumptions based on previous studies.

In order to look more deeply into the radius influence and Urban Weather Generator behavior, for the simulations, we differentiated three different periods, annual, December, and July, and three different time spans, as a whole day, day hours, and night hours. Moreover, we had measured data in different conditions such as building shade, full sun exposure, tree shade, wind protected, and wind exposure; this fact gave us the possibility to simulate and perform comparisons between different conditions as well.

While creating and simulating the model, we faced some limitations, including a simplified model for vegetation evapotranspiration, single surface type consideration, and no water body inclusion from the engine. To overcome the single surface limitation, we calculated the weighted average albedo value of different surfaces. Moreover, in this study we have considered a constant sensible anthropogenic heat value to not have another varying parameter.

Comparisons were performed by considering different statistical approaches, as Mean Absolute Error, Linear Regression Analysis, Mean Bias Error and most important Root Mean Square Error. The comparisons were made between simulated and measured dry bulb temperature values in place and between simulated and airport values. We have done these comparisons for each radius, time span and period span that we have simulated. After having the results of comparison for each radius, specifically Root Mean Square Errors, we looked if there is any pattern with the variation of the radius and

performed a Spearman's correlation between the radius and the obtained error. Furthermore, intercomparisons were made for same conditions but different period, and different conditions but same period.

We compiled our findings related to the radius behavior and influence into a table. These results were scaled for Local Climate Zone 2, and may be considered as a guideline. It may be beneficial for other studies, and in the same time as a starting point for future researches to look into the radius influence in other cities with Local Climate Zone 2 or analyses regarding other local climate zones. Another subject for future studies, is to look into the simulated relative humidity data and the radius influence, or generally the comparison of simulated relative humidity data to measured values. To our knowledge there are no previous studies. We did not consider the relative humidity data, since we did not have the appropriate form of the measured values.

We believe that the key findings of this study will help urban planners to appropriately design and simulate urban areas considering urban climate analysis and other stakeholders to make the right decisions.

Key findings:

- Munich International Airport serves as a suitable rural station, this fact will help the urban planners to use it as an input for the climate analysis for the city of Munich.

- Urban Weather Generator is an easy-to-use tool for climate analysis that provides simulated urban dry bulb temperature values with low error rates compared to measured data.

- Errors in dry bulb temperature predictions vary across different time spans and period spans, we suggest urban planners to differentiate between time and period spans for better estimation of urban heat island effect, and carefully look into the conditions of the measured data.

- There is no specific radius/boundary that displays the lowest error in all cases, conditions. This implies that when in doubt about the area size for climate analysis one should consider the period, time span, condition and see the radius as a conglomeration of other urban morphology parameters.

7. List of figures

Figure 1 Representation of spatial scales in climate modeling [28, p. 1615]..... 18
Figure 2 Information exchanged between the four modules of the UWG [23]..... 20
Figure 3 UWG inputs from the urban and reference site environments [42] 22
Figure 4 Methodology scheme..... 26
Figure 5 Period spans, time spans and different conditions used in the study..... 27
Figure 6 Software and tools used in the study 28
Figure 7 CADMAPPER website [48] 29
Figure 8 3D view of the model created with CADMAPPER 29
Figure 9 Model created with Elk and OSM..... 30
Figure 10 3D view of the model from the .stl file 30
Figure 11 3D view of the model after using AntFarm 31
Figure 12 Simplified scheme with DF and UWG tools based on [59]..... 33
Figure 13 Location of the case study, Bordeauxplatz, Munich [84]..... 38
Figure 14 Various land use..... 38
Figure 15 Recreational area 38
Figure 16 Various businesses..... 39
Figure 17 Isar River 39
Figure 18 Top-View Bordeauxplatz, location of i-Buttons devices, P.Stark [87]..... 40
Figure 19 GH Script for area selection..... 40
Figure 20 Area and elements selected automatically, example radius 500 m, FS..... 41
Figure 21 Map of Buildings' age [90]..... 44
Figure 22 Buildings' facades..... 47
Figure 23 Buildings' roof, Bordeauxplatz [84]..... 47
Figure 24 Albedo values for wall and roof [100, p. 33] 47
Figure 25 GH script for assigning buildings' properties, residential example..... 48
Figure 26 Part of the model and the embedded map 49
Figure 27 Terrain division 50
Figure 28 Tree crown curves, from shape file 52
Figure 29 Union of tree crowns as surfaces..... 53
Figure 30 GH script for creating the epw file 54
Figure 31 Properties of reference rural/airport site..... 55
Figure 32 Airport site, model created with the vegetation curves 55
Figure 33 GH script to run the UWG 56
Figure 34 Monthly averages diurnal cycles 2022, Munich..... 58
Figure 35 July monthly-average diurnal cycle, DBT, Munich..... 59
Figure 36 Barcelona Case Study Results (July monthly-average diurnal cycle) [41] .. 59
Figure 37 Singapore Case Study July 2010, Seletar (rural station) [129] 59
Figure 38 January monthly-average diurnal cycle, DBT, Munich..... 60
Figure 39 Barcelona Case Study Results (monthly-average diurnal cycle) [41] 60
Figure 40 Hourly values of DBT for the whole year 2022, simulated..... 61
Figure 41 Hourly DBT values for the whole year 2022, Munich Airport 61
Figure 42 MAE analysis results for July FS, all month hours..... 63
Figure 43 Linear Regression Analysis results for July FS, all month hours 63
Figure 44 MBE analysis results for July FS, all month hours..... 64
Figure 45 RMSE analysis results for July FS, all month hours 64
Figure 46 MAE analysis results for July FS, day hours 65
Figure 47 Linear Regression Analysis results for July FS, day hours..... 65
Figure 48 MBE analysis results for July FS, day hours 66

Figure 49 RMSE analysis results for July FS, day hours 66
Figure 50 MAE analysis results for July FS, night hours..... 67
Figure 51 Linear Regression Analysis results for July FS, night hours 67
Figure 52 MBE analysis results for July FS, night hours..... 68
Figure 53 RMSE analysis results for July FS, night hours 68
Figure 54 RMSE vs Radius in R studio for July FS, all month hours 69
Figure 55 RMSE vs Radius in R studio for July FS, day hours 70
Figure 56 RMSE vs Radius in R studio for July FS, night hours 71
Figure 57 RMSEs measured comparison for different time spans, July FS 72
Figure 58 RMSE analysis results for December FS, all month hours 74
Figure 59 RMSE analysis results for December FS, day hours 75
Figure 60 RMSE analysis results for December FS, night hours 75
Figure 61 RMSEs measured comparison for different time spans, December FS 76
Figure 62 RMSE analysis results for annual FS, all year hours 77
Figure 63 RMSE analysis results for annual FS, day hours..... 77
Figure 64 RMSE analysis results for annual FS, night hours..... 78
Figure 65 RMSEs measured comparison for different time spans, annual FS 79
Figure 66 RMSEs measured comparisons different periods and time spans, FS 80
Figure 67 RMSEs measured comparisons different periods and time spans, BS 80
Figure 68 RMSEs measured comparisons FS, BS, and AV for July 81
Figure 69 RMSEs measured comparisons FS, BS for December..... 82
Figure 70 RMSEs measured comparisons FS, BS for annual data 82
Figure 71 Summary of the results, case study Bordeauxplatz Munich, guideline..... 84
Figure 72 Statistical results, Raval station, Barcelona [41] 85
Figure 73 Statistical results, BUBBLE and CAPITOUL case study [23] 85
Figure 74 Statistical results based on 3 rural stations, Carmes [37] 86
Figure 75 Munich district division [91] 93
Figure 76 MAE analysis results for annual FS, all year hours..... 98
Figure 77 Linear Regression Analysis results for annual FS, all year hours 98
Figure 78 MBE analysis results for annual FS, all year hours..... 99
Figure 79 MAE analysis results for annual FS, day hours 99
Figure 80 Linear Regression Analysis results for annual FS, day hours 100
Figure 81 MBE analysis results for annual FS, day hours 100
Figure 82 MAE analysis results for annual FS, night hours 100
Figure 83 Linear Regression Analysis results for annual FS, night hours 101
Figure 84 MBE analysis results for annual FS, night hours 101
Figure 85 RMSE vs Radius in R studio for annual data FS, all year hours 102
Figure 86 RMSE vs Radius in R studio for annual data FS, day hours 102
Figure 87 RMSE vs Radius in R studio for annual data FS, night hours 103
Figure 88 MAE analysis results for December FS, all month hours 104
Figure 89 Linear Regression Analysis results for December FS, all month hours..... 104
Figure 90 MBE analysis results for December FS, all month hours 105
Figure 91 MAE analysis results for December FS, day hours..... 105
Figure 92 Linear Regression Analysis results for December FS, day hours 106
Figure 93 MBE analysis results for December FS, day hours..... 106
Figure 94 MAE analysis results for December FS, night hours..... 107
Figure 95 Linear Regression Analysis results for December FS, night hours 107
Figure 96 MBE analysis results for December FS, night hours..... 108
Figure 97 RMSE vs Radius in R studio for December FS, all month hours 108
Figure 98 RMSE vs Radius in R studio for December FS, day hours 109
Figure 99 RMSE vs Radius in R studio for December FS, night hours 109
Figure 100 RMSE analysis results for annual BS, all year hours 110

Figure 101 RMSE analysis results for annual BS, day hours 110
Figure 102 RMSE analysis results for annual BS, night hours 111
Figure 103 RMSE analysis results for December BS, all month hours 112
Figure 104 RMSE analysis results for December BS, day hours..... 112
Figure 105 RMSE analysis results for December BS, night hours..... 113
Figure 106 RMSE analysis results for July BS, all month hours 114
Figure 107 RMSE analysis results for July BS, day hours..... 114
Figure 108 RMSE analysis results for July BS, night hours..... 115
Figure 109 RMSE analysis results for July TS, all month hours 115
Figure 110 RMSE analysis results for July TS, day hours..... 116
Figure 111 RMSE analysis results for July TS, night hours..... 116
Figure 112 RMSE analysis results for July WE, all month hours 117
Figure 113 RMSE analysis results for July WE, day hours..... 118
Figure 114 RMSE analysis results for July WE, night hours..... 118
Figure 115 RMSE analysis results for July WP, all month hours 119
Figure 116 RMSE analysis results for July WP, day hours..... 119
Figure 117 RMSE analysis results for July WP, night hours..... 120
Figure 118 RMSE analysis results for July AV, all month hours 120
Figure 119 RMSE analysis results for July AV, day hours..... 121
Figure 120 RMSE analysis results for July AV, night hours..... 121
Figure 121 Detailed summary of the results, Bordeauxplatz Munich 122

8. List of tables

Table 1 Variations of each parameter for the test 34
Table 2 Buildings' function and assigned available programs 42
Table 3 Buildings' functions and their floor to floor heights 43
Table 4 Buildings' construction year and their U values of the glass 46
Table 5 Albedo values variation for different surface types 50
Table 6 Urban morphology parameters combinations for different radii 62
Table 7 Summary of Spearman's correlation and Δ_{RMSE} for July FS 69
Table 8 Overheating hours and tropical nights (in terms of hours) July FS 73
Table 9 Summary of Spearman's correlation and Δ_{RMSE} December FS 76
Table 10 Summary of Spearman's correlation and Δ_{RMSE} annual FS 78
Table 11 Year of construction for residential buildings Munich, until 2011 [91] 94
Table 12 Year of construction for residential buildings Munich, until 2011 [91] 94
Table 13 Different MFH with their window to wall ratio based on [93] 95
Table 14 Urban morphology parameters combinations for different radii, FS 97
Table 15 Summary of Spearman's correlation and Δ_{RMSE} annual BS 111
Table 16 Summary of Spearman's correlation and Δ_{RMSE} December BS 113
Table 17 Summary of Spearman's correlation and Δ_{RMSE} July BS 115
Table 18 Summary of Spearman's correlation and Δ_{RMSE} July TS 117
Table 19 Summary of Spearman's correlation and Δ_{RMSE} July WE 118
Table 20 Summary of Spearman's correlation and Δ_{RMSE} July WP 120
Table 21 Summary of Spearman's correlation and Δ_{RMSE} July AV 121

Appendix A

A.1 Buildings' properties

Buildings' age

The map below in Figure 75, shows the areas related to the two data sets provided by the Statistics Office of Munich, where the blue marked show the small area while the red one is related to the second data set of the greater area.

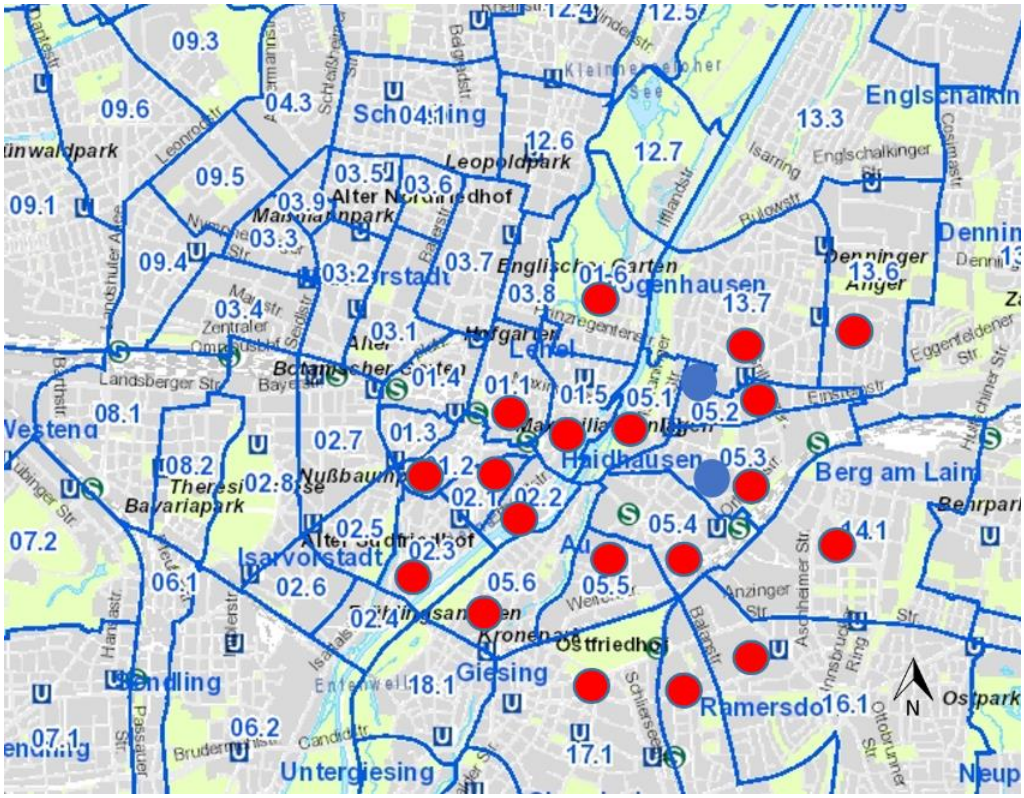

Figure 75 Munich district division [91]

From Table 11 is shown that nearly 79% of the buildings is built before 1980.

Table 11 Year of construction for residential buildings Munich, until 2011 [91]

District division 05.3 & 05.2

Year of construction	Number of buildings
Before 1919	8390
1919-1949	665
1950-1959	1717
1960-1969	1333
1970-1979	398
1980 - 1989	1500
1990-1999	872
2000-2005	260
2006 and later	732

From table 12 is presented that nearly 81% of the buildings is built before 1980.

Table 12 Year of construction for residential buildings Munich, until 2011 [91]

District division 01.1, 01.2, 01.5, 01.6, 02.1, 02.2, 02.3, 05.1, 05.2, 05.3, 05.4, 05.5, 05.6, 13.6, 13.7, 14.1, 16.1, 16.2, 17.1

Year of construction	Number of buildings
Before 1919	29469
1919-1949	17136
1950-1959	29583
1960-1969	23859
1970-1979	12736
1980 - 1989	11837
1990-1999	7135
2000-2005	3500
2006 and later	3394

For each area of consideration we see that the majority of the buildings is built before 1980.

Glass ratio calculation for the residential buildings

Table 13 Different MFH with their window to wall ratio based on [93]

Typology of buildings	Type	WWR
MFH_A	MFH	0.14542713
MFH_B	MFH	0.38410959
MFH_C	MFH	0.22612351
MFH_D	MFH	0.21800866
MFH_E	MFH	0.24986758
MFH_F	MFH	0.24791667
MFH_G	MFH	0.22671259
MFH_H	MFH	0.21037687
MFH_I	MFH	0.23684967
MFH_J	MFH	0.18297998
K.MFH - Referenz-Ausführung EnEV 2009	MFH	0.24426732
L.MFH - Referenz-Ausführung EnEV 2009	MFH	0.24426732
K.MFH - Variante 001	MFH	0.24426732
L.MFH - Variante 001	MFH	0.24426732
Average value		**0.23610297**

A.2 Creation of the terrain

Albedo values

Many papers consider different albedo values depending on the condition and age of asphalt. A study focused on the parameters that affect the albedo state that the variation is 0.1-0.15 for the aged and 0.05 for the new one [104]. We must mention that the component of the terrain in the DF, suggests that the fresh asphalt has a value of 0.1

which opposes the values of the previous study. According to a research that investigates the effect of ground albedo on the performance of PV systems shows asphalt's albedo as 0.05-0.2, where they decide to consider 0.2 [105]. Also in a case study in Rome it was observed a value of 0.2 [106]. In the Kempten case study a value of 0.20225 was used [88]. This value was an average of the results from a case study in Illinois, USA, asphalt of different ages were considered. We could not find any information about the age of the asphalt for our area, but during our site analysis we observed that it was not freshly poured so the value cannot be 0.1. On the other side we considered that it goes under a periodic maintenance, so we decide for a value of 0.2 for the asphalt.

Concrete was part of the pavements, near the buildings and also part of the railways, so is important to consider also its albedo value. Analysis done in the field shows that the new concrete pavement can have a value of 0.35 - 0.4, as it ages it darkens and the values can drop to 0.2-0.3 [108]. Another study shows that concrete values vary 0.3-0.32 [109]. Since we did not know the age of our concrete we decided to have a value of 0.3. The same value was chosen for the railway.

The green, grass surfaces usually have an albedo value varying from 0.18-0.22 [109] a previous study shows a variation of 0.16-0.27 [110] we decided to use 0.2 albedo value in our case study.

As it concerns the soil's albedo it varies from 0.05-0.5 from dark, wet to light, dry [111]. Since we are modeling for the summer months, we will consider a value of 0.4 for the soil.

Important elements of the terrain are also sidewalks (mostly out of concrete material), moreover some squares and roads are composed of sanpietrini, of conventional and permeable pattern. The sanpietrini has an albedo value of 0.4, [106] and since we consider side walks, and sanpietrini squares and roads all together we took an average value of 0.35 (concrete 0.3 and sanpietrini 0.4).

In the terrain division, we also took in consideration the water areas. For high solar elevation locations (northern hemisphere) the albedo of water varies 0.03-0.1 [112], in another study the albedo value is considered to be 0.05 [113], since Munich is also on the northern hemisphere we take an average value of 0.065.

Appendix B

B.1 Urban morphology parameters combination for different radii

Table 14 shows the combinations of the urban morphology parameters for the full sun condition (the center of the radius matches the position of the i-Button device for full sun condition). For other conditions, the combinations are different especially for small radius, while for greater ones they tend to be comparable and similar.

Table 14 Urban morphology parameters combinations for different radii, FS

Radius	Average Height	Footprint Density	Facade to site	Tree cover	Grass cover	Terrain's albedo
10 m	3 m	0	0.03	0	0.98	0.202
30 m	22.4 m	0.02	0.47	0.18	0.34	0.211
50 m	19.6 m	0.24	1.65	0.27	0.28	0.223
100 m	15.8 m	0.39	2.14	0.49	0.32	0.234
200 m	15.8 m	0.38	2.03	0.56	0.37	0.251
300 m	15.2 m	0.4	1.99	0.54	0.3	0.256
400 m	14.5 m	0.36	1.41	0.53	0.31	0.258
500 m	14.3 m	0.32	1.55	0.46	0.28	0.263
600 m	14.4 m	0.31	1.41	0.46	0.28	0.265
700 m	14.7 m	0.31	1.44	0.47	0.29	0.264
800 m	14.9 m	0.31	1.39	0.48	0.3	0.264
900 m	15.1 m	0.31	1.33	0.49	0.32	0.262
1000 m	15.3 m	0.3	1.25	0.52	0.34	0.259
1100 m	15.4 m	0.29	1.17	0.51	0.35	0.255
1200 m	15.4 m	0.27	1.11	0.54	0.36	0.251
1300 m	15.4 m	0.27	1.11	0.55	0.36	0.25
1400 m	15.4 m	0.27	1.1	0.57	0.37	0.249
1500 m	15.3 m	0.27	1.1	0.59	0.38	0.248

B.2 Comparison results

Annual FS

Whole day hours, other statistical analyses

Figure 76 presents MAE values, for different radii. The error of the comparison between simulated and airport are higher compared to the error between simuated and measured for all the radii. On the other hand, we see that the error is higher in the small radii values, but the highest difference between MAEs measured is of 0.05 ºC negligible since the engine displays one digit after the decimal point.

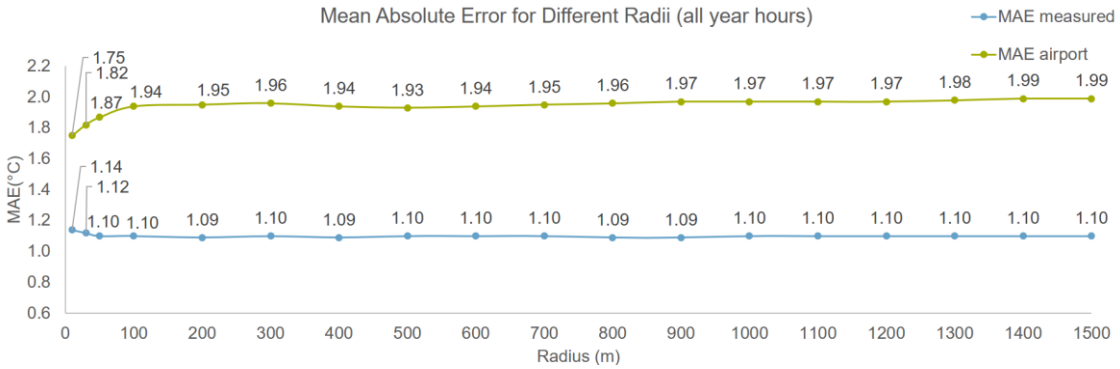

Figure 76 MAE analysis results for annual FS, all year hours

As can be seen in figure 77, there is no change happening to R^2 measured as radius changes, while R^2 airport changes.

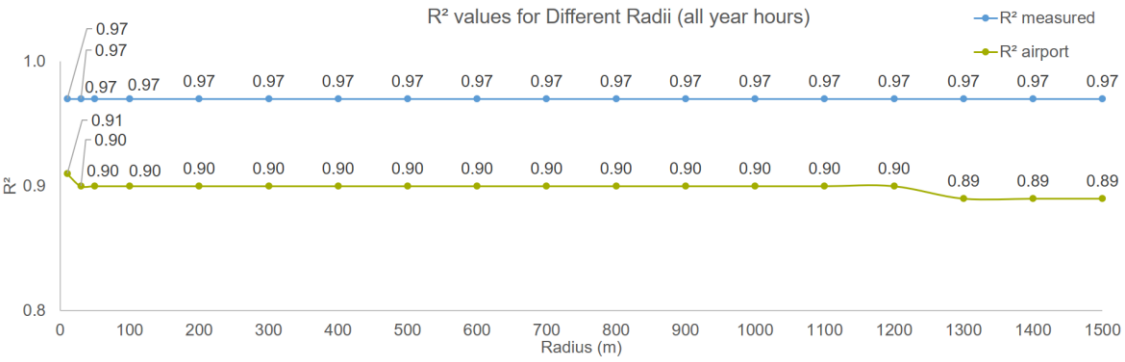

Figure 77 Linear Regression Analysis results for annual FS, all year hours

As it concerns the MBE analysis we see an overestimation of the engine compared to the measured values, and underestimation compared to airport values, displayed in Figure 78.

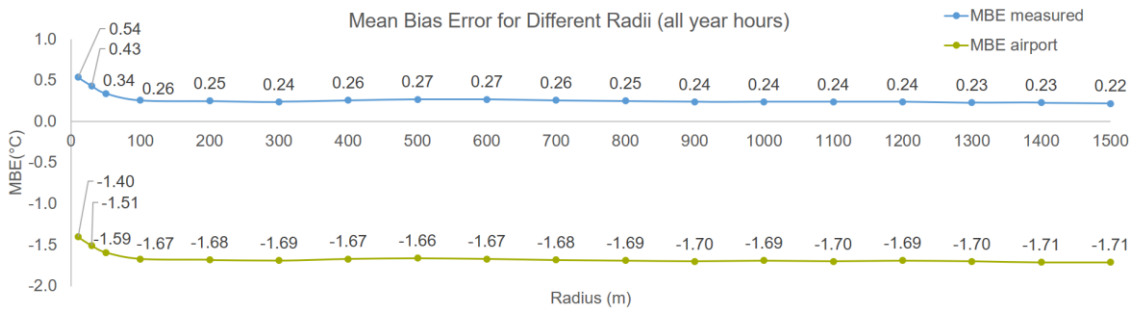

Figure 78 MBE analysis results for annual FS, all year hours

Day hours, other statistical analyses

Referring to Figure 79, the highest difference in MAEs measured values is 0.06 ºC .No pattern is observed. MAE measured is higher compared to MAE airport.

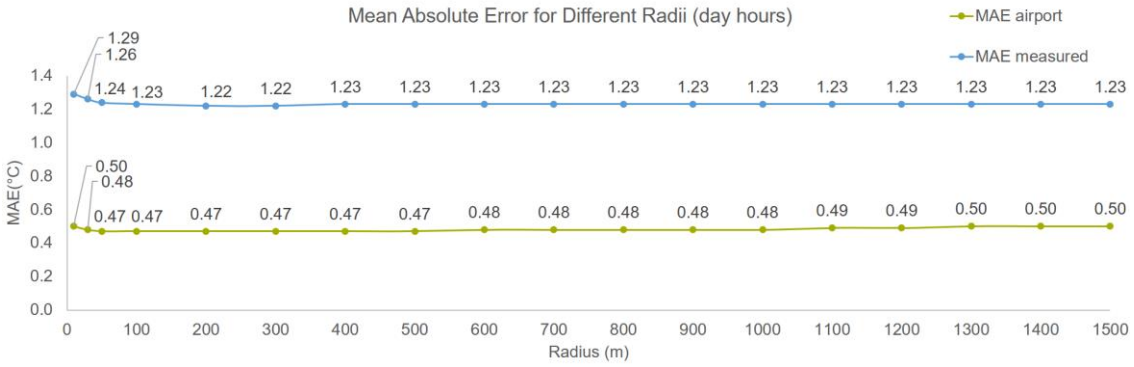

Figure 79 MAE analysis results for annual FS, day hours

As it concerns the regression analysis, we see constant values throughout the change of radius being it for the measured or also airport consideration. There is a better fitting of the simulated data to airport data, Figure 80.

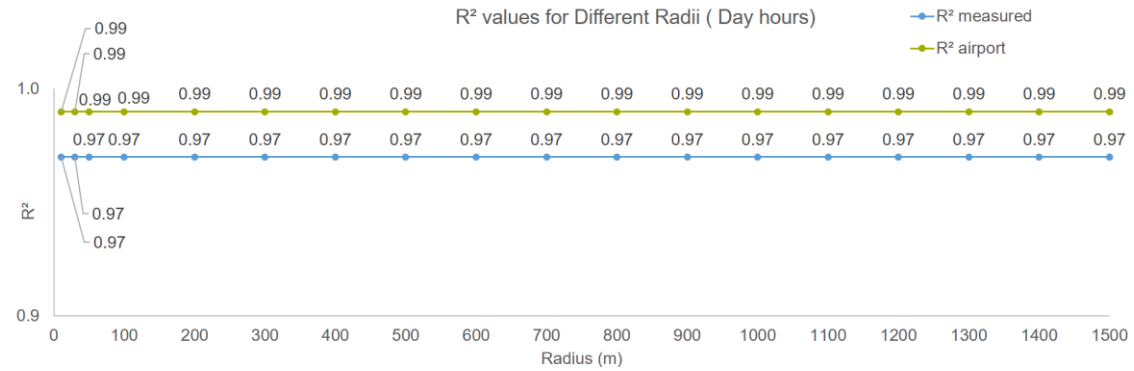

Figure 80 Linear Regression Analysis results for annual FS, day hours

Regarding the MBE analysis, Figure 81, we observe an overestimation of the engine regarding the measured and airport values.

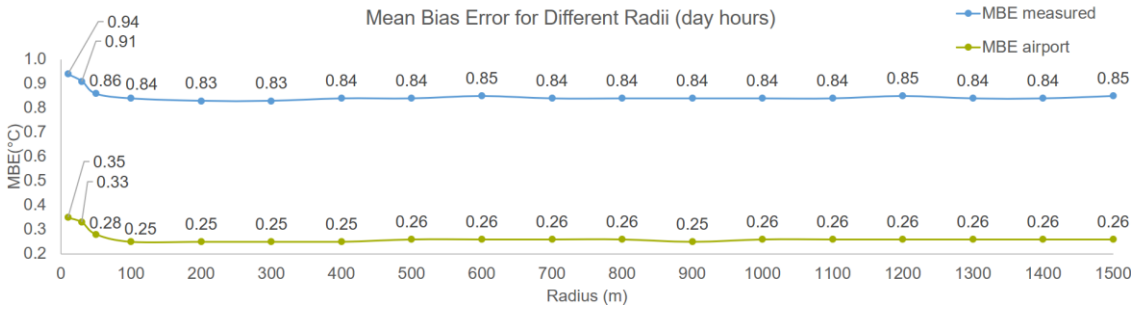

Figure 81 MBE analysis results for annual FS, day hours

Night hours, other analyses

The MAE related to measured data is lower at lower radii, the highest difference between these errors is of 0.04 ºC, which is considered as negligible. As it concerns the MAE airport it is higher for the night span compared to MAE measured.

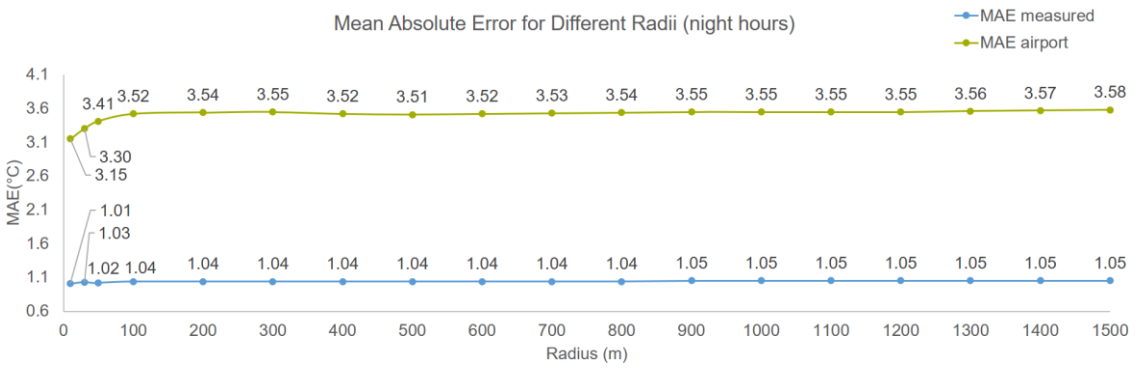

Figure 82 MAE analysis results for annual FS, night hours

The regression analysis in Figure 83, displays a constant value for the simulated data fitting the measured data, a high value of 0.97. As it concerns R^2 airport there is only the 10 m radius that displays a higher value. Again we see that the R^2 of airport is lower than the fitting of the measured data.

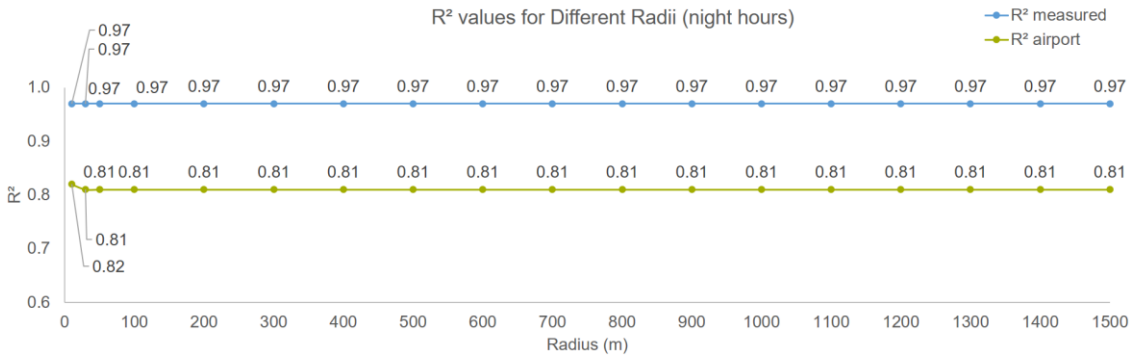

Figure 83 Linear Regression Analysis results for annual FS, night hours

Regarding MBE, Figure 84, we see mostly an underestimation (except small radii values) of the engine towards the measured and the airport values.

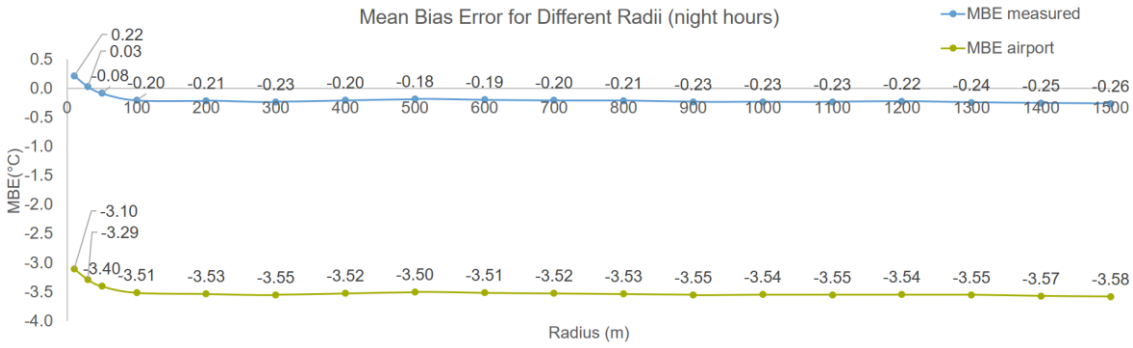

Figure 84 MBE analysis results for annual FS, night hours

Spearman's correlation between RMSE and radius for whole day, day and night

When considering the whole day hours, looking into the RMSE measured and performing the correlation in regard to the radius, there was no correlation found. The graph from R studio is shown in Figure 85.

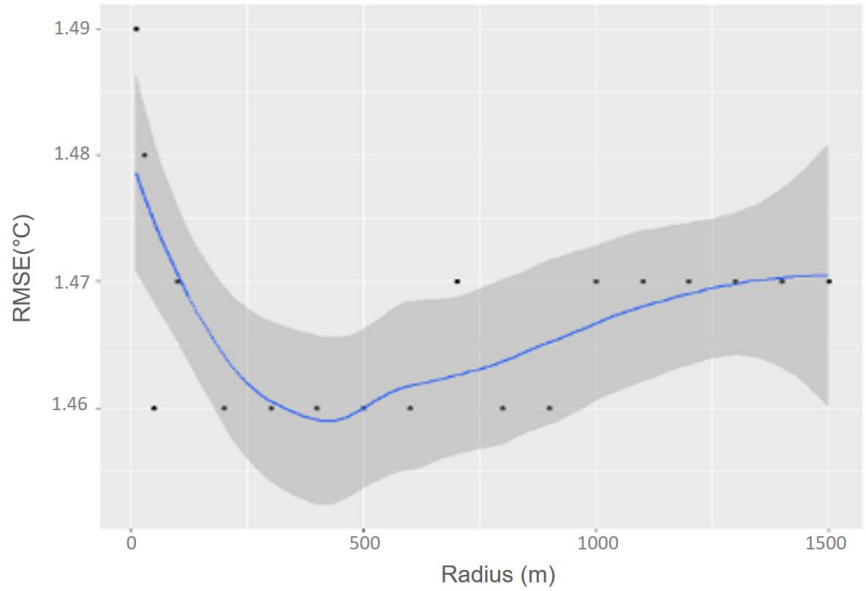

Figure 85 RMSE vs Radius in R studio for annual data FS, all year hours

For the day time hours, there was again no correlation. In this case the difference between RMSEs measured values is 0.08 ºC (1.71 ºC -1.63 ºC), we see the highest drop (in terms of errors) happens in the small radii, for this reason we suggest a radius of at least 50 m for this condition, time span and period. The graph from R studio is shown in Figure 86.

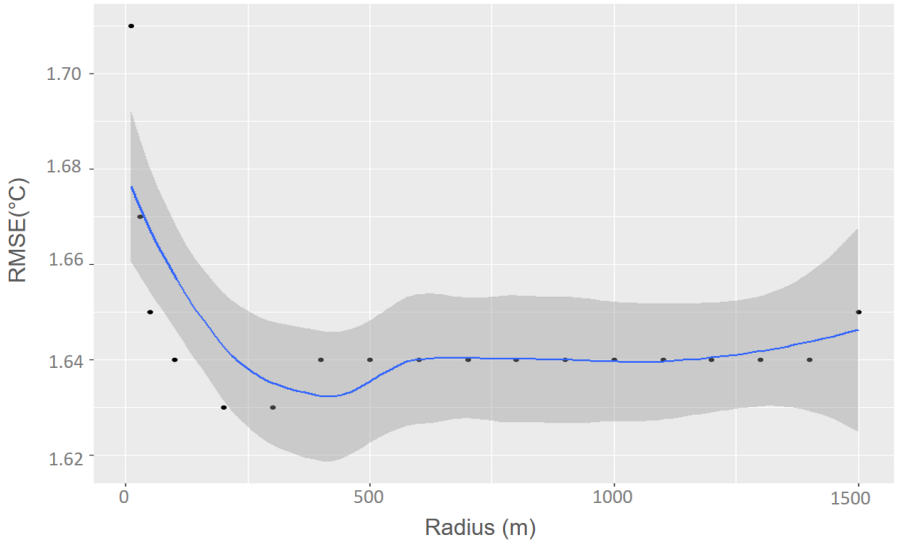

Figure 86 RMSE vs Radius in R studio for annual data FS, day hours

As it concerns the night span we found a correlation between the radius and the RMSE measured values with a correlation coefficient ρ = 0.95 and significance level of the

correlation p-value = 1.43 x 10^{-9}. On the other hand we also have a difference of 0.08 ºC (1.40 ºC -1.32 ºC). For this case we suggest to run the simulations with an urban area of a radius equal or smaller than 100 m. Figure 87 displays the graph obtained in R studio.

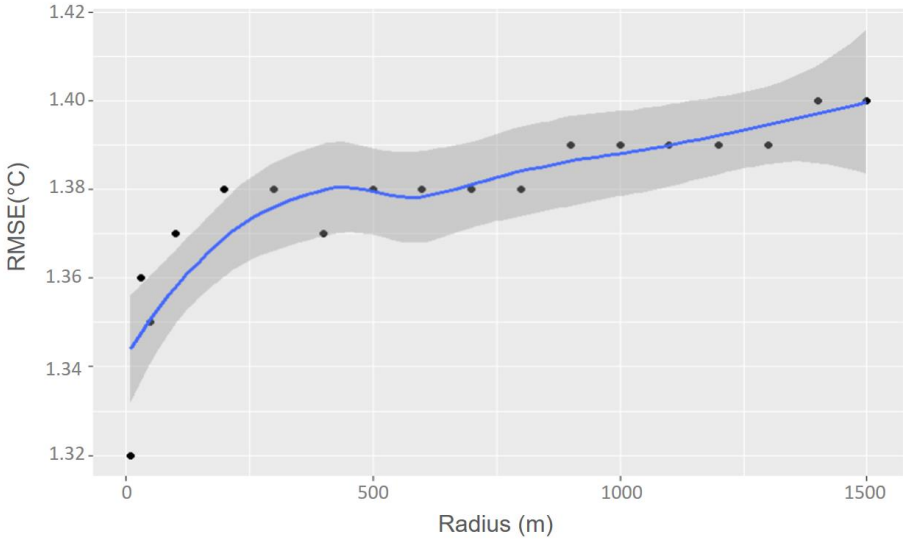

Figure 87 RMSE vs Radius in R studio for annual data FS, night hours

December FS

Whole day hours, other analyses

The highest MAEs measured values are observed for small radii values, as shown in Figure 88. We can see a decreasing pattern. The highest difference in error is of 0.25 ºC (1.2 ºC – 0.95 ºC). The variation can also be seen for the MAE of the airport when we have small radii values. We also see that the error of simulated-measured is higher than the MAE of simulated-airport.

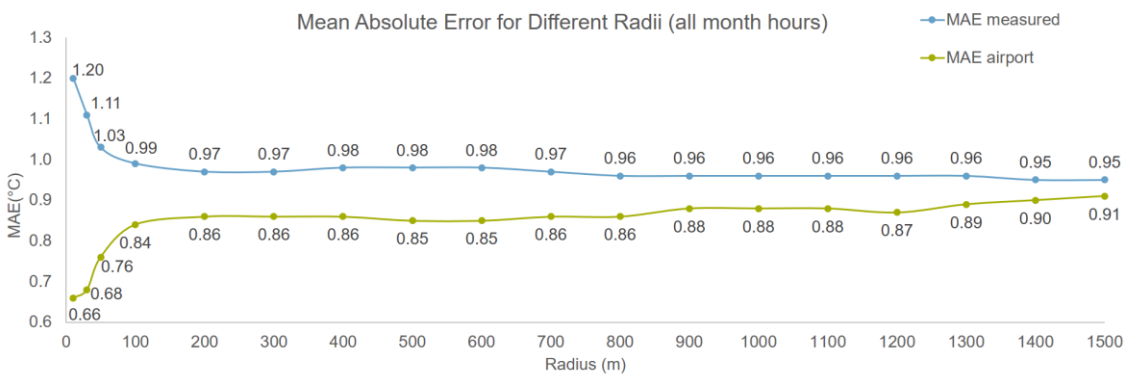

Figure 88 MAE analysis results for December FS, all month hours

Figure 89 presenting the regression analysis for whole day hours for December, displays that nearly all of the radius are related to the same R^2 measured value of 0.94, except some deviation where a smaller value of 0.93 is seen at the radius of 100 m and 300 m. Also the values of the airport are comparable to the R^2 related to measured data.

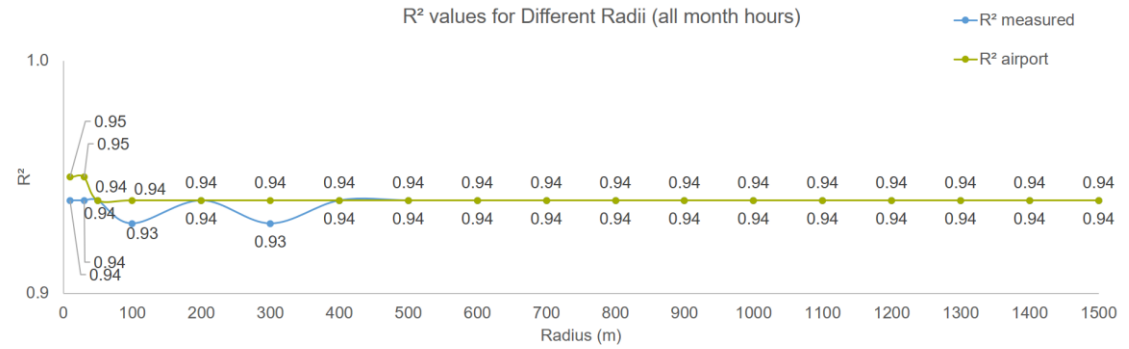

Figure 89 Linear Regression Analysis results for December FS, all month hours

Referring to Figure 90, the mean bias error shows an overestimation of the engine values to the measured data, while for the airport we see an underestimation.

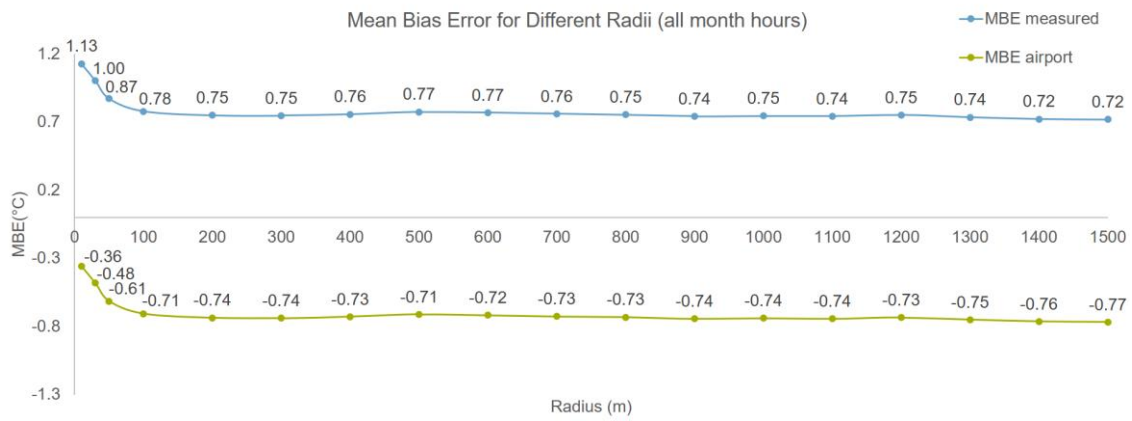

Figure 90 MBE analysis results for December FS, all month hours

Day hours, other analyses

Figure 91 displays higher MAE measured for the small radii values, while after 100 m the highest difference of MAEs measured is small as 0.01 ºC – 0.02 ºC.

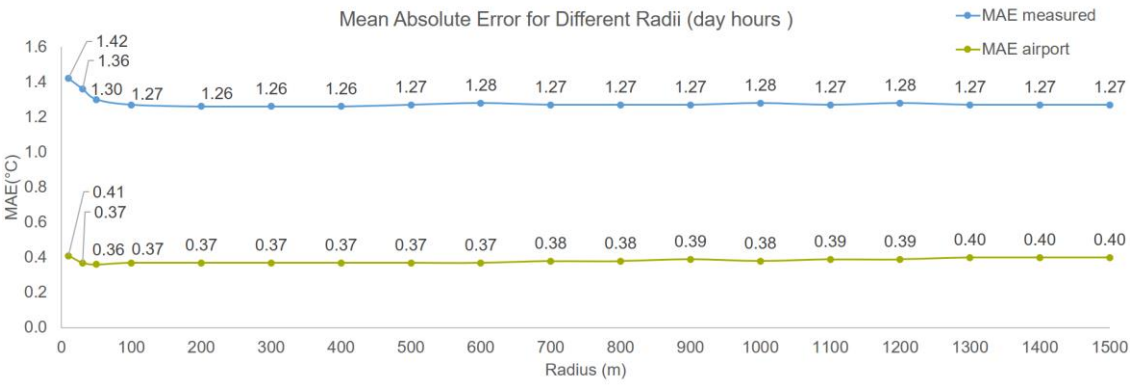

Figure 91 MAE analysis results for December FS, day hours

For the regression analysis, there is no pattern of increasing or decreasing in the simulated-measured comparison, we see that the values are 0.92 or 0.93, while the R^2 related to the airport stays constant and shows a better fitting of the simulated data to the airport, Figure 92.

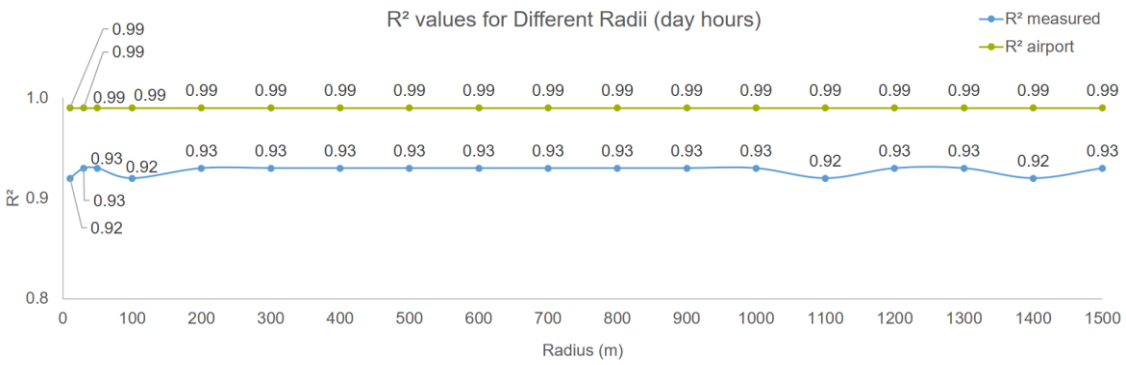

Figure 92 Linear Regression Analysis results for December FS, day hours

For day hours the simulated values are overestimated compared to the measured data, and an overestimation is observed compared to the airport values as well, as displayed in Figure 93.

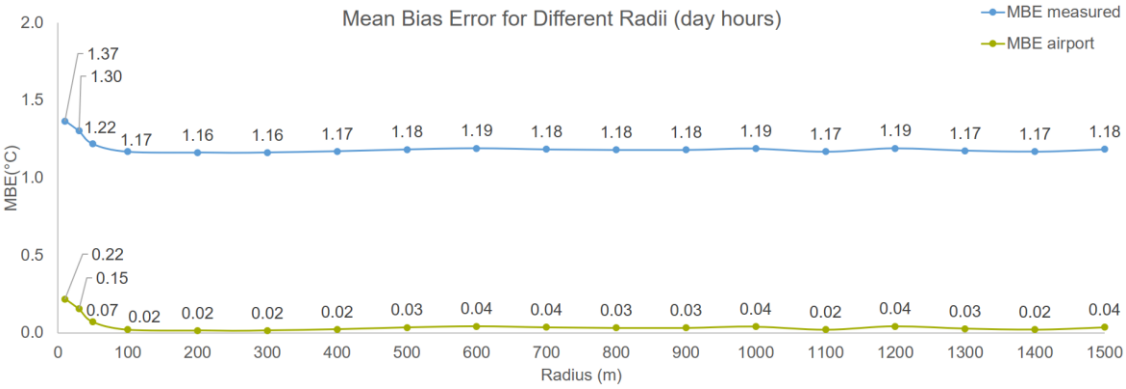

Figure 93 MBE analysis results for December FS, day hours

Night hours, other analyses

We observed that MAE measured is higher compared to MAE airport for small radii, while the opposite happens after the radius of 100 m, as shown in Figure 94. As it concerns the highest difference of MAEs measured is 0.28°C, and the highest drop is seen from 10 m to 100 m with 0.23°C.

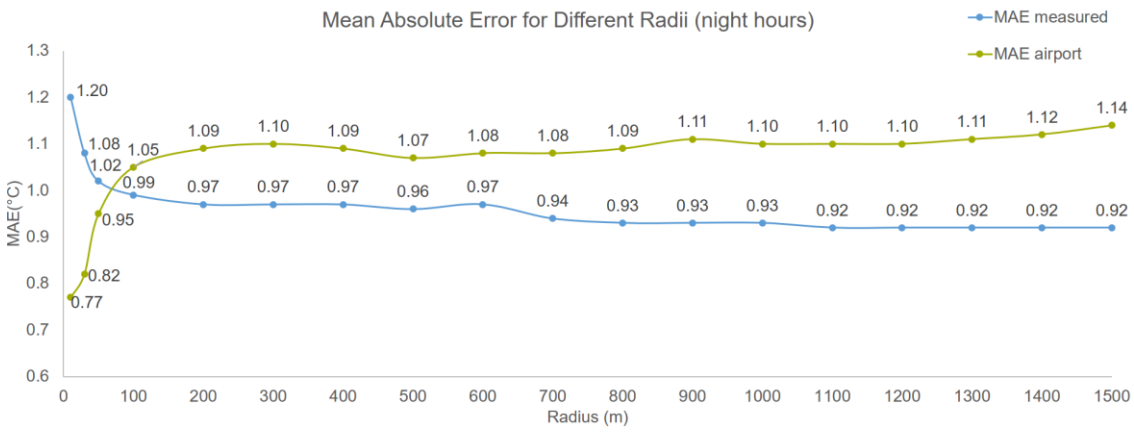

Figure 94 MAE analysis results for December FS, night hours

Upon conducting regression analysis, shown in Figure 95, it was observed that the R^2 value related to measured data remains constant with varying radii. Therefore, no conclusions can be drawn from this analysis in this case. On the other hand we see a variation on the airport values.

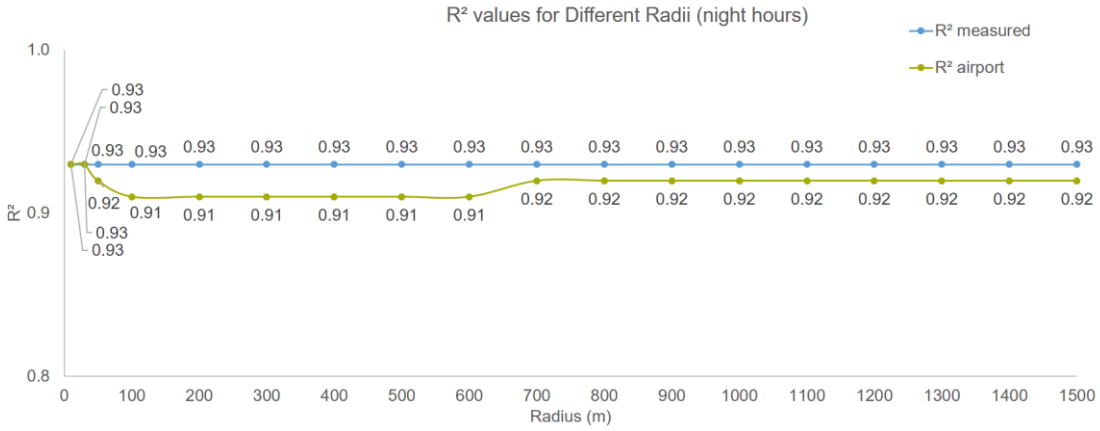

Figure 95 Linear Regression Analysis results for December FS, night hours

In Figure 96, the MBE measured shows an overestimation, and the MBE airport shows an underestimation. We can see as well that for the small radii the MBE measured values are further from zero.

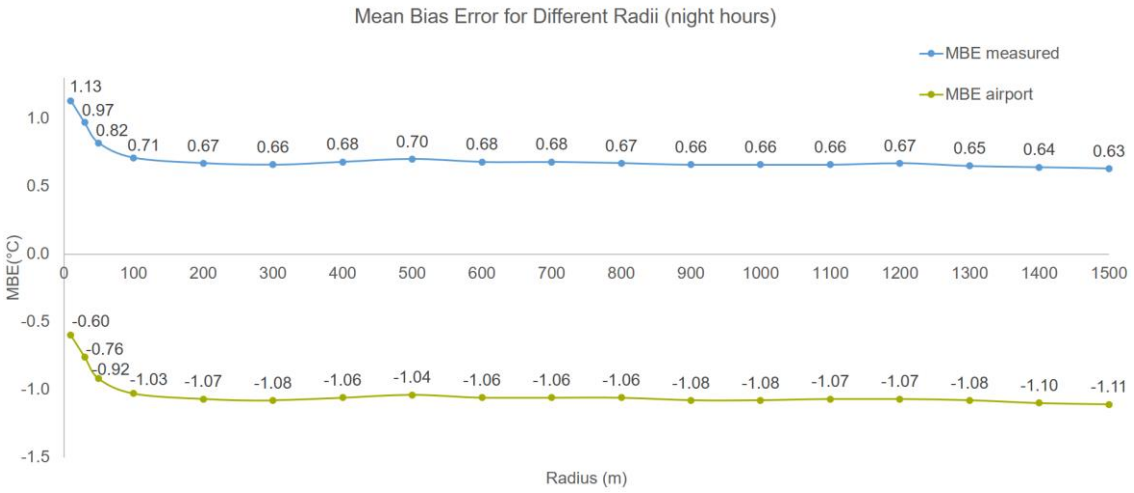

Figure 96 MBE analysis results for December FS, night hours

Spearman's correlation between RMSE and radius for whole day, day, night

For the whole day RMSE regarding simulated-measured comparison, we obtained a negative correlation with a coefficient of ρ = -0.95 and significance p-value = 1.25×10^{-9}, as discussed before we also have a high difference between the RMSE of radii as of 0.23 ºC. Considering the high range of error change and also the correlation, we suggest that in this case a value of at least 200 m should be considered in the design. Figure 97 displays the graph obtained in R studio.

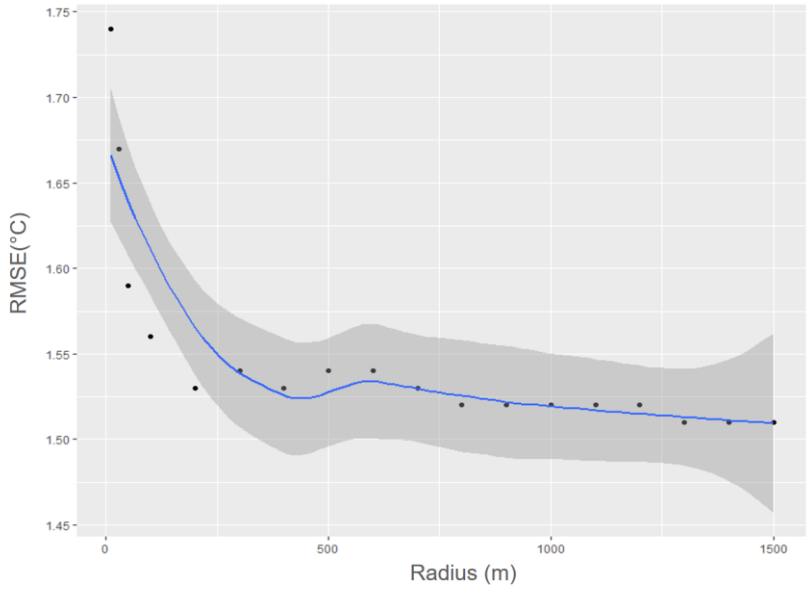

Figure 97 RMSE vs Radius in R studio for December FS, all month hours

For the day hours there was no correlation, but considering the difference of 0.15 ºC between RMSEs values, we suggest using a radius for the model of at least 100 m. Figure 98 displays the graph created in R studio.

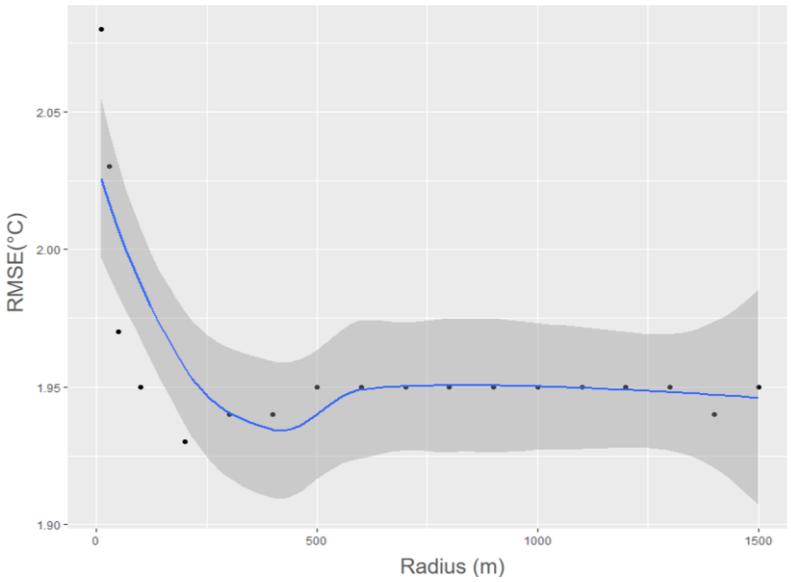

Figure 98 RMSE vs Radius in R studio for December FS, day hours

While at nighttime we see the highest correlation ρ = -0.98 and significance p-value = 2.05×10^{-12}. We already mentioned that it has the highest range of change as 0.29 ºC. and we suggested a radius of at least 700 m.

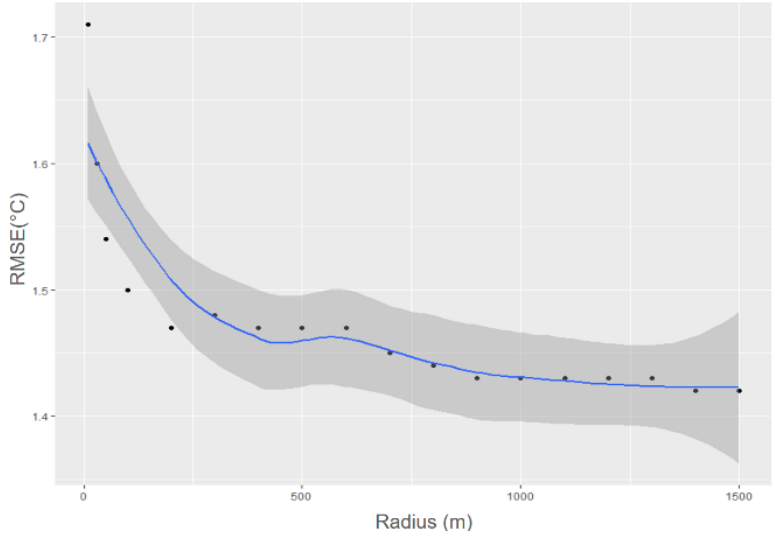

Figure 99 RMSE vs Radius in R studio for December FS, night hours

Annual, BS

Whole day hours, RMSE analysis

Considering Figure 100, the highest difference between RMSEs measured is only 0.03 ºC (1.34 ºC – 1.31 ºC) negligible for our engine. The RMSE measured is smaller than the RMSE airport.

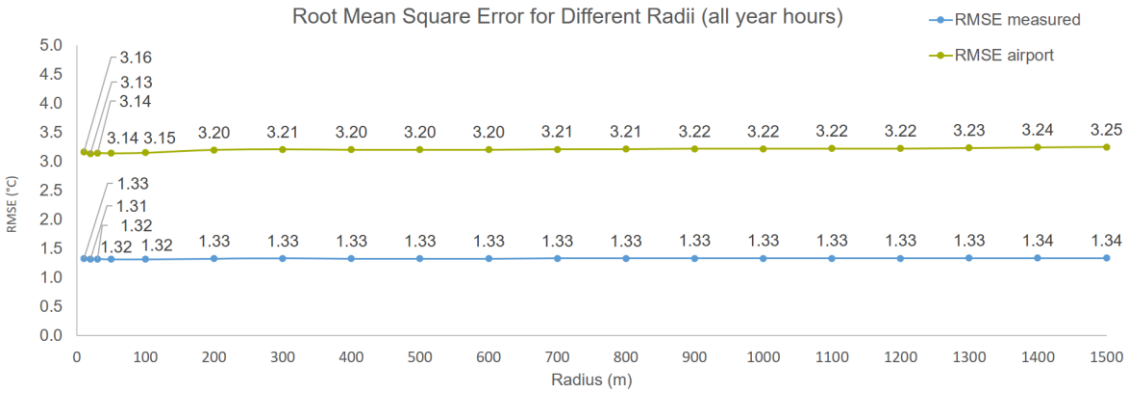

Figure 100 RMSE analysis results for annual BS, all year hours

Day hours, RMSE analysis

As can be observed in Figure 101, for annual day hours the highest RMSE measured difference is of only 0.01 ºC (1.32 ºC – 1.31 ºC), negligible. On the other hand, RMSE measured is higher than the RMSE airport for day hours.

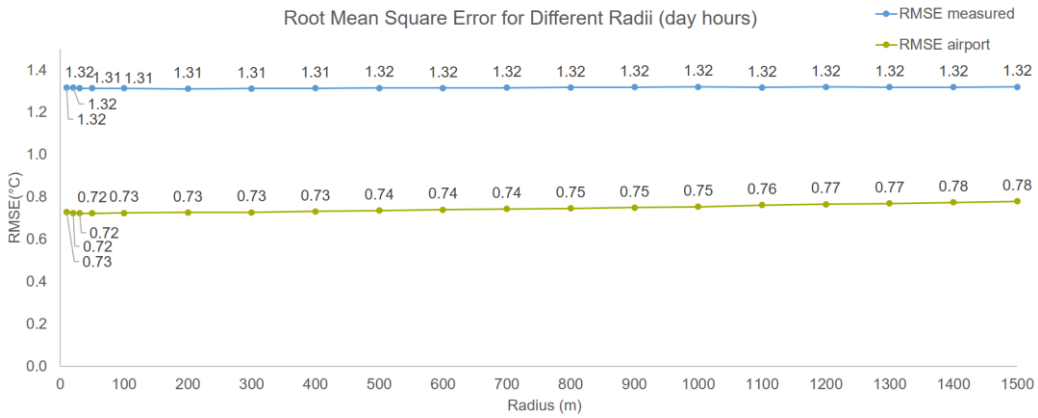

Figure 101 RMSE analysis results for annual BS, day hours

Night hours, RMSE analysis

In Figure 102, we can see that the small radii values, are related to smaller RMSE measured data. The highest difference between RMSEs measured values is 0.05ºC (1.39 ºC – 1.34 ºC). As expected RMSE airport is higher than RMSE measured.

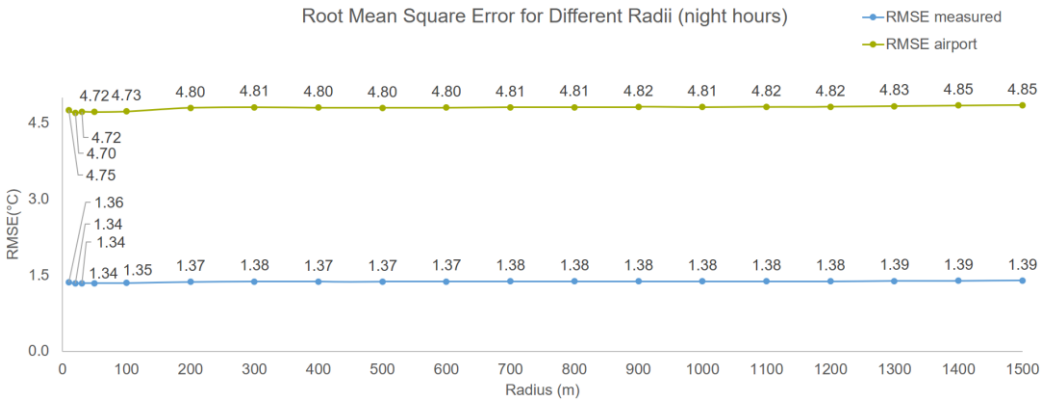

Figure 102 RMSE analysis results for annual BS, night hours

Spearman's correlation between RMSE and radius for whole day, day and night

Table 15 Summary of Spearman's correlation and Δ_{RMSE} annual BS

	Spearman's correlation	**ρ**	**Significance p**	**Δ_{RMSE}**
Whole day hours	Applicable	+0.75	2×10^{-4}	0.03 ºC
Day hours	Not applicable	-	-	0.01 ºC
Night hours	Applicable	+0.92	2.784×10^{-8}	0.05 ºC

December BS

Whole day hours, RMSE analysis

Referring to Figure 103, we observe that the higher errors compared to measured values are in small radii values. The highest difference between these RMSEs values is of 0.08 ºC (1.31 ºC – 1.23 ºC). As expected RMSE airport is higher than RMSE measured.

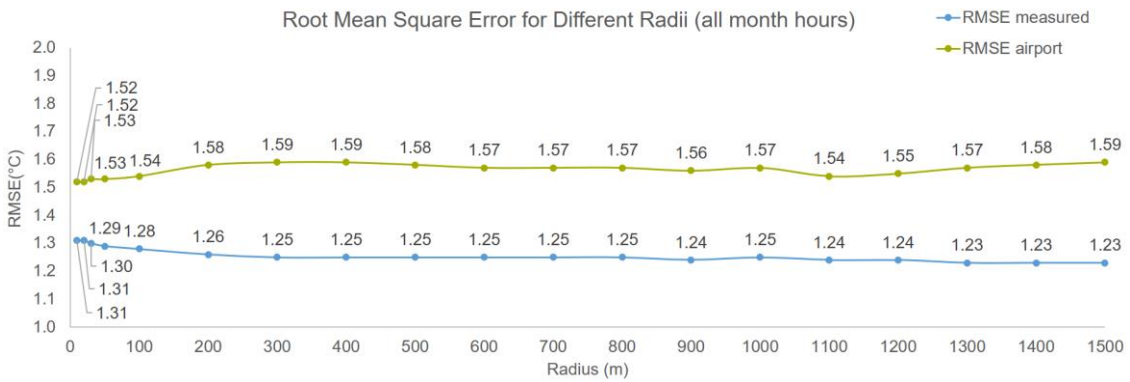

Figure 103 RMSE analysis results for December BS, all month hours

Day hours, RMSE analysis

Regarding the RMSE analysis for day hours, in Figure 104, the highest difference between RMSE measured is 0.04 ºC (1.54 ºC – 1.50 ºC). RMSE airport for the day hours is seen to be smaller compared to RMSE measured.

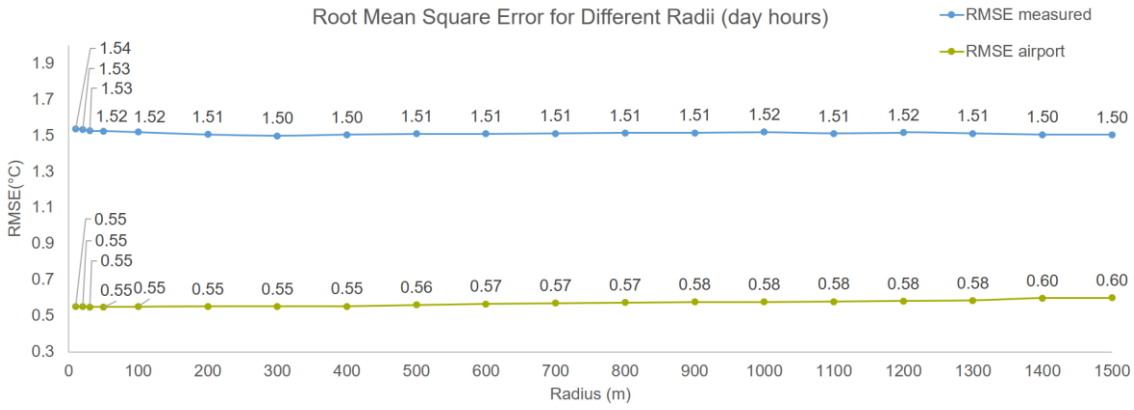

Figure 104 RMSE analysis results for December BS, day hours

Night hours, RMSE analysis

For the night hours we see a higher difference between RMSEs measured, as 0.12 ºC (1.29 ºC - 1.17 ºC). As expected we observe that RMSE airport is smaller than RMSE measured, referring to Figure 105.

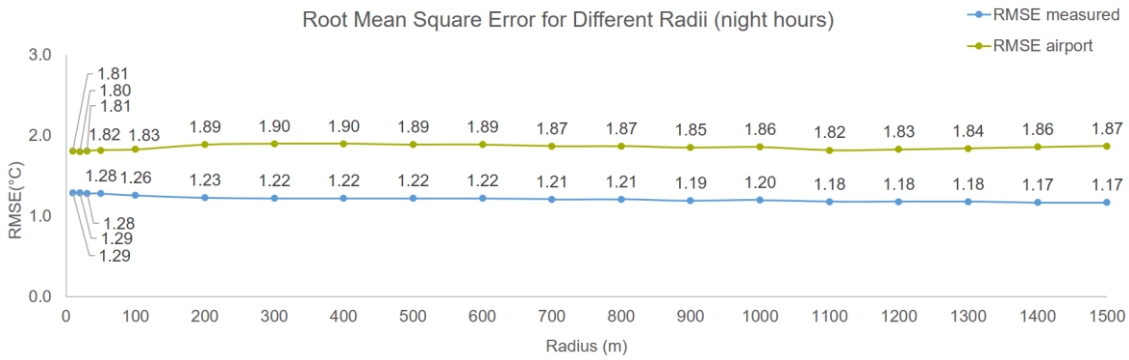

Figure 105 RMSE analysis results for December BS, night hours

Spearman's correlation between RMSE and radius for whole day, day and night

Table 16 Summary of Spearman's correlation and Δ_{RMSE} December BS

	Spearman's correlation	**ρ**	**Significance p**	**Δ_{RMSE}**
Whole day hours	Applicable	-0.96	5.101×10^{-11}	0.08 ºC
Day hours	Not applicable	-	-	0.04 ºC
Night hours	Applicable	-0.99	2.046×10^{-12}	0.12 ºC

July BS

Whole day hours, RMSE analysis

In this case as shown in Figure 106, higher RMSEs measured are related to greater values of radius. The difference between these erros is 0.03 ºC (1.22 ºC - 1.19 ºC) insignificant. Moreover as seen previously in whole day hours analyses the RMSE measured is lower than RMSE airport.

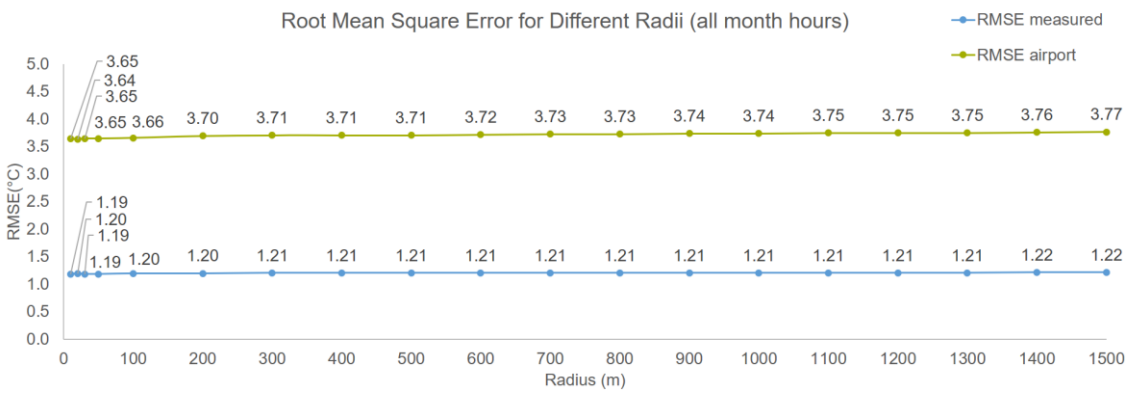

Figure 106 RMSE analysis results for July BS, all month hours

Day hours, RMSE analysis

In day hours analysis Figure 107, smaller errors are observed for small radii values, even though the difference between RMSEs measured data is negligible, 0.02 ºC (1.10 ºC - 1.08 ºC). RMSE airport is lower compared to RMSE measured for all radii values.

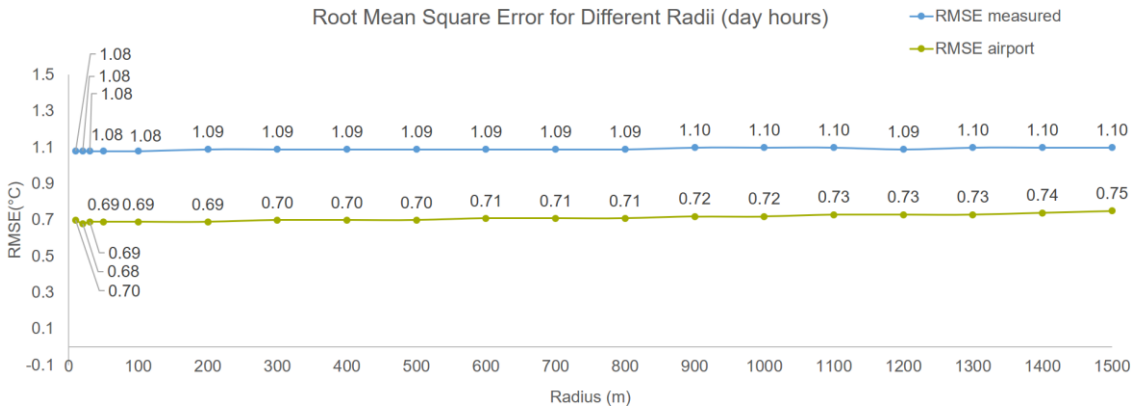

Figure 107 RMSE analysis results for July BS, day hours

Night hours, RMSE analysis

The errors from the comparison to measured data, are higher for high radii values in this case as can be seen in Figure 108, the highest difference between these errors is 0.09 ºC (1.21 ºC - 1.12 ºC). Moreover, we observe very high errors in terms of airport comparison, this may account as the UHI intensity.

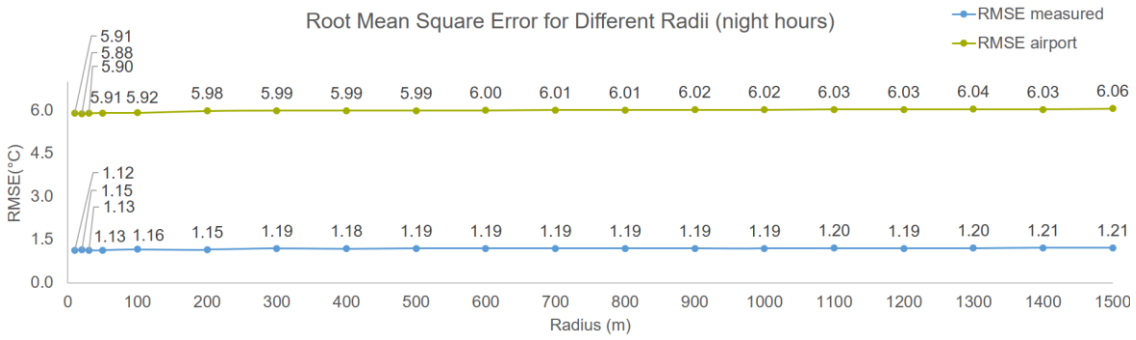

Figure 108 RMSE analysis results for July BS, night hours

Spearman's correlation between RMSE and radius for whole day, day and night

Table 17 Summary of Spearman's correlation and Δ_{RMSE} July BS

	Spearman's correlation	ρ	Significance p	Δ_{RMSE}
Whole day hours	Applicable	+0.88	5.875×10^{-7}	0.03 ºC
Day hours	Applicable	+0.89	1.86×10^{-7}	0.02 ºC
Night hours	Applicable	+0.93	5.612×10^{-9}	0.09 ºC

July TS

Whole day hours, RMSE analysis

Referring to Figure 109, we see that the highest errors of the comparison to measured data are related to small radii values. The highest difference between these errors is 0.03 ºC (1.26 ºC – 1.23 ºC). The errors from the airport comparison are higher for all radii values.

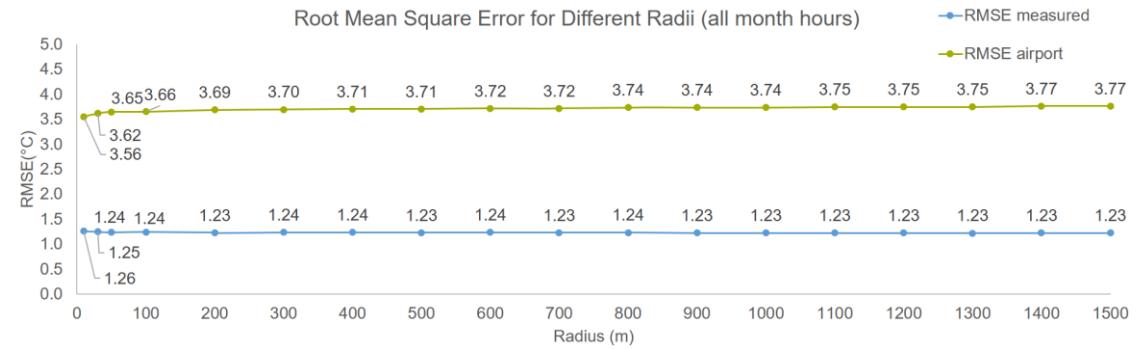

Figure 109 RMSE analysis results for July TS, all month hours

Day hours, RMSE analysis

For day hours the highest difference between RMSEs measured values is 0.02 ºC (1.05 ºC – 1.03 ºC), as shown in Figure 110. There is no pattern observed. As expected for the day span, the RMSE airport values are lower than the RMSE measured.

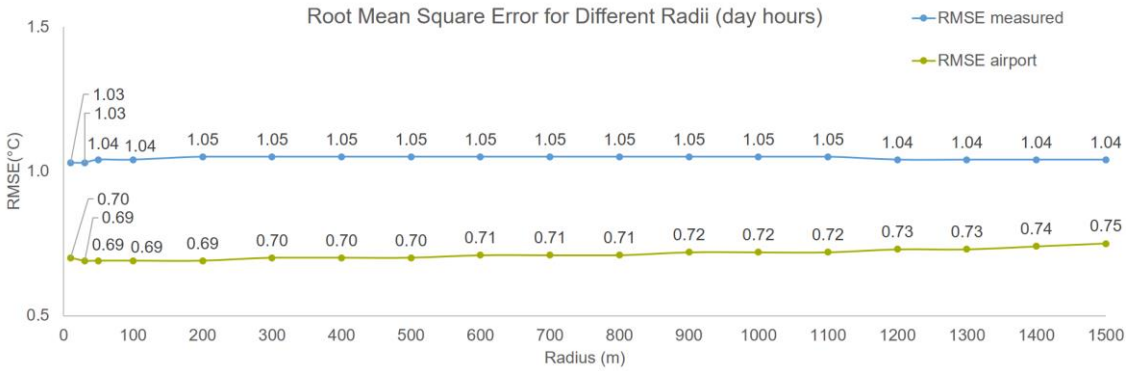

Figure 110 RMSE analysis results for July TS, day hours

Night hours, RMSE analysis

For the night span even in this condition, we have high value of errors regarding the airport accounting for UHI effect, as shown in Figure 111. On the other hand, the RMSEs measured are not patterned and have the highest difference between them as 0.07 ºC (1.11 ºC – 1.04 ºC).

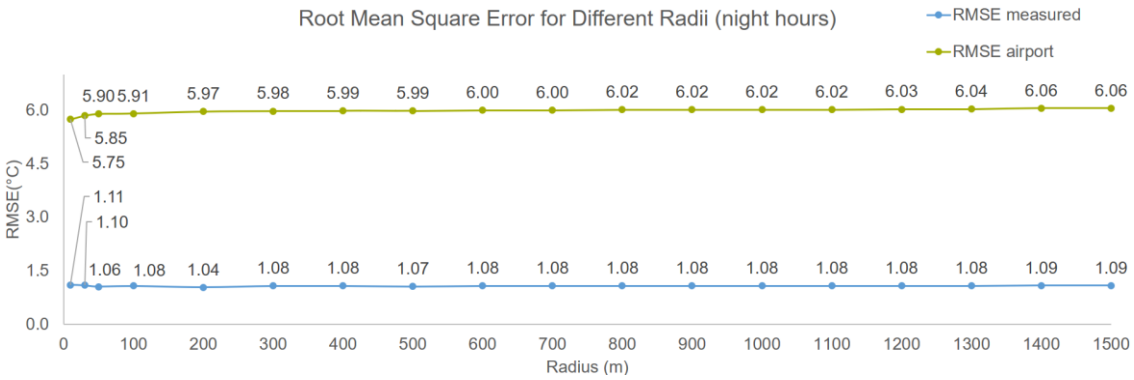

Figure 111 RMSE analysis results for July TS, night hours

Spearman's correlation between RMSE and radius for whole day, day, and night

Table 18 Summary of Spearman's correlation and Δ_{RMSE} July TS

	Spearman's correlation	ρ	Significance p	Δ_{RMSE}
Whole day hours	Not applicable	-	-	0.03 ºC
Day hours	Not applicable	-	-	0.02 ºC
Night hours	Not applicable	-	-	0.07 ºC

July wind exposed condition

Whole day, RMSE analysis

Smaller errors are seen at the small radii values, regarding RMSE measured, as can be seen in Figure 112. The highest difference is 0.07 ºC (1.31 ºC – 1.24 ºC). As it concerns the RMSE airport we see that the values are higher compared to RMSE measured for all radii values.

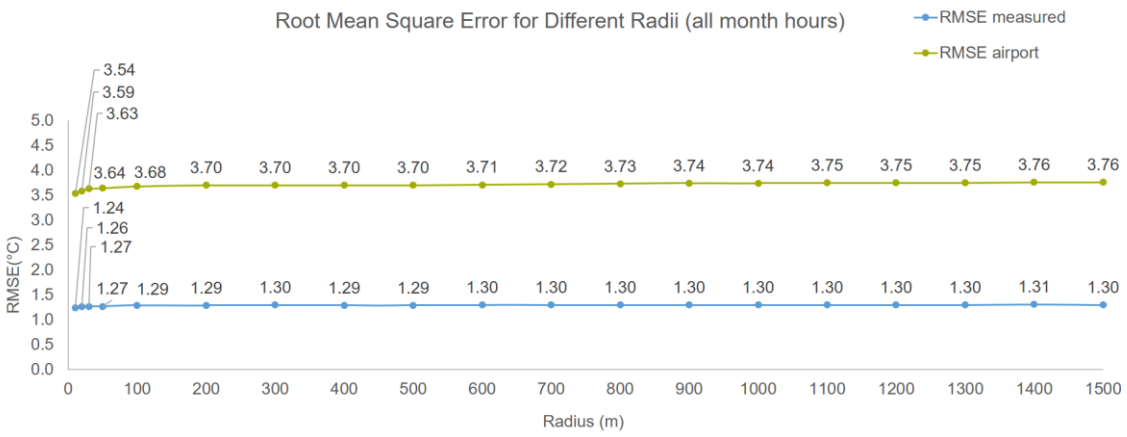

Figure 112 RMSE analysis results for July WE, all month hours

Day hours, RMSE analysis

For the day span the highest difference of the errors related to measured data is 0.06 ºC (1.27 ºC – 1.21 ºC). Again at the day span case, we observe in Figure 113 higher error related to measured data than the errors related to airport data.

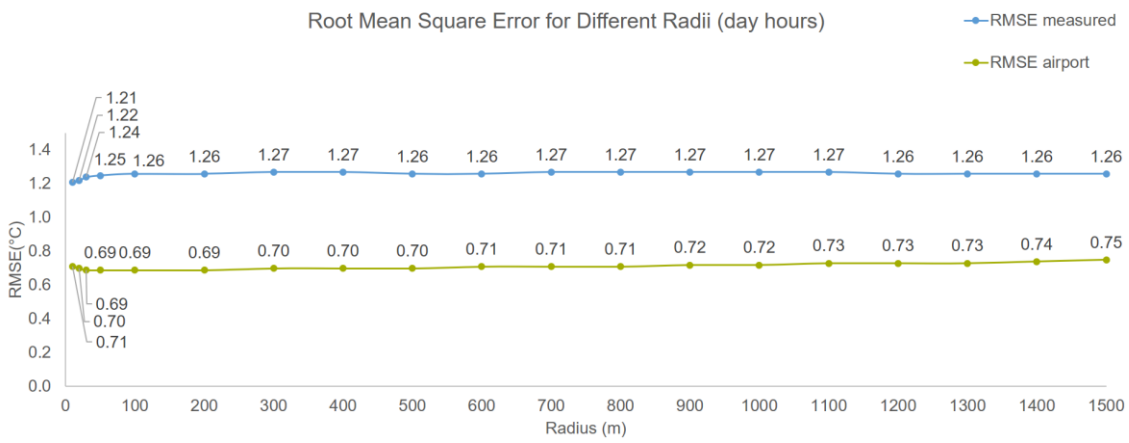

Figure 113 RMSE analysis results for July WE, day hours

Night hours, RMSE analysis

The highest difference between the RMSEs measured values related to night span is 0.15 ºC (1.23 ºC – 1.08 ºC). We also observe lower errors at the small radii values. On the other hand the errors related to the airport values are high, as displayed in Figure 114.

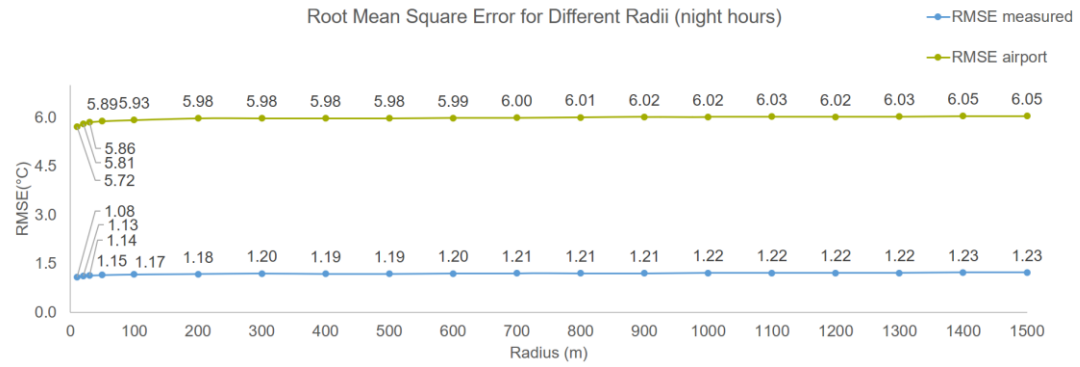

Figure 114 RMSE analysis results for July WE, night hours

Spearman's correlation between RMSE and radius for whole day, day, and night

Table 19 Summary of Spearman's correlation and Δ_{RMSE} July WE

	Spearman's correlation	ρ	Significance p	Δ_{RMSE}
Whole day hours	Applicable	+0.88	5.791×10^{-7}	0.07 ºC
Day hours	Not applicable	-	-	0.06 ºC
Night hours	Not applicable	+0.98	1.597×10^{-14}	0.15 ºC

July WP

Whole day hours, RMSE analysis

In this case, Figure 115, the difference between RMSEs measured values is negligible 0.03 ºC (1.24 ºC – 1.21 ºC). As expected the RMSE airport is higher than RMSE measured.

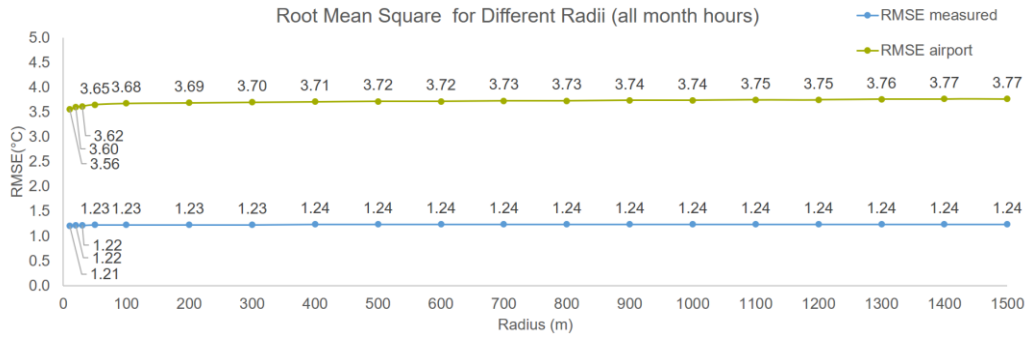

Figure 115 RMSE analysis results for July WP, all month hours

Day hours, RMSE analysis

Again for the day span the difference is negligible as 0.03 ºC (0.91 ºC – 0.88 ºC), Figure 116. As seen previously for the day span RMSE airport is lower than RMSE measured.

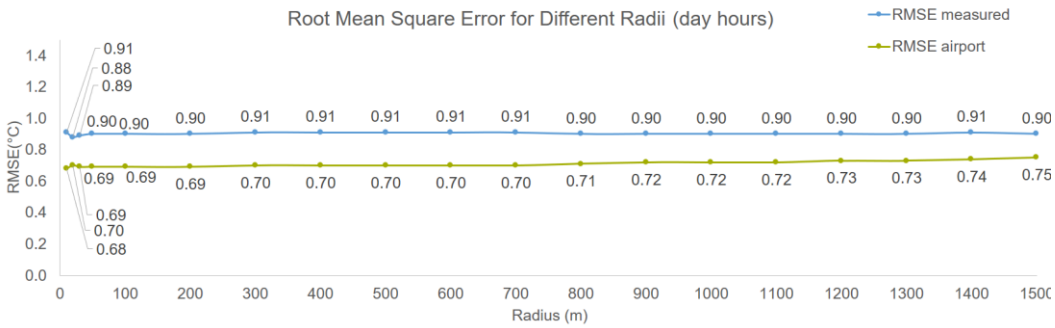

Figure 116 RMSE analysis results for July WP, day hours

Night hours, RMSE analysis

The highest difference between the RMSEs measured for the night span is 0.13 ºC (1.27 ºC – 1.14 ºC) as can be seen in Figure 117. As it concerns the RMSE airport it shows high values, as it may account for the UHI effect.

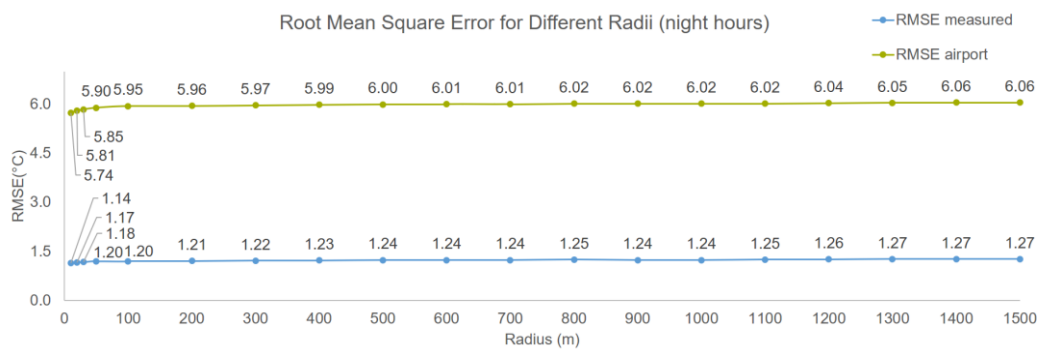

Figure 117 RMSE analysis results for July WP, night hours

Spearman's correlation between RMSE and radius for whole day, day, and night

Table 20 Summary of Spearman's correlation and Δ_{RMSE} July WP

	Spearman's correlation	ρ	Significance p	Δ_{RMSE}
Whole day hours	Applicable	+0.48	0.034	0.03 ºC
Day hours	Not applicable	-	-	0.03 ºC
Night hours	Not applicable	+0.98	1.045×10^{-12}	0.13 ºC

July AV

Whole day hours, RMSE analysis

In the average condition RMSE analysis Figure 116, we see that the highest difference between RMSEs measured is 0.02 ºC (1.18 ºC – 1.16 ºC). For this time span as observed in previous cases RMSE airport is higher than RMSE measured, displayed in Figure 118.

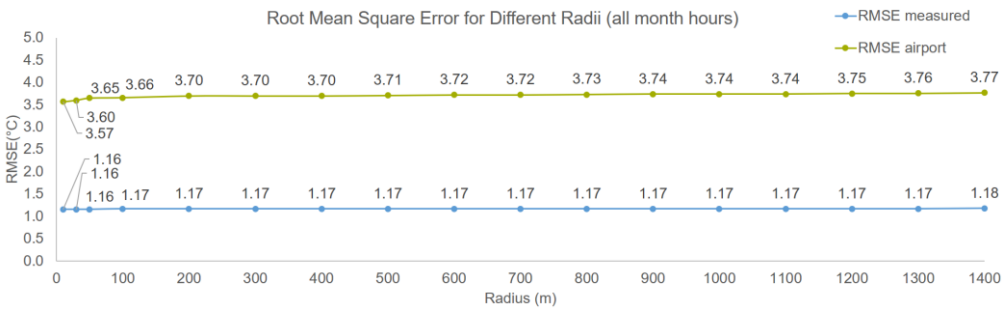

Figure 118 RMSE analysis results for July AV, all month hours

Day hours, RMSE analysis

For the day span again the RMSE airport is lower than RMSE measured, as can be observed in Figure 119. Related to the highest difference of RMSEs measured values, it is 0.03 ºC (0.89 ºC – 0.86 ºC).

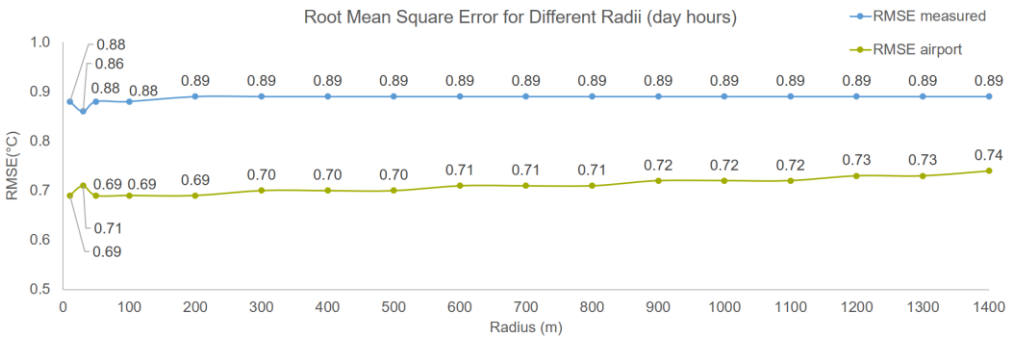

Figure 119 RMSE analysis results for July AV, day hours

Night hours, RMSE analysis

For the night span, Figure 120, the highest difference for the errors related to measured data is 0.08 ºC (1.17 ºC – 1.09 ºC). The error is lower for small radii values. As it concerns the RMSE related to airport it is higher than RMSE measured.

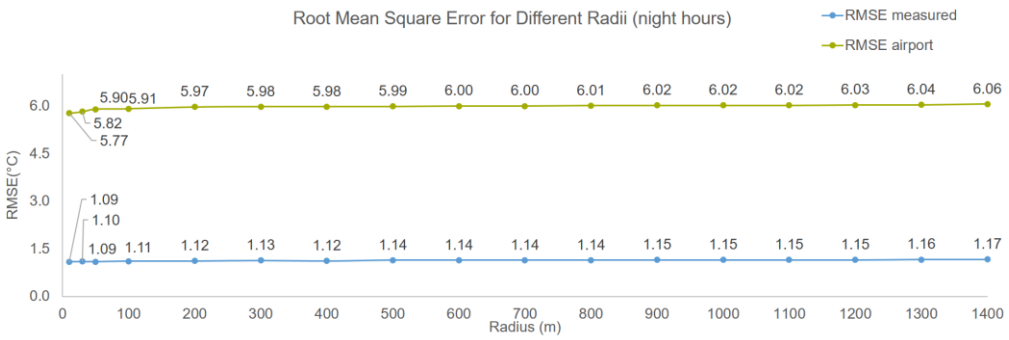

Figure 120 RMSE analysis results for July AV, night hours

Table 21 Summary of Spearman's correlation and Δ_{RMSE} July AV

	Spearman's correlation	**ρ**	**Significance p**	**Δ_{RMSE}**
Whole day hours	Applicable	+0.74	6×10^{-4}	0.02 ºC
Day hours	Applicable	+0.73	8×10^{-4}	0.03 ºC
Night hours	Applicable	+0.98	9.096×10^{-12}	0.08 ºC

B.3 Detailed summary of the results

	Annual		December		July					
	BS	FS	BS	FS	BS	FS	TS	WP	WE	AV
Whole Day	+ 0.03	0 0.03	- 0.08 Rs ≥ 200m	- 0.23 Rs ≥ 200 m	+ 0.03	0 0.02	0 0.03	+ 0.03	+ 0.07 Rs ≤ 50 m	+ 0.02
Day	0 0.01	0 0.08 Rs ≥ 50 m	0 0.04	0 0.15 Rs ≥100 m	+ 0.02	0 0.04	0 0.02	0 0.03	0 0.06 Rs ≤ 50 m	+ 0.03
Night	+ 0.05	+ 0.08 Rs ≤ 100 m	- 0.12 Rs ≥ 900 m	- 0.29 Rs ≥ 700 m	+ 0.09 Rs ≤ 200 m	+ 0.09 Rs ≤ 100 m	0 0.07 Rs= 50 m; 200 m	+ 0.13 Rs ≤ 30 m	+ 0.15 Rs <30 m	+ 0.08 Rs ≤ 200 m

Spearman correlation → 0 no correlation; + positive correlation; - negative correlation

Range of Change for RMSE → ≤ 0.05 insignificant; > 0.05 significant

Radius suggested → Rs

Figure 121 Detailed summary of the results, Bordeauxplatz Munich

9. References

[1] B. Bera, S. Chinta, D. A. Mahajan, A. Sailaja, and R. Mahajan, "Urbanization and Its Impact on Environmental Sustainability: A Comprehensive Review," 1006-7043, Aug. 2023.

[2] B. Venditti, *This chart shows the impact rising urbanization will have on the world*: World Economic Forum, 2022. [Online]. Available: https://www.weforum.org/agenda/2022/04/global-urbanization-material-consumption/

[3] The World Bank, *Advancing Climate Action and Resilience through an Urban Lens.* [Online]. Available: https://www.worldbank.org/en/topic/urbandevelopment/brief/climate-action-through-an-urban-lens

[4] United Nations, "World Urbanization Prospects The 2018 Revision," Department of Economic and Social Affairs, 2019.

[5] European Comission, *Buildings and construction.* [Online]. Available: https://single-market-economy.ec.europa.eu/industry/sustainability/buildings-and-construction_en (accessed: Jan. 17 2024).

[6] Deutscher Wetterdienst, *The weather in Germany – Year 2022*, 2022. [Online]. Available: https://www.dwd.de/EN/press/press_release/EN/2022/20221230_the_weather_in_germany_in_year_2022.pdf?__blob=publicationFile&v=4

[7] M. Ichimura, "ASIA-PACIFIC FORUM FOR ENVIRONMENT AND DEVELOPMENT EXPERT MEETING," PFED3/EM/03/Doc.5, Jan. 2003.

[8] L. Zhao *et al.,* "Interactions between urban heat islands and heat waves," *Environ. Res. Lett.*, vol. 13, no. 3, p. 34003, 2018, doi: 10.1088/1748-9326/aa9f73.

[9] R. J. Klein, S. Huq, F. Denton, T. E. Downing, and R. G. Richels, "Inter-relationships between adaptation and mitigation," 745-777, 2007.

[10] F. Banihashemi, R. Reitberger, and W. Lang, "Investigating Urban Heat Island and Vegetation Effects Under the Influence of Climate Change in Early Design Stages," in *Proceedings of the 27th Conference on Computer Aided Architectural Design Research in Asia (CAADRIA) [Volume 2]*, Sydney, Australia, 2022, pp. 679–688.

[11] A. Mueller, *Urban Development in Germany: Experiences in Framing the Urban Future*. Singapore: Springer, Singapore, 2020. [Online]. Available: https://link.springer.com/chapter/10.1007/978-981-15-3738-7_14

[12] TUM, *Research Training Group 2679 - Urban Green Infrastructure.* [Online]. Available: https://www.gs.tum.de/en/grk/urban-green-infrastructure/ (accessed: Feb. 11 2024).

[13] L. Bande *et al.,* "Validation of UWG and ENVI-Met Models in an Abu Dhabi District, Based on Site Measurements," *Sustainability*, vol. 11, no. 16, p. 4378, 2019, doi: 10.3390/su11164378.

[14] T. R. Oke, "CITY SIZE AND THE URBAN HEAT ISLAND," *Atmospheric Environment*, vol. 7, pp. 769–779, 1973.

[15] A. El Hibaoui, M. Essaaidi, and Y. Zaz, Eds., *Proceedings of 2019 7th International Renewable and Sustainable Energy Conference (IRSEC)*. Piscataway, NJ: IEEE, 2019. [Online]. Available: https://ieeexplore.ieee.org/servlet/opac?punumber=9067801

[16] US EPA, *Learn About Heat Islands | US EPA.* [Online]. Available: https://www.epa.gov/heatislands/learn-about-heat-islands#_ftn1 (accessed: Jan. 17 2024).

[17] J. Gregory, H. Azarijafari, and A. Logan, *Urban Heat Islands.* [Online]. Available: https://climate.mit.edu/explainers/urban-heat-islands (accessed: Jan. 17 2024).

[18] I. D. Stewart and T. R. Oke, "Local Climate Zones for Urban Temperature Studies," *Bulletin of the American Meteorological Society*, vol. 93, no. 12, pp. 1879–1900, 2012, doi: 10.1175/BAMS-D-11-00019.1.
[19] K. Hibbard *et al.,* "Ch. 10: Changes in Land Cover and Terrestrial Biogeochemistry. Climate Science Special Report: Fourth National Climate Assessment, Volume I," 2017.
[20] K. Ward, S. Lauf, B. Kleinschmit, and W. Endlicher, "Heat waves and urban heat islands in Europe: A review of relevant drivers," *The Science of the total environment*, 569-570, pp. 527–539, 2016, doi: 10.1016/j.scitotenv.2016.06.119.
[21] S. W. Kim and R. D. Brown, "Urban heat island (UHI) intensity and magnitude estimations: A systematic literature review," *The Science of the total environment*, vol. 779, p. 146389, 2021, doi: 10.1016/j.scitotenv.2021.146389.
[22] D. Erlström, "Outdoor thermal comfort in Drottninghög, Helsingborg: A study on the effects of urban densification in a warmer climate," Bachelor, Department of Physical Geography and Ecosystem Science, Lund University, Sweden, 2020.
[23] B. Bueno, L. Norford, J. Hidalgo, and G. Pigeon, "The urban weather generator," *Journal of Building Performance Simulation*, vol. 6, no. 4, pp. 269–281, 2012, doi: 10.1080/19401493.2012.718797.
[24] M. Santamouris, *Minimizing energy consumption, energy poverty and global and local climate change in the built environment: Innovating to zero : casualties and impacts in a zero concept world*. Amsterdam: Elsevier, 2019. [Online]. Available: https://www.sciencedirect.com/science/book/9780128114179
[25] N. Singh, S. Singh, and R. K. Mall, "Chapter 17 - Urban ecology and human health: implications of urban heat island, air pollution and climate change nexus," in *Urban Ecology: Emerging Patterns and Social-Ecological Systems*, P. Singh, P. Verma, A. S. Raghubanshi, and R. Singh, Eds.: Elsevier, 2020, pp. 317–334. [Online]. Available: https://www.sciencedirect.com/science/article/pii/B9780128207307000173
[26] F. Teichmann, C. M. Baumgartner, A. Horvath, M. Luisser, and A. Korjenic, "Simulation of urban microclimate with uhiSolver: software validation using simplified material data," *Ecol Process*, vol. 10, no. 1, 2021, doi: 10.1186/s13717-021-00336-y.
[27] P. A. Mirzaei and F. Haghighat, "Approaches to study Urban Heat Island – Abilities and limitations," *Building and Environment*, vol. 45, no. 10, pp. 2192–2201, 2010, doi: 10.1016/j.buildenv.2010.04.001.
[28] Y. Toparlar, B. Blocken, B. Maiheu, and G. van Heijst, "A review on the CFD analysis of urban microclimate," *Renewable and Sustainable Energy Reviews*, vol. 80, pp. 1613–1640, 2017, doi: 10.1016/j.rser.2017.05.248.
[29] D. B. Crawley, "Estimating the impacts of climate change and urbanization on building performance," *Journal of Building Performance Simulation*, vol. 1, no. 2, pp. 91–115, 2008, doi: 10.1080/19401490802182079.
[30] M. A. Street, "Comparison of Simplified Models of Urban Climate for Improved Prediction of Building Energy Use in Cities," Master of Science in Building Technology, Massachusetts Institute of Technology, Massachusetts, USA, 2013.
[31] T. Fink and K. Reinhard, Eds., *Integrated Parametric Urban Design in Grasshopper / Rhinoceros 3D: Demonstrated on a Master Plan in Vienna*. Portugal, 2019.
[32] D. Kodikara and N. Perera, "Urban Heat Island Minimisation, Local Climate Zones and Parametric Optimisation: A “Grasshopper” Based Model," in *5th International Conference on Countermeasures to Urban Heat Islands*, Dec. 2019, p. 412.

[33] C. Mackey, *Dragonfly 0.0.3 and Urban Weather Generator 5.0 Released! - grasshopper / dragonfly-legacy - Ladybug Tools | Forum.* [Online]. Available: https://discourse.ladybug.tools/t/dragonfly-0-0-3-and-urban-weather-generator-5-0-released/3250 (accessed: Feb. 4 2024).
[34] GitHub, *GitHub - ladybug-tools/uwg: :city_sunrise: The Urban Weather Generator (uwg) is a Python application for modeling the urban heat island effect.* [Online]. Available: https://github.com/ladybug-tools/uwg (accessed: Feb. 4 2024).
[35] B. Bueno and A. Nakano, "Urban Weather Generator - a Novel Workflow for Integrating Urban Heat Island Effect within Urban Design Process," Dec. 2015.
[36] B. Bueno, G. Pigeon, L. K. Norford, K. Zibouche, and C. Marchadier, "Development and evaluation of a building energy model integrated in the TEB scheme," *Geosci. Model Dev.*, vol. 5, no. 2, pp. 433–448, 2012, doi: 10.5194/gmd-5-433-2012.
[37] H. Hamdi, L. Roupioz, T. Corpetti, and X. Briottet, "Evaluation of the Urban Weather Generator on the City of Toulouse (France)," *Applied Sciences*, vol. 14, no. 1, p. 185, 2024, doi: 10.3390/app14010185.
[38] M. W. Rotach *et al.,* "BUBBLE – an Urban Boundary Layer Meteorology Project," *Theor. Appl. Climatol.*, vol. 81, 3-4, pp. 231–261, 2005, doi: 10.1007/s00704-004-0117-9.
[39] V. Masson *et al.,* "The Canopy and Aerosol Particles Interactions in TOulouse Urban Layer (CAPITOUL) experiment," *Meteorol Atmos Phys*, vol. 102, 3-4, pp. 135–157, 2008, doi: 10.1007/s00703-008-0289-4.
[40] B. Bueno, M. Roth, L. Norford, and R. Li, "Computationally efficient prediction of canopy level urban air temperature at the neighbourhood scale," *Urban Climate*, vol. 9, pp. 35–53, 2014, doi: 10.1016/j.uclim.2014.05.005.
[41] A. Salvati, H. Coch Roura, and C. Cecere, "Urban heat island prediction in the mediterranean context: an evaluation of the urban weather generator model," *ACE: Architecture, City and Environment*, vol. 11, no. 32, pp. 135–156, 2016, doi: 10.5821/ace.11.32.4836.
[42] A. Nakano, "Urban Weather Generator User Interface Development: Towards a Usable Tool for Integrating Urban Heat Island Effect within Urban Design Process," Master Thesis, Department of Architecture, Massachusetts Institure of Technology, Massachusetts, USA, 2015.
[43] Deutscher Wetterdiesnt, *Climate Data Center.* [Online]. Available: https://cdc.dwd.de/portal/202209231028/mapview (accessed: Jan. 18 2024).
[44] J. Azevedo, L. Chapman, and C. Muller, "Quantifying the Daytime and Night-Time Urban Heat Island in Birmingham, UK: A Comparison of Satellite Derived Land Surface Temperature and High Resolution Air Temperature Observations," *Remote Sensing*, vol. 8, no. 2, p. 153, 2016, doi: 10.3390/rs8020153.
[45] Bayerische Vermessungsverwaltung, *OpenData.* [Online]. Available: https://geodaten.bayern.de/opengeodata/OpenDataDetail.html?pn=lod2 (accessed: Jan. 19 2024).
[46] P. Chelyshkov, S. Volkov, and E. Babushkin, "DATA-flow in the field of urban planning: basics, concept, methodology," *E3S Web Conf.*, vol. 258, p. 9054, 2021, doi: 10.1051/e3sconf/202125809054.
[47] A. Borrmann, J. Beetz, C. Koch, T. Liebich, and S. Muhic, "Industry Foundation Classes: A Standardized Data Model for the Vendor-Neutral Exchange of Digital Building Models," in *Building Information Modeling*, A. Borrmann, M. König, C. Koch, and J. Beetz, Eds., Cham: Springer International Publishing, 2018, pp. 81–126.
[48] *CADMAPPER.* [Online]. Available: https://cadmapper.com/pro/home (accessed: Jan. 19 2024).

[49] Food4Rhino, *Elk.* [Online]. Available: https://www.food4rhino.com/en/app/elk (accessed: Jan. 19 2024).
[50] R. McNeel, *Supported File Formats.* [Online]. Available: https://www.rhino3d.com/features/file-formats/ (accessed: Jan. 20 2024).
[51] K.-H. Häfele, *KIT - IAI - Downloads - FZKViewer.* [Online]. Available: https://www.iai.kit.edu/english/1648.php (accessed: Jan. 20 2024).
[52] C. Hartz, *AntFarm - data management for Rhino and GH - Pre-Release out now - News - McNeel Forum.* [Online]. Available: https://discourse.mcneel.com/t/antfarm-data-management-for-rhino-and-gh-pre-release-out-now/143129 (accessed: Jan. 21 2024).
[53] BKG, *BKG - Homepage - Updated 3D building model in Level of Detail 2 available for federal facilities.* [Online]. Available: https://www.bkg.bund.de/SharedDocs/Produktinformationen/BKG/DE/P-2020/201204_LoD2.html (accessed: Jan. 21 2024).
[54] S. Schlueter and U. Gruber, *External Code List enumerating the values for the attribute BuildingFuctionType.xml.* [Online]. Available: https://repository.gdi-de.org/schemas/adv/citygml/Codelisten/BuildingFunctionTypeAdV.xml (accessed: Jan. 21 2024).
[55] McNeel Forum, *Open Mesh to Closed Polysurfaces / BREP watertight solid objects.* [Online]. Available: https://discourse.mcneel.com/t/open-mesh-to-closed-polysurfaces-brep-watertight-solid-objects/161272
[56] Food4Rhino, *Urbano.* [Online]. Available: https://www.food4rhino.com/en/app/urbano (accessed: Jan. 21 2024).
[57] T. Fröch and O. Wysocki, *GitHub - tum-gis/CityGML2OBJv2: Command line converter of CityGML (.gml) to OBJ (.obj) files, while maintaining the semantics.* [Online]. Available: https://github.com/tum-gis/CityGML2OBJv2 (accessed: Jan. 21 2024).
[58] F. Biljecki, H. Ledoux, and R. Peters, *GitHub - tudelft3d/CityGML2OBJs: An experimental utility to convert CityGML data to OBJ, featuring decoupling of objects and conversion of attributes to colours.* [Online]. Available: https://github.com/tudelft3d/CityGML2OBJs (accessed: Jan. 21 2024).
[59] *Dragonfly Primer.* [Online]. Available: https://docs.ladybug.tools/dragonfly-primer/
[60] *Building from Solid.* [Online]. Available: https://docs.ladybug.tools/dragonfly-primer/components/0_create/building_from_solid (accessed: Jan. 21 2024).
[61] *Context Shade.* [Online]. Available: https://docs.ladybug.tools/dragonfly-primer/components/0_create/contextshade (accessed: Jan. 21 2024).
[62] *DF Model.* [Online]. Available: https://docs.ladybug.tools/dragonfly-primer/components/0_create/model
[63] *Assign Model UWG Properties.* [Online]. Available: https://docs.ladybug.tools/dragonfly-primer/components/4_alternativeweather/assign_model_uwg_properties
[64] *UWG Simulation Parameter.* [Online]. Available: https://docs.ladybug.tools/dragonfly-primer/components/4_alternativeweather/uwg_simulation_parameter
[65] *Run Urban Weather Generator.* [Online]. Available: https://docs.ladybug.tools/dragonfly-primer/components/4_alternativeweather/run_urban_weather_generator
[66] J. M. Finkelstein and R. E. Schafer, "Improved Goodness-Of-Fit Tests," *Biometrika*, vol. 58, no. 3, p. 641, 1971, doi: 10.2307/2334400.
[67] M. Ozdenefe and J. Dewsbury, "Simulation and real weather data: A comparison for Cyprus case," *Building Services Engineering Research and Technology*, vol. 37, no. 3, pp. 288–297, 2016, doi: 10.1177/0143624415603581.

[68] S. Pusat, İ. Ekmekçi, and M. T. Akkoyunlu, "Generation of typical meteorological year for different climates of Turkey," *Renewable Energy*, vol. 75, pp. 144–151, 2015, doi: 10.1016/j.renene.2014.09.039.
[69] A. L. Chan, T. T. Chow, S. K. Fong, and J. Z. Lin, "Generation of a typical meteorological year for Hong Kong," *Energy Conversion and Management*, vol. 47, no. 1, pp. 87–96, 2006, doi: 10.1016/j.enconman.2005.02.010.
[70] A. J. Peña Quiñones, G. Hoogenboom, M. R. Salazar Gutiérrez, C. Stöckle, and M. Keller, "Comparison of air temperature measured in a vineyard canopy and at a standard weather station," *PloS one*, vol. 15, no. 6, e0234436, 2020, doi: 10.1371/journal.pone.0234436.
[71] J. Le Bras and V. Masson, "A fast and spatialized urban weather generator for long-term urban studies at the city-scale," *Front. Earth Sci.*, vol. 3, 2015, doi: 10.3389/feart.2015.00027.
[72] M. Cajias, *Empirical Methods in Real Estate*.
[73] Zach, "MSE vs. RMSE: Which Metric Should You Use?," *Statology*, 30 Sep., 2021. https://www.statology.org/mse-vs-rmse/ (accessed: Feb. 13 2024).
[74] Thieu, *MBE - Mean Bias Error — Permetrics 1.4.3 documentation.* [Online]. Available: https://permetrics.readthedocs.io/en/latest/pages/regression/MBE.html (accessed: Feb. 13 2024).
[75] P. Bhandari, "Correlation Coefficient | Types, Formulas & Examples," *Scribbr*, 02 Aug., 2021. https://www.scribbr.com/statistics/correlation-coefficient/ (accessed: Feb. 13 2024).
[76] TUM|Stat, *Statistical consulting TUM|Stat - Department of Mathematics - TUM.* [Online]. Available: https://www.math.cit.tum.de/en/math/department/statistical-consulting/#c10260 (accessed: Feb. 13 2024).
[77] Landeshauptstadt München, "Munich Facts and Figures 2023," 2023.
[78] S. Alavipanah, M. Wegmann, S. Qureshi, Q. Weng, and T. Koellner, "The Role of Vegetation in Mitigating Urban Land Surface Temperatures: A Case Study of Munich, Germany during the Warm Season," *Sustainability*, vol. 7, no. 4, 2015, doi: 10.3390/su7044689.
[79] Deutscher Wetterdienst. [Online]. Available: https://www.dwd.de/DE/klimaumwelt/cdc/cdc_node.html
[80] D. Gondhalekar and T. Ramsauer, "Nexus City: Operationalizing the urban Water-Energy-Food Nexus for climate change adaptation in Munich, Germany," *Urban Climate*, vol. 19, pp. 28–40, 2017, doi: 10.1016/j.uclim.2016.11.004.
[81] Muenchen.de, *Haidhausen.* [Online]. Available: https://www.muenchen.de/stadtteile/haidhausen-wissenswertes-tipps-und-infos
[82] Muenchen.de, *Bordeauxplatz Munich: Oasis of calm in the hustle and bustle of the big city* (accessed: 2024).
[83] L. Parhizgar, "Effect of trees on the cooling of squares in Munich in the course of the year," Master thesis, Chair of Forest Growth and Yield Science, Technical University of Munich, Munich, 2022.
[84] Google Earth. [Online]. Available: https://earth.google.com/web/search/Bordeauxplatz,+W%c3%b6rthstra%c3%9fe,+Munich/@48.13193344,11.60507765,531.82781777a,2633.318872d,35y,0h,0t,0r/data=CigiJgokCX_O4WW5wTRAEXzO4WW5wTTAGXDlUZR5qEJAIVbk0bvCTVDAOgMKATA
[85] Maxim Integrated Product ®, *i-Button sensor description.* [Online]. Available: https://www.analog.com/en/product-category/ibutton-and-memory.html (accessed: Feb. 14 2024).
[86] *Lehrstuhl für Waldwachstumskunde: City Trees in Munich.* [Online]. Available: https://www.waldwachstum.wzw.tum.de/en/research/projects/city-trees-in-munich/ (accessed: Feb. 20 2024).

[87] Bayerische Vermessunsverwaltung, *BayernAtlas.* [Online]. Available: https://geoportal.bayern.de/bayernatlas/?lang=de&topic=ba&bgLayer=atkis&catalogNodes=11 (accessed: Feb. 21 2024).
[88] E. Kalaj, "The change in outdoor thermal comfort due to different densification scenarios (horizontal/vertical).: The effect of greening scenarios as a mitigation measure in case of densification.," Master Thesis, Chair of Energy Efficient and Sustainable Design and Building, Technical University of Munich, Munich, 2022.
[89] *Construction Set by Climate.* [Online]. Available: https://docs.ladybug.tools/hb-energy-primer/components/0_basicproperties/construction_set_by_climate
[90] Geoportal Munich, *Energieportal: Buildings' age.* [Online]. Available: https://geoportal.muenchen.de/portal/energie/#
[91] Statistisches Amt München – Auskunftsbüro: *Statistisches Amt München – Auskunftsbüro,* (in de). [Online]. Available: https://stadt.muenchen.de/rathaus/verwaltung/direktorium/statistisches-amt.html
[92] *TABULA WebTool.* [Online]. Available: https://webtool.building-typology.eu/#bm (accessed: Jan. 23 2024).
[93] Loga *et al., Deutsche Wohngebäudetypologie: Beispielhafte Maßnahmen zur Verbesserung der Energieeffizienz von typischen Wohngebäuden ; erarbeitet im Rahmen der EU-Projekte TABULA - "Typology approach for building stock energy assessment", EPISCOPE - "Energy performance indicator tracking schemes for the continous optimisation of refurbishment processes in European housing stocks",* 2nd ed. Darmstadt: IWU, 2015. [Online]. Available: http://www.building-typology.eu/downloads/public/docs/brochure/DE_TABULA_TypologyBrochure_IWU.pdf
[94] Umwelt und Klimapakt Bayern, *Effiziente Energienutzung bei Büro- und Verwaltungsgebäuden - IZU.* [Online]. Available: https://www.umweltpakt.bayern.de/index.php (accessed: Jan. 23 2024).
[95] F. Goia, "Search for the optimal window-to-wall ratio in office buildings in different European climates and the implications on total energy saving potential," *Solar Energy*, vol. 132, pp. 467–492, 2016, doi: 10.1016/j.solener.2016.03.031.
[96] M. Lange and Unfallkasse Hessen, "Kindertageseinrichtungen sicher gestalten: Leitfaden für Bauherren, Architekten und Planungsämter zur sicherheitsgerechten Gestaltung von Kindertageseinrichtungen," Nov. 2020. [Online]. Available: https://www.mkk.de/media/resources/pdf/mkk_de_1/buergerservice_1/lebenslagen_1/familie__kinder_und_jugendliche_1/51180/arbeitshilfen_kita/UKH_Band_8_Kitas_sicher_gestalten_final_web.pdf
[97] S. Cesari, P. Valdiserri, M. Coccagna, and S. Mazzacane, "Energy savings in hospital patient rooms: the role of windows size and glazing properties," *Energy Procedia*, vol. 148, pp. 1151–1158, 2018, doi: 10.1016/j.egypro.2018.08.027.
[98] Y. Zhang, C. Zhao, T. Olofsson, G. Nair, B. Yang, and A. Li, "Field measurements and numerical analysis on operating modes of a radiant floor heating aided by a warm air system in a large single-zone church," *Energy and Buildings*, vol. 255, 2022.
[99] Fensterversand, *Der g-Wert oder Gesamtenergiedurchlassgrad von Verglasungen.* [Online]. Available: https://www.fensterversand.com/info/qualitaet/g-wert-fenster.php (accessed: Jan. 23 2024).
[100] A. Misni, G. Baird, and P. Allan, "The Effect of Landscaping on the Thermal Performance of Housing," *IRSPSD International*, vol. 1, no. 1, pp. 29–48, 2013, doi: 10.14246/irspsd.1.1_29.
[101] *Terrain.* [Online]. Available: https://docs.ladybug.tools/dragonfly-primer/components/4_alternativeweather/terrain (accessed: Sep. 11 2023).

[102] Ladybug Tools | Forum, *Modeling Water Bodies in Dragonfly - grasshopper / dragonfly-legacy - Ladybug Tools | Forum.* [Online]. Available: https://discourse.ladybug.tools/t/modeling-water-bodies-in-dragonfly/3985 (accessed: Jan. 23 2024).
[103] Ladybug Tools | Forum, *Terrain Variation for DF model to use UWG - grasshopper / dragonfly - Ladybug Tools | Forum.* [Online]. Available: https://discourse.ladybug.tools/t/terrain-variation-for-df-model-to-use-uwg/22160 (accessed: Jan. 23 2024).
[104] A. Sweeney, R. P. West, and C. O'Connor, "PARAMETERS AFFECTING THE ALBEDO EFFECT IN CONCRETE," 2010. [Online]. Available: https://www.semanticscholar.org/paper/PARAMETERS-AFFECTING-THE-ALBEDO-EFFECT-IN-CONCRETE-Sweeney-West/40d9b90a4191441d28c48cd68f87a878d563cc57
[105] Y. Kotak, M. S. Gul, T. Muneer, and S. M. Ivanova, Eds., *Investigating the Impact of Ground Albedo on the Performance of PV Systems*, 2015.
[106] L. Moretti *et al.,* "Effect of Sampietrini Pavers on Urban Heat Islands," *International journal of environmental research and public health*, vol. 18, no. 24, 2021, doi: 10.3390/ijerph182413108.
[107] S. Sen and J. Roesler, "Aging albedo model for asphalt pavement surfaces," *Journal of Cleaner Production*, vol. 117, pp. 169–175, 2016, doi: 10.1016/j.jclepro.2016.01.019.
[108] ACPA, "ALBEDO: A MEASURE OF PAVEMENT SURFACE REFLECTANCE," 2002. [Online]. Available: http://overlays.acpa.org/Downloads/RT/RT3.05.pdf
[109] F. P. Torgal, L. Czarnecki, A. L. Pisello, L. F. Cabeza, and C. G. Granqvist, Eds., *Eco-efficient materials for reducing cooling needs in buildings and construction: Design, properties and applications*. Duxford: Woodhead Publishing, an imprint of Elsevier, 2021.
[110] W. R. van Wijk and D. W. Scholte Ubing, "Radiation. Physics of plant environment: North-Holland," pp. 62–101, 1963.
[111] T. R. Oke, *Boundary layer climates. 2nd ed*. London: Methuen (reprinted by Routledge), 1987.
[112] G. Sumner, *Precipitation: Process and analysis*. Chichester: Wiley, 1988.
[113] P. T. Hu, M. Negnevitsky, and M. A. Kashem, "Loading Capabilities Assessment of Power Transmission Lines," 2014.
[114] Y. Wang, Y. Li, S. Di Sabatino, A. Martilli, and P. W. Chan, "Effects of anthropogenic heat due to air-conditioning systems on an extreme high temperature event in Hong Kong," *Environ. Res. Lett.*, vol. 13, no. 3, p. 34015, 2018, doi: 10.1088/1748-9326/aaa848.
[115] D. J. Sailor, "A review of methods for estimating anthropogenic heat and moisture emissions in the urban environment," *Intl Journal of Climatology*, vol. 31, no. 2, pp. 189–199, 2011, doi: 10.1002/joc.2106.
[116] K. KLYSIK, "SPATIAL AND SEASONAL DISTRIBUTION OF ANTHROPOGENIC HEAT EMISSIONS IN LODZ, POLAND KAZIMIERZ KLYSIK," *Elsevier*, vol. 30, 1996.
[117] *Traffic Parameters.* [Online]. Available: https://docs.ladybug.tools/dragonfly-primer/components/4_alternativeweather/traffic_parameters (accessed: Jan. 25 2024).
[118] Ladybug Tools | Forum, *UWG, season change - grasshopper / dragonfly - Ladybug Tools | Forum.* [Online]. Available: https://discourse.ladybug.tools/t/uwg-season-change/23115 (accessed: Jan. 25 2024).
[119] Ladybug Tools | Forum, *Tree coverage ratio calculation - grasshopper / dragonfly - Ladybug Tools | Forum.* [Online]. Available: https://discourse.ladybug.tools/t/tree-coverage-ratio-calculation/18301/3 (accessed: Jan. 25 2024).

[120] M. Münzinger, N. Prechtel, and M. Behnisch, "Mapping the urban forest in detail: From LiDAR point clouds to 3D tree models," *Urban Forestry & Urban Greening*, vol. 74, p. 127637, 2022, doi: 10.1016/j.ufug.2022.127637.
[121] Ladybug Tools | Forum, *Trees in UWG simulation - grasshopper / dragonfly - Ladybug Tools | Forum.* [Online]. Available: https://discourse.ladybug.tools/t/trees-in-uwg-simulation/22779 (accessed: Jan. 25 2024).
[122] L. T. LLC, *EPW Map.* [Online]. Available: https://www.ladybug.tools/epwmap/ (accessed: Jan. 25 2024).
[123] climate.onebuilding.org, *\climatewebsite\WMO_Region_6_Europe\DEU_Germany.* [Online]. Available: https://climate.onebuilding.org/WMO_Region_6_Europe/DEU_Germany/index.html (accessed: Jan. 25 2024).
[124] *Create EPW.* [Online]. Available: https://docs.ladybug.tools/dragonfly-primer/components/4_alternativeweather/create_epw (accessed: Jan. 26 2024).
[125] T. R. Oke, "Initial guidance to obtain representative meteorological observations at urban sites," 2006.
[126] Food4Rhino, *TT Toolbox.* [Online]. Available: https://www.food4rhino.com/en/app/tt-toolbox (accessed: Jan. 26 2024).
[127] *Monthly Chart.* [Online]. Available: https://docs.ladybug.tools/ladybug-primer/components/2_visualizedata/monthly_chart (accessed: Jan. 27 2024).
[128] *Hourly Plot.* [Online]. Available: https://docs.ladybug.tools/ladybug-primer/components/2_visualizedata/hourly_plot (accessed: Jan. 27 2024).
[129] B. Bueno, A. Nakano, and L. Norford, "Urban weather generator: a method to predict neighborhood-specific urban temperatures for use in building energy simulations," in *9th International Conference on Urban Climate jointly with 12th Symposium on the Urban Environment*, 2015.
[130] J. Mittermüller, S. Erlwein, A. Bauer, T. Trokai, S. Duschinger, and M. Schönemann, "Context-Specific, User-Centred: Designing Urban Green Infrastructure to Effectively Mitigate Urban Density and Heat Stress," *UP*, vol. 6, no. 4, pp. 40–53, 2021, doi: 10.17645/up.v6i4.4393.
[131] Deutscher Wetterdiesnt, *Tropennacht.* [Online]. Available: https://www.dwd.de/DE/service/lexikon/Functions/glossar.html?lv3=102802&lv2=102672 (accessed: Feb. 17 2024).
[132] M. Demuzere *et al.,* "A global map of local climate zones to support earth system modelling and urban-scale environmental science," *Earth Syst. Sci. Data*, vol. 14, no. 8, pp. 3835–3873, 2022, doi: 10.5194/essd-14-3835-2022.
[133] *Global LCZ Map.* [Online]. Available: https://lcz-generator.rub.de/global-lcz-map (accessed: Feb. 19 2024).